

THE PHYSICS OF EXCLUSIVE REACTIONS IN QCD: THEORY AND PHENOMENOLOGY

N. G. STEFANIS *

Institut für Theoretische Physik II

Ruhr-Universität Bochum

D-44780 Bochum, Germany

(June 15, 2018)

Abstract

The modern formulation of exclusive reactions within Quantum Chromodynamics is reviewed, the emphasis being placed on the pivotal ideas and methods pertaining to perturbative and non-perturbative topics. Specific problems, related to scale locality, infrared safety, gluonic radiative corrections (Sudakov effects), and the role of hadronic size effects (intrinsic transverse momentum), are studied. These issues are more precisely analyzed in terms of the essential mechanisms of momentum transfer to a hadron while remaining intact. Different factorization schemes are considered and the conceptual lacunas are pointed out. The quite technical subject of renormalization-group evolution is given a detailed account. By combining analytical and numerical algorithms, the one-gluon exchange nucleon evolution equation is diagonalized and next-to-leading eigenfunctions are calculated in terms of Appell polynomials. The corresponding anomalous dimensions of trilinear quark operators are found to form a degenerate system whose envelope shows logarithmic large-order behavior. Selected applications of this framework are presented, focusing on the helicity-conserving elastic form factors of the pion and the nucleon. The theoretical constraints imposed by QCD sum rules on the moments of nucleon distribution amplitudes are used to determine a whole spectrum of optional solutions. They organize themselves along an “orbit” characterized by a striking scaling relation between the form-factor ratio $R = |G_M^n|/G_M^p$ and the projection coefficient B_4 on to the corresponding eigensolution. The main reasons for the failure of the present theoretical predictions to match the experimental data are discussed and workable explanations are sketched.

11.10.Hi, 12.38.Aw, 12.38.Bx, 12.38.Cy, 12.38.Lg, 13.40.Gp, 13.40.Hq, 14.40.Aq

Typeset using REVTeX

*E-mail: stefanis@tp2.ruhr-uni-bochum.de

Contents

I	PREFACE	3
II	INTRODUCTION	3
III	STANDARD CONVOLUTION SCHEME	14
A	FACTORIZATION	14
B	SHORT DISTANCE PART	15
C	LARGE DISTANCE PART: PERTURBATIVE ASPECTS	17
1	Renormalization	17
2	Meson evolution equation	19
3	Nucleon evolution equation	24
D	LARGE DISTANCE PART: NON-PERTURBATIVE ASPECTS	32
E	NUCLEON DISTRIBUTION AMPLITUDES	41
F	DELTA DISTRIBUTION AMPLITUDES	51
IV	ELECTROWEAK FORM FACTORS	55
A	NUCLEON FORM FACTORS	56
B	NUCLEON-DELTA TRANSITION FORM FACTOR	62
V	CHARMONIUM DECAYS	66
VI	MODIFIED CONVOLUTION SCHEME	68
A	MODIFIED FACTORIZATION	69
B	MODIFIED NUCLEON FORM FACTOR	74
1	Screening of α_s singularities	79
2	Numerical form-factor analysis	85
3	Higher-order nucleon distribution amplitudes	93
4	Global pattern of nucleon distribution amplitudes	95
VII	CONCLUSIONS AND OUTLOOK	97
	APPENDIXES	101
A	EIGENFUNCTIONS OF THE NUCLEON EVOLUTION EQUATION	101
B	ELASTIC FORM FACTORS OF THE NUCLEON	103

I. PREFACE

Quantum Chromodynamics (QCD) is that part of the Standard Model which is supposed to describe the strong interactions at the microscopic level. However, despite the numerous phenomenological successes of this theory in regimes where perturbation theory applies, several conceptual and technical challenges concerning the large-distance domain still remain.

Understanding the questions and fixing the problems is possibly not enough to yield convincing quantitative answers towards an analytic description of confinement and the formation of hadronic bound states. Especially the theoretical analysis of exclusive processes, in which *intact* hadrons appear in the initial and final states, involves the detailed calculation of hadronic wave functions – incalculable within a perturbative framework. Nevertheless, it is tempting to analyze the current status of knowledge by exposing physical scenarios pertinent to understanding some basic features in the transition from the perturbative to the non-perturbative phase. Probably the greatest technical barrier here is the mutation of light current quarks – the degrees of freedom of high-energy QCD – to massive constituent quarks, operative after gluon bosonization in low-energy effective theories.

By now the pure perturbative QCD option to large-momentum transfer exclusive processes has been proved elusive. The troubles may be a reflexion of the poorly known complex substructure of hadrons (intrinsically linked to the non-perturbative QCD vacuum); or the faults may lie elsewhere, e.g., in the limited knowledge of higher-order perturbative corrections and the possible lack of convergence of the perturbative expansion. A common key element of these difficulties is infrared (IR) sensitivity due to incomplete factorization of short from large-distance effects. As a consequence, either there are intrusions in forbidden kinematical regimes – invalidating the initial factorization assumptions – or in order to preserve IR finiteness, severe IR-cutoff prescriptions have to be employed – resulting in a depletion of the perturbative contributions.

This report focuses on these problems from a user’s perspective, identifying the principal drawbacks, and trying to set benchmarks for future developments. We concentrate on two major subjects: (i) hadron distribution amplitudes and elastic form factors, and (ii) implementation of the renormalization group within appropriate factorization schemes. To set the stage, we discuss and review problems relating to the momentum (mass) scales involved in form factor calculations: scale locality, IR safety, gluonic radiative corrections (Sudakov-type form factors), and the role of hadronic size effects (intrinsic transverse momenta). In addition, we give a systematic non-perturbative analysis for determining hadron distribution amplitudes in conjunction with QCD sum rules. These issues are related to distinct mechanisms by which a large space-like momentum is transferred to an intact hadron and we use detailed calculations to investigate how these mechanisms influence the predictions for $F_\pi(Q^2)$, $G_M^p(Q^2)$, $G_M^n(Q^2)$, and $G_M^*(Q^2)$ relative to existing data. Other phenomenological applications in this context are also discussed.

II. INTRODUCTION

Lack of precise knowledge about the large-scale inter-quark forces and the mathematical intractability of the nonlinear structure of the QCD dynamics preclude an *ab initio* analytical

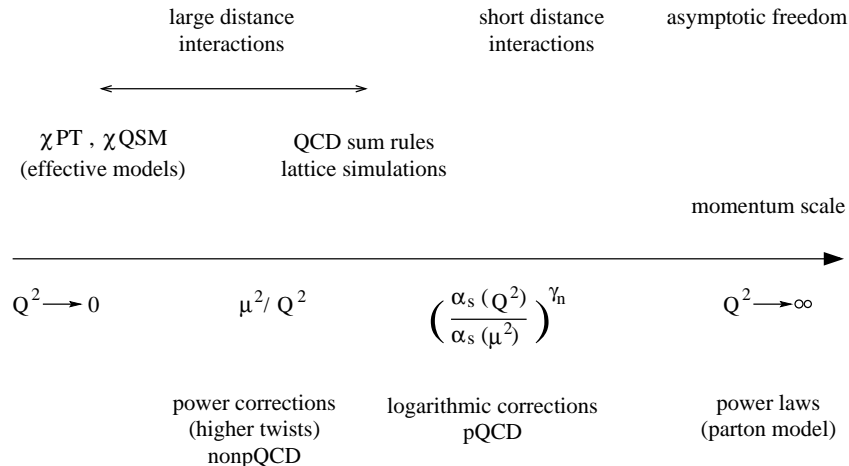


Figure 1. Perception of strong-interaction dynamics with momentum flow.

calculation of quantities like the hadron wave functions. Of the various approaches now being studied, those employing quark/gluon condensates, the order parameters of non-perturbative QCD, are among the most successful – albeit not without their loose ends. In particular, nonlocal condensates [1] which ascribe a nonzero average virtuality to vacuum quarks and gluons (a technical review with earlier references is given in [2]) may enable one to do more realistic calculations of hadron wave functions, but such techniques are still in an embryonic phase of development. Thus far the non-locality of quark/gluon condensates appears only in model form, though it was found by lattice calculations [3] that it decreases exponentially with the coordinates.

Frameworks which are capable of simulating the non-perturbative regime of QCD, either in the continuum (e.g., via QCD sum rules [4]), or numerically on the lattice [5], have been widely used during the last decade. Although modern lattice calculations in the strong-coupling regime are very promising, there are conceptual and technical limitations: e.g., the properties of a single proton cannot be determined properly at present. Especially the computation of higher-order moments (corresponding to higher derivatives acting on local operators) of light-cone distribution amplitudes appears very difficult at present [6]. On the other hand, since hadron wave functions enter only *integrated* quantities, like form factors, their extraction directly from the data is still in its infancy, and much more experimental input is needed to make significant progress here.

In the past few years, there have been several theoretical attempts to emulate low-energy QCD by using effective chiral (χ) actions, e.g., the Nambu-Jona-Lasinio model (for a recent review, see, e.g., [7] and references cited therein). Such approaches implement chiral symmetry breaking and are, in principle, deducible from the instanton model of the QCD vacuum [8], albeit a rigorous derivation is still rudimentary, and the range of their validity is limited to momentum values below an ultraviolet (UV) cutoff scale of about 1 GeV.

The perception of strong-interaction dynamics at different resolution (energy) scales is illustrated in Fig. 1.

Exclusive processes in QCD are therefore particularly interesting because they provide the possibility of analyzing hadron wave functions in terms of their quark and gluon de-

degrees of freedom. In order to take advantage of perturbative QCD in exclusive processes,¹ a short-distance amplitude has to be isolated and proved to be IR finite. This provides a useful handle on strong-interaction amplitudes and one is in the position to make quantitative computations in a systematic fashion. Formally, this corresponds to the procedure of multiplicative separation (factorization) of regimes, ubiquitous in many areas of theoretical physics. It is the property of cross sections (in inclusive processes) or amplitudes (in exclusive processes) that high-momenta (“hard”) and low-momenta (“soft”) regions can be disentangled in such a way that the factorized parts depend only on the dynamics specific for the corresponding scale.

Proofs of factorization theorems [9,10], both for inclusive cross sections and exclusive amplitudes, have reached a certain level of sophistication, but the subject is still open (for a comprehensive review, we refer to [11]). For instance, the generalization of factorization theorems beyond leading twist faces severe problems due to incomplete Bloch-Nordsieck (BN) cancellation [12] of IR divergences [13,14]. Along similar lines of argument, uncanceled IR divergences near the boundary of phase space (the so-called endpoint region) have to be re-summed by improving renormalization group techniques to render the perturbative calculation sound. Completing this procedure, the second step is to interphase the factorized parts to renormalization.

According to these ideas, the asymptotic, i.e., large Q^2 -behavior of electroweak form factors can be calculated with perturbative QCD by simply assuming free valence quarks entering and exiting the hard-scattering region, without any recourse to confinement. It is clear that as the external momentum becomes smaller, the resolution scale decreases, quantum modes with corresponding wavelengths emerge and the pure perturbative picture of quasi-free quarks bound together by single-gluon exchange breaks down. At this point, fluctuations of the background fields of the non-trivial QCD vacuum interfere and a self-consistent computation must take them into account. Where this transition of the pure perturbative phase to the non-perturbative one takes place is a point of ongoing controversy [15,16,17,18].

A useful framework for describing exclusive processes along these premises is the convolution scheme of Brodsky and Lepage [19,20,21]. [A somewhat different approach to hard processes was developed independently by Efremov and Radyushkin [16,22,23].] Within this scheme, the reaction amplitude becomes the product (the convolution) of two or more factors, each depending only on the dynamics specific for that particular momentum (or distance scale), and the evolution of the factorized parts is renormalization group controlled. More important, the hard part of the process becomes amenable to the methodology of QCD perturbation theory. To enforce IR finiteness, subtractions of IR singularities are imposed. The guiding idea is that the time scale involved in the hard part of the amplitude and that one for the formation of the intact hadron in the final state(s) are disparate, so that the corresponding dynamics are uncorrelated (impulse approximation). As a consequence of the sudden character of the hard interactions, the perturbed quantum mechanical state remains unchanged and time evolution is governed by the perturbed Hamiltonian.

¹“Exclusive” means that the momenta of all individual hadrons participating in the process are measured.

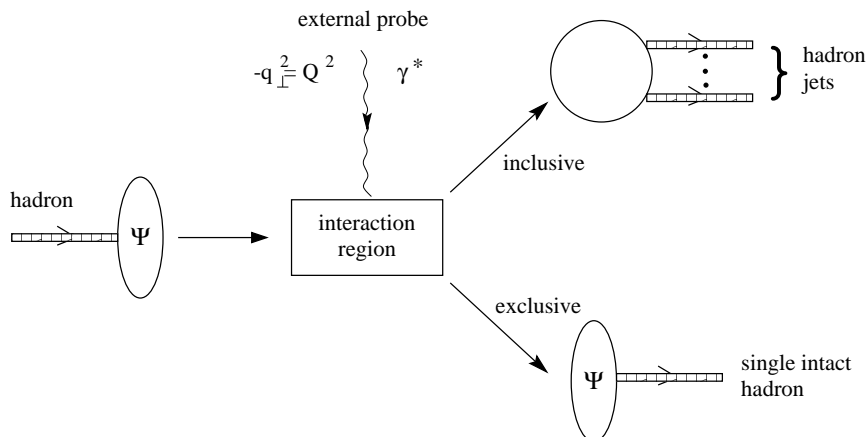


Figure 2. Inclusive versus exclusive reactions in QCD.

In leading order of the coupling constant, large-momentum transfer quark-gluon subprocesses can be adequately described by one-gluon exchange kernels, the justification being provided by asymptotic freedom [24]. We will call this approach in the following “the standard convolution scheme” of exclusive processes. Detailed applications of this type of QCD analysis to hadronic form factors and decay amplitudes are given in later sections of this survey.

Having extracted a (process-dependent) hard-scattering amplitude, the remaining soft contributions responsible for the bound-state dynamics are encapsulated in universal (but *factorization-scheme dependent* [25]) hadron distribution amplitudes. In axial gauges (e.g., the light-cone gauge, $A^+ = 0$), the distribution amplitude is the probability amplitude for the hadron to consist of valence quarks with (longitudinal) momentum fractions $0 \leq x_i \leq 1$, $\sum_i x_i = 1$ (in an infinite momentum frame) moving collinearly up to the factorization scale. Restricting the flow of soft transverse momenta into the distribution amplitudes amounts to subtracting their high-momentum tails, and is tantamount to avoid double counting and ensure that all vertices and propagators entering the microscopic processes of a Feynman graph are entirely governed by perturbative QCD.² The practical utility of this picture, besides being physically appealing, resides in the fact that presciently dissecting the reaction amplitude in the form of a convolution of soft and hard parts, its evolution behavior, i.e., the variation of the parts with momentum, is completely controlled by the large scale of the process. In fact, if the momentum transfer Q^2 is very large, the UV regularization scale of the renormalization group can be safely traded for Q^2 to give rise to renormalization group evolution. As the momentum transfer imparted to the hadron by the external electromagnetic probe increases, inclusive channels are gradually triggered, and the probability that the hadron rebounds without going apart diminishes. This behavior is illustrated in Fig. 2.

A theoretical tool to calculate hadron wave functions is provided by the operator product expansion [26]. In the operator product expansion language, the hard-scattering amplitude (small-distance interaction) corresponds to the Wilson coefficient function, whereas

²A more technical discussion of these points is postponed to a following section.

the initial- and final-state hadron wave functions (large-distance interactions) derive from the matrix elements of local operators with appropriate quantum numbers for each channel. A complicating factor in the operator product expansion analysis is that the identification of a short-distance part in the exclusive amplitude is not *a priori* obvious and has to be determined process by process.

At leading-twist level, the soft parts of the factorized exclusive amplitude are represented by the valence-state wave functions on the light cone and describe the distribution in longitudinal momentum fractions, being averaged over transverse momenta up to values of the factorization scale. Contributions from higher Fock states with additional $q\bar{q}$ -pairs and gluons (higher twists) are suppressed by powers of the momentum transfer. Such contributions correspond in the operator product expansion to composite quark-gluon operators with progressively higher dimensions, the inclusion of which introduces new order parameters that have to be estimated.

Applications of QCD sum rules to exclusive processes started already in the early eighties by computing the meson and nucleon form factors [27,28], as well as the first moment (i.e., the f_π decay constant) of the pion distribution amplitude. Following a different strategy, V. L. Chernyak, A. R. Zhitnitsky, and I.R. Zhitnitsky (CZ) attempted to reconstruct model distribution amplitudes from their few first moments for the pion [29], the nucleon [30], and other hadrons [31]. The values of the moments were restricted in their approach by constraints extracted from QCD sum rules, and model distribution amplitudes as polynomials in the longitudinal momenta of the valence quarks were derived by means of moment inversion. Fixing the second and fourth moment of the pion distribution amplitude, CZ proposed a “double-humped” model which brings the value of the pion form factor close to the data for a value of the strong coupling constant α_s as low as 0.3. This was considered a remarkable success because the asymptotic prediction yields the value $Q^2 F_\pi(Q^2) \approx 0.13$ which falls short a factor of three compared to the experimental data [32] (though the accuracy of the present data is rather poor to be conclusive). A similar analysis for the nucleon on the basis of the first- and second-order moments, led the same authors to propose a nucleon distribution amplitude which shows considerable asymmetry in the distribution of the longitudinal momentum of the valence quarks.

Soon an alternative nucleon distribution amplitude was suggested by Gari and Stefanis (GS) [33], constructed with the aim to yield helicity-conserving nucleon form factors which account for the possibility that the electron-neutron differential cross section is dominated by G_E^n , while G_M^n is asymptotically small or equivalently that there is a sizeable neutron Pauli form factor overwhelming the Dirac one at all Q^2 values. The GS model gives very good agreement with the latest high- Q^2 SLAC data [34] on G_M^p (or F_1^p) and makes realistic predictions for the corresponding neutron form factor in the high-momentum region [35]. In contrast, as effected in [35], the CZ model overestimates both form factors almost by a factor of two in the region of 10-20 GeV^2 , if realistic values of Λ_{QCD} around 200 MeV are used.³ But, on the theoretical side, a heavy price is paid: some moments of the GS model distribution amplitude cannot match the requirements set by the CZ moment sum

³In the original CZ analysis, the value $\Lambda_{\text{QCD}} = 100 \text{ MeV}$ was used. Such a low value is now de facto excluded by experiment.

rules in the allowed saturation range [35]. Moreover, as it was shown later by Chernyak and coworkers [36], this model leads to a prediction for the $^3S_1 \rightarrow p\bar{p}$ decay width of charmonium which is several orders of magnitude smaller than the experimental value.⁴

In 1987 the moment sum rules were re-evaluated by King and Sachrajda (KS) [37], spotting the gaps in the CZ analysis and shifting the range of the moment sum rules, albeit the gross features of the method were confirmed as was the basic shape of the nucleon distribution amplitude.

A couple of years later, Chernyak, Ogloblin, and I. R. Zhitnitsky (COZ) [38] refined their previous moment sum rules for the second-order moments and extended their method to third-order moments. Their new moment sum rules comprise 18 terms with restricted margins of uncertainty relative to the previous CZ analysis and, in general, comply with the results of the KS computation, but contradict those obtained on the lattice for the lowest two moments [39]. The same authors have also proposed a new model distribution amplitude for the nucleon – still restricted to polynomials of second degree in the longitudinal momentum – which satisfies all, but 6 of the new moment sum rules, whereas the CZ amplitude and the GS one violate, respectively, 13 and 14 of them. The KS amplitude provides almost the same quality as that of COZ, with only 7 broken moment sum rules. In the same year, Schäfer [40] presented a variety of model distribution amplitudes for the nucleon, which incorporate polynomials of degree three in the longitudinal momentum, and found that such contributions play a token role, if properly incorporated.

The essence of these investigations is that distribution amplitudes extracted from moment sum rules are much broader than the asymptotic solution (to the evolution equation) and have a rich structure that is reflected in a quite asymmetric balance in the distribution of longitudinal momentum fractions among the valence quarks, accentuated by nodes. The latter may be understood in the following way: A valence quark embedded in the non-perturbative QCD vacuum rebounds differently from one in “free space”. Hence, quark/gluon condensates act somewhat like a dispersive medium in which different components of a wave propagate with different speeds and tend to change phase with respect to each other [35]. Regions of different phases in the nucleon distribution amplitude may be interpreted as evidence for binding effects inside the nucleon, amounting perhaps to diquark formation. A full-fledged discussion of these issues will be given in the course of this work.

The next major step in the determination of nucleon distribution amplitudes was done in the early nineties by Stefanis and Bergmann with the invention of the *heterotic conception* [41,42] (Fig. 3).⁵ Previously, the CZ model (or its descendants: KS and COZ models) on one hand and the GS model on the other hand were treated in the literature as competing alternatives – mutually excluding each other. In addition, either way, it was not possible to reconcile the theoretical moment sum rules constraints with the experimental data because none of these models is able to give, simultaneously, a quantitatively satisfactory agreement with the form-factor and charmonium-decay data.

Perhaps understandably, in view of such distinctive models and predictions, the con-

⁴Provided one uses again the favored value of the strong coupling constant $\alpha_s = 0.3$.

⁵“Heterosis” in Greek means increased vigor due to cross-breeding.

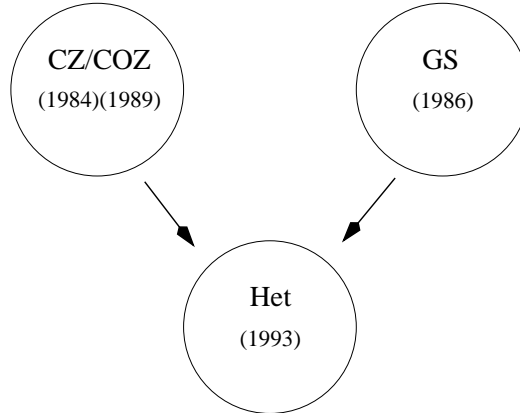


Figure 3. Heterotic conception of the nucleon distribution amplitude. The heterotic model amalgamates typical characteristics of COZ-like and GS-like amplitudes.

ventional view has been one of fragmentation. But the new idea, underlying the nucleon heterotic model, makes it possible to amalgamate the best features of COZ-type and GS-type distribution amplitudes into a single mold, thus lifting the disparity between theory and experiment. As it will become more transparent in the following sections, the heterotic distribution amplitude is a “hybrid” – sort of – and seems to have a foot in each of the previous models. This duality is also reflected in its profile which, though distinctive in overall shape from both the COZ and the GS distribution amplitudes, bears geometrical characteristics typical for both models.

Similar ideas of heterosis were then applied by the same authors [43] to the distribution amplitude of the $\Delta^+(1232)$ isobar, treating the moment sum rules of Farrar et al. (FZOZ) [44] and those by Carlson and Poor (CP) [45] in combination. Again a heterotic distribution amplitude was determined in between the CP and the FZOZ model distribution amplitudes. Using the heterotic distribution amplitudes for the nucleon and the Δ , the transition form factor G_M^* was calculated [42,43] within the standard convolution scheme and remarkable agreement with the available data was found. Even more, a recent reanalysis by Stuart et al. [46,47], of the inclusive $e - p$ data in the $\Delta(1232)$ region by the SLAC experiment NE11, combined with low Q^2 data, high Q^2 data from the SLAC experiment E133, and missing mass squared data, finds results for the transition form factor systematically higher than the previous data analysis by Stoler [48] and confirms within the errors the “heterotic” predictions [49].

These developments gave rise to a more general picture (Stefanis and Bergmann) [49,50,51,52], which deals with *global* features of nucleon distribution amplitudes. The crucial question is: If it is possible to synthesize *one* hybrid-type distribution amplitude, namely the heterotic one, is it then possible to find also other distribution amplitudes with elements belonging to different classes of solutions to the moment sum rules? That the moment sum rules are not stringent enough to fix the shape of the nucleon distribution amplitude uniquely was already pointed out by Gari and Stefanis [53], and in more mathematical detail by Ste-

fanis [35]. A similar analysis for the pion distribution amplitude was given by Mikhailov and Radyushkin [54].

To determine the possible variation of distribution amplitudes allowed by moment sum rules, one has first to identify appropriate order parameters in order to classify the obtained solutions. It turns out that the crucial parameters are: (1) the expansion coefficient B_4 in the eigenfunctions decomposition of the nucleon distribution amplitude, (2) the form-factor ratio $R \equiv |G_M^n|/G_M^p$, and (3) a χ^2 criterion in the moment sum rules analysis that accounts for the higher stability of the lower moment sum rules relative to the higher ones [35]. In addition, one can define a “hybridity” angle [52] which quantifies the information about the mixing of geometrical characteristics of distribution amplitudes associated with different sorts of (asymmetric) longitudinal momentum balance. The upshot of this treatment is a pattern of unity in diversity. One is able to track the “metamorphosis” of the heterotic distribution amplitude across an orbit in the plane spanned by B_4 and R as it transforms into the COZ one. Furthermore, the orbit turns out to be finite, starting at small R -values, associated with the heterotic distribution amplitude, and terminating at a COZ-like distribution amplitude which is a fixed point of the transformation. Interpolating solutions with comparable χ^2 -values are also determined, showing various degrees of “hybridity”. In effect, the emerging orbit provides at a glance a global, and perhaps more perspicacious, perspective on the information encapsulated in available moment sum rules [38,37] for the structure of nucleon distribution amplitudes.

Regardless of the degree of conviction of particular model distribution amplitudes, problems are lurking in the endpoint region of phase space, where the typical gluon virtualities are much smaller than the external high momentum. Indeed, Isgur and Llewellyn-Smith [15], and also Radyushkin [16,17], have pointed out that the contributions from this region in fact dominate the pion and nucleon form factors, rendering a perturbative treatment at accessible momentum transfers questionable. Their main conclusion is that the observed power-law behavior of the hadron form factors is not due to the perturbative contribution via hard-gluon exchange, but rather a reflection of the finite size of the hadrons. The perturbative contribution takes over, they argue, at momentum-transfer values too high to be measured in the foreseen future. Similar thoughts were more recently expressed by Bolz and Kroll [18,55] on a phenomenological basis. These authors claim that the broad flat maximum of the (soft) overlap contributions to the pion and nucleon form factors in the intermediate momentum-transfer region “mimics” the Q^2 -dependence of the short-distance term. Again the conclusion is that the bulk of the existing data can be explained by the soft contribution alone without resort to the small perturbative contribution. Such statements could be construed as indicating that perturbative QCD is irrelevant for this sort of exclusive processes at laboratory Q^2 .

A serious criticism in this context concerns whether asymmetric distribution amplitudes, as those discussed above, are reliable. It was noted by Stefanis [35] that a *finite* set of low-order moments cannot provide a unique solution, and that the ensuing variation is inherent in the technique of moments inversion that is unable to render the diversity of possible solutions small. It is exactly because of this reason that a “hierarchical” χ^2 criterion, which weighs the moment sum rules according to their order, was used in the “heterotic” approach, proposed in [42,43]. Imposing such a *global* criterion, the sensitivity to disregarded higher-order terms is *de facto* averted [51].

Another objection, intimately tied to the QCD sum-rule method, was raised by Radyushkin and expounded in several articles (see, e.g., [17]). The point is that *local* condensates assign zero virtuality to vacuum quarks corresponding, equivalently, to infinite correlation lengths of vacuum field fluctuations and, since the higher-order moments are sensitive to the size of the non-locality (or inverse quark virtuality), this effect should be taken into account. This is perhaps a turning point in the conceptual evolution of QCD sum rules, but crucial technical challenges remain, e.g., the operator product expansion has to be generalized to nonlocal operators. Nevertheless, following this rationale, Mikhailov and Radyushkin [56], and Bakulev and Radyushkin [57] (see also [58]) were able to obtain pion wave functions, modeling the vacuum quark virtuality distribution by a Gaussian around an average virtuality ranging from 0.4 GeV^2 [59] to 1.2 GeV^2 [60]. A more recent analysis by Dorokhov, Esaibegyan, and Mikhailov [61] attempts to calculate quark and gluon virtualities within the model of the liquid instanton vacuum [8,60]. The wave functions derived this way are broader than the asymptotic solution of perturbative QCD, but, unlike the CZ amplitude, have no dip in the central region. It goes without saying that the corresponding second and fourth order moments are close to their asymptotic values. These investigations seem to confirm again the dominance of the soft contribution to the pion form factor at intermediate values of momentum transfer.

Unfortunately, the extension of this method to the nucleon case is not straightforward. New nonlocal quark-gluon condensates of higher dimension emerge, which have to be estimated, but cannot be reduced to condensates of lower dimension because they explicitly violate the “factorization hypothesis” [4].

Putting our comments so far together, we draw two important conclusions: (1) the endpoint region of exclusive processes is IR sensitive and has to be considered very carefully; (2) the moment sum rules have defined a much more profitable goal to work towards than an elaborate formalism for calculating reliable distribution amplitudes. But however incompletely we may comprehend the details of how the complex structure of the non-perturbative QCD vacuum works, we all understand that until more advanced techniques are really available, the moment sum rules and the herewith derived model distribution amplitudes are revealing. In succeeding sections, we focus on the ramifications and implications of issue (1) considering assessment (2) as a sound working hypothesis.

While the non-perturbative non-locality of condensates may eliminate a source of errors in the determination of wave-function moments, another type of non-locality, namely in transverse configuration space, may help out in restoring the validity of the perturbative treatment in the endpoint region by permitting the divergences due to soft gluons to be *screened* by means of (re-summed) Sudakov effects. We do not propose to review these extensive investigations in great detail here, but we do sketch the key ideas in connection with form-factor calculations and complete this review in Sec. VI with some concrete examples.

In Abelian theories, like Quantum Electrodynamics (QED), the emission of soft real (*bremsstrahlung*) quanta prevents the vanishing of the cross section by giving rise to BN cancellation between (soft) real and virtual photons [12]. This cancellation does not occur within perturbation theory because these two different sorts of soft quanta correspond to different powers of the coupling constant, rent by the iteration procedure. Hence, one needs closed-form all-order expressions to accomplish cancellation. In the IR regime of non-Abelian theories (like QCD), where the ratios of all physical scales relative to the IR-cutoff scale are

large, cross sections of non-forward processes involving *isolated* colored particles, whether or not an infinite number of soft gauge bosons (gluons) are included, vanish in the IR limit. In contrast, processes involving only neutral (composite) particles have non-vanishing cross sections in this limit. It transpires that colored amplitudes at large momentum transfers are suppressed by damping exponential (Sudakov) factors – one for each non-color-singlet, near mass-shell particle [62].

The Sudakov form factor is the probability for no emission of soft photons (gluons) with increasing momentum transfer in hard photon-electron scattering within QED (QCD). Sudakov found [63] that the one-loop result exponentiates to give a double logarithm of the form $\exp[-(\alpha/c\pi)\ln^2(Q^2/\mu^2)]$, μ being the small scale of the system; e.g., the invariant squared mass of the electron [63] ($c = 2$), or an auxiliary photon mass in the case of on-shell external fermions ($c = 4$) [64,65,66]. The dominance of the leading double-logarithmic term in the high-momentum limit was confirmed by Mueller [67], and Collins [68] by re-summing non-leading single logarithms to all orders of the fine-coupling constant α . The upshot is that, asymptotically, the Sudakov form factor drops to zero faster than any power of Q^2 .

The generalization of this type of calculations to QCD was initiated by Cornwall and Tiktopoulos [62]. They computed the non-Abelian vertex function up to the three-loop order and conjectured exponentiation of the leading double-logarithmic result. The formal proof of exponentiation was provided by Belokurov and Ussyukina [69], and by Dahmen and Steiner [70]. The inclusion of single-logarithmic terms was supplied by Sen [71], along the lines of Collins' previous QED analysis [68]. An elaborate and systematic re-summation approach for leading and non-leading logarithms was conducted by Collins and Soper [72] (see also [73,74]), using eikonalization and renormalization group type equations in the axial gauge, with recourse to the Grammer-Yennie method [75]. They found that the leading contributions stem from integration regions where either all four-momentum components of gluons are small ("soft region") or from gluons collinear to external (massless) quark lines.⁶ When such loop momenta regions overlap they give rise to double logarithms of the generic form $\exp\left\{-c\ln\left(\frac{Q^2}{\mu^2}\right)\ln\left[\frac{\ln(Q^2/\Lambda_{\text{QCD}}^2)}{\ln(\mu^2/\Lambda_{\text{QCD}}^2)}\right]\right\}$, in which the constant c depends on the color algebra via the renormalization group effective coupling $\beta_0 = (11 - 2n_f/3)/4$, where n_f is the number of quark flavors. In our considerations to follow n_f is taken to be equal to 3.

One crucial clue of Sudakov effects in exclusive processes came into view, largely as the result of work by Botts and Sterman [76]. They realized that the IR cutoff in the Sudakov function can be traded for the inter-quark separation in transverse configuration space (after Fourier transformation), thus providing an *in situ* regularization of IR divergences without introducing external IR regulators. Conventionally, transverse momenta in the hard-scattering amplitude are dispensed with on the assumption that they are negligible compared to the large scale Q^2 . This is true – no doubt – as long as all momentum flows within a Feynman graph are large. However, in the endpoint region, as already mentioned, some momentum can formally come close to zero, becoming smaller than the neglected transverse momentum. Retaining the flow of transverse momenta into the hard-scattering region, is actually tantamount to modifying factorization because the momentum region at

⁶Whether a gluon belongs to the soft or the collinear set depends on the gauge.

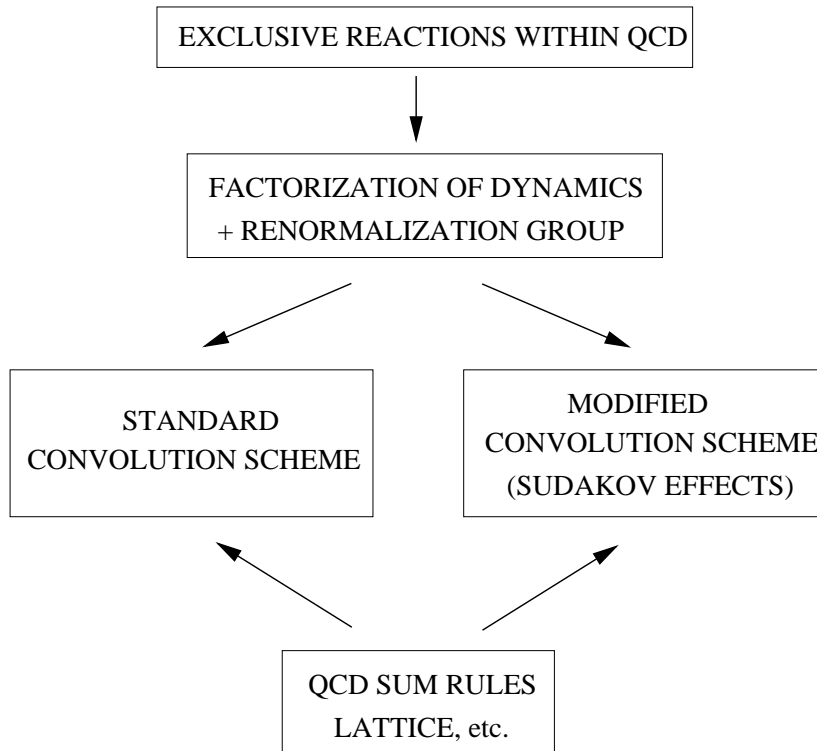


Figure 4. Flow chart illustrating two possible ways of realizing factorization of exclusive reactions in convolution form within QCD.

the interface between the true confinement regime – parameterized in the wave functions – and the true hard regime – expressed through the short-distance part – is explicitly taken into account in the convolution of the reaction amplitude. In the axial gauge, all Sudakov effects can be encapsulated in wave-function-like factors, one for each incoming and outgoing quark line, that link the soft wave functions with the hard scattering region. This amounts to a *finite* wave function renormalization (Stefanis [25]). The modified convolution (factorization) scheme is illustrated in Fig. 4.

In this vein, Li and Sterman [77] were able to show that in the pion case there is strong Sudakov suppression for large inter-quark separation as Q^2 increases. Whence, contributions from the endpoint region, where perturbation theory fails, become less and less important. Indeed, the bulk of the pion form factor accumulates in regions where the coupling constant is less than about 0.7 and the transverse distances are moderate. This is a remarkable result, for no external regulators are needed to saturate the strong coupling at small momenta, the IR protection being intrinsically provided by the transverse inter-quark separation alone.

As regards three-quark states, the situation is more complicated because several transverse scales are involved and therefore IR protection is not automatically accomplished. It was shown by Kroll and Stefanis, and their respective collaborators [78], that the simple extension of the pion analysis to the nucleon case by Li [79] fails. The main reason is that there exist kinematical regimes where none of the Sudakov factors provides suppression for arbi-

trary choices of the inter-quark distances. One has to correlate the different transverse scales and adopt a *common* IR cutoff scale that is taken to be the maximum transverse separation (“MAX” prescription). The underlying physical idea is that due to the color neutrality of a hadron, its quark distribution cannot be resolved by gluons with a wavelength much larger than an average inter-quark separation scale. Thus, gluons with wavelengths large compared to the (transverse) hadron size probe the hadron as a whole, i.e., in a color-singlet state and decouple. As a result, quarks in such configurations act *coherently* and therefore (soft) gluon radiation is dynamically inhibited.

The particular advantage of this approach [78,25] is that (1) it suffices to protect the amplitudes from becoming singular for all possible kinematical configurations, and (2) it yields a perturbative contribution to the nucleon form factors which *saturates*, i.e., which is rather insensitive to distances of order $1/\Lambda_{\text{QCD}}$. Other IR regularization choices, for instance that adopted by Li, may lead to un-compensated singularities (see for more details, in Sect. VI). Results for both the proton [78] as well as the neutron form factors [80] were obtained, taking also into account the intrinsic transverse momenta in the nucleon wave function in the realm of the pion analysis of Jakob and Kroll [81]. The dark side of these theoretical improvements is that the calculated nucleon form factors fall short by at least a factor of two relative to the experimental data. The possible reasons for this depletion will be discussed in subsequent sections.

The remaining part of this report is divided into two main parts. The first part deals with hadron distribution amplitudes (Sect. III) and form factors (Sect. IV) within the standard convolution scheme. In the second part (Sect. VI) we treat similar topics within the modified convolution scheme. We close this review with a further in-depth discussion of the whole picture, attempting at providing a stimulating outlook for the future. Some important technical issues and useful formulae are collected in the appendixes.

III. STANDARD CONVOLUTION SCHEME

The theoretical tools for the description of exclusive processes are the hard-scattering amplitude – which describes the process-dependent quark-gluon interactions within perturbative QCD – and the probability amplitude for finding the lowest-twist Fock state (*alias* the distribution amplitude for the valence state) in a hadron. The total exclusive amplitude is then represented by the convolution of these three factors [21,23], assuming factorization of large-momentum flow regions from those of soft transverse momenta, necessary to form bound states. In terms of the operator product expansion, this corresponds to truncation at leading twist (t =dimension–spin) level, namely $t = 2$ (meson case) and $t = 3$ (nucleon case). Higher-twist components, corresponding to a higher number of partons (quark-pairs and gluons), are suppressed by powers of the large scale, i.e., the momentum transfer Q^2 . To clarify the physical meaning of these statements, we now turn to factorization.

A. FACTORIZATION

Factorization theorems are of central importance in quantum field theory. The basic idea is that one can separate high-momentum from low-momentum dependence in a multiplica-

tive way. For example, proving that UV divergences occurring in Feynman graphs can be absorbed into multiplicative renormalization factors (infinite constants) is instrumental in establishing renormalizability. The technical challenge is to prove factorization of a particular QCD process to *all orders* in the coupling constant going beyond leading logarithms [11]. These difficulties derive from the fact that in QCD a new type of IR-divergence is encountered, the *collinear* divergence, and that in higher orders the self-coupling of gluons becomes important in the exponentiation of IR divergences.

The realization of factorization when applying to elastic form factors can be written in the form of a convolution of the hard-scattering amplitude (dubbed T_H) and two soft wave functions corresponding to the incoming and out-coming hadron (termed Φ). Generically (i.e., absorbing all integrations over internal variables into \otimes), one has

$$F(Q^2) = \Phi^{\text{out}}(m/\mu) \otimes T_H(\mu/Q) \otimes \Phi^{\text{in}}(m/\mu) , \quad (1)$$

where m sets the typical (small) virtuality in the soft parts and Q is the (external) large scale, characteristic of the hard (parton) subprocesses.

The matching scale μ at which factorization has been performed is arbitrary and, assuming that $\mu \gg m$, it can be safely identified with the renormalization scale – unavoidable in any perturbative calculation – by virtue of the renormalization group equations. In this way, F can be rewritten as a function only of the coupling constant operative at that same scale, the latter being identified with the large external scale.

As long as *scale locality* is preserved, i.e., as long as the variation of the effective coupling constant with μ is governed by the *same* momentum scale, and the limit $m \rightarrow 0$ is finite, Eq. (1) is valid because *intrusions* from the hard into the soft regime are prohibited. Potential IR divergences in T_H are removed by subtractions on account of the properties of the wave function parts. This means that T_H in leading order is by definition insensitive to long-distance interactions, i.e., it is *IR safe*. All IR-sensitivity resides in the hadron distribution amplitudes $\Phi^{\text{in(out)}}$ which are peaked around small transverse momenta of the order m^{-1} with their large-momentum tails removed by cutting off from above the integration over transverse momenta. Their dependence on the cutoff scale is mild and is governed by renormalization group-evolution. Both the subtraction procedure of the large momentum tails in the soft parts and the cancellation of IR divergences in the hard part are not unique. They actually define the factorization procedure adopted, thus imposing an *implicit* factorization-scheme dependence on the hadron distribution amplitudes [82]. Of course the asymptotic behavior of F should not be affected and still be determined by the asymptotic distribution amplitude evolved with the leading (i.e., lowest-order) anomalous dimension, associated with vertex and quark self-energy corrections.

B. SHORT DISTANCE PART

Invoking factorization, the leading order expression for the helicity-conserving hadron form factor can be cast in the form

$$F(Q^2) = \int_0^1 [dx] \int_0^1 [dy] \Phi^*(y_i, \tilde{Q}_y) T_H(x_i, y_i, Q) \Phi(x_i, \tilde{Q}_x) , \quad (2)$$

where

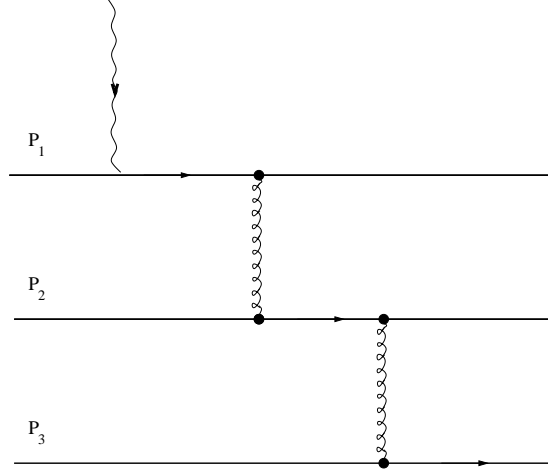


Figure 5. Example of a Feynman graph contributing to the nucleon form factor at tree level.

$$[dx] = \delta \left(1 - \sum_{i=1}^n x_i \right) \prod_{j=1}^n dx_j \quad (3)$$

($n = 2$ for mesons and $n = 3$ for baryons), and $\tilde{Q}_x = \min(x_i Q)$ or $\tilde{Q}_x = \min((1 - x_i)Q)$ with analogous definitions for the y variable. The form factor is the probability for the hadron to absorb large transverse momentum while remaining intact. The bound-state (i.e., confining) dynamics is encoded in Φ , while in the hard-scattering amplitude T_H the hadron is simulated by on-mass-shell (but off-light-cone energy) valence quarks with negligible mass and transverse momentum. To leading order α_s , T_H is the sum of all Born diagrams contributing to the particular process. The transition from the initial to the final state is supposed to go via hard gluon re-scattering which involves a factor $(\alpha_s(Q^2)/Q^2)$, ($Q^2 \equiv q_\perp^2 = -q^2$) after one quark was derailed from the initial to the final direction. To leading order, the contributions of $q\bar{q}$ -irreducible diagrams to the pion form factor amount to the hard-scattering amplitude

$$T(x, y, Q) = \frac{16\pi C_F \alpha_s(Q^2)}{\bar{x}\bar{y}Q^2}, \quad (4)$$

where the abridged notation $\bar{x} = 1 - x$, $\bar{y} = 1 - y$ has been used, $C_F = (N_c^2 - 1)/2N_c = 4/3$ is the Casimir operator of the fundamental representation of $SU(3)_c$, and $\alpha_s(Q^2) = (4\pi/\beta_0 \ln(Q^2/\Lambda_{\text{QCD}}^2))$ is the running coupling constant in the one-loop approximation.

In the nucleon case, there is a total of 14 Born diagrams with different topologies out of which only 8 give non-zero contributions. A complete list of these diagrams is compiled in [31]; the Feynman rules for light-cone perturbation theory are given in [21]. A typical diagram contributing to the nucleon form factor is depicted in Fig. 5. The quark-propagator denominators along the first and the second quark lines are, respectively: $-Q^2\bar{x}_1$ and $-Q^2x_3\bar{y}_1$; those of the gluon propagators which channel the external momentum flow from the struck quark to the spectator quarks are: $-Q^2\bar{x}_1\bar{y}_1$ and $-Q^2x_3y_3$, where all quark masses and k_\perp -momenta have been set equal to zero (collinear approximation). Recall that in the light-

cone frame, parton “i” in a hadron has four-momentum $p_i = x_i P + k_i = (p^+, p^-, p_\perp)$, where $x_i = \frac{p_i^+}{P^+}$ and $k_i = (0, k^-, \mathbf{k}_\perp)$. Momentum conservation implies

$$\sum_{i=1}^n x_i = 1 ; \quad \sum_{i=1}^n \mathbf{k}_{\perp i} = 0 . \quad (5)$$

Quarks are on-mass shell, i.e., $p_i^2 = m_i^2$ but off the light-cone energy:

$$p_i^- = \frac{(\mathbf{p}_{\perp i} + \mathbf{k}_{\perp i})^2 + m_i^2}{2p_i^+} . \quad (6)$$

In a frame where $P = (P^+ = 1, 0, 0_\perp)$ and for massless quarks, this relation simplifies to

$$p_i^- = \frac{\mathbf{k}_{\perp i}^2}{2x_i} . \quad (7)$$

Note that the sum over all p_i^- is not equal P^- . The difference is a boost-invariant measure of how far off energy shell a Fock state is [21,83]. This off-shellness is large in the kinematic endpoint region, i.e., when $\mathbf{k}_{\perp i}^2$ or x_i is small and, as a consequence, the hadron wave function should vanish in these limits. Hence, formally, all wave functions should satisfy the boundary conditions

$$\begin{aligned} \mathbf{k}_{\perp i}^2 \psi_n(x_i, \mathbf{k}_{\perp i}, \lambda_i) &\rightarrow 0 & \text{as} & & \mathbf{k}_{\perp i}^2 &\rightarrow \infty \\ \psi_n(x_i, \mathbf{k}_{\perp i}, \lambda_i) &\rightarrow 0 & \text{as} & & x_i &\rightarrow 0 \end{aligned} \quad (8)$$

if the free-particle Hamiltonian is to have a finite expectation value (λ_i denotes here parton’s “i” helicity). None of these conditions is generally satisfied in the absence of UV ($\mathbf{k}_\perp \rightarrow \infty$) and IR ($x \rightarrow 0$) regulators (for a further discussion of these subtle issues, we refer to [83]).

C. LARGE DISTANCE PART: PERTURBATIVE ASPECTS

1. Renormalization

The function $\Phi(x_i, \tilde{Q})$ is the probability distribution amplitude for finding the hadron to consist of valence quarks each carrying a fraction $0 \leq x_i \leq 1$ of the hadron’s longitudinal momentum P^+ ($P^\pm = (P^0 \pm P^3)/\sqrt{2}$) at transverse separations (relative to the hadron’s P^+ momentum) not smaller than \tilde{Q}^{-1} . We work in the infinite momentum frame, where $\vec{P} = (0, 0, P^3)$ and $P^3 = |\vec{P}| \rightarrow \infty$. In this frame the p^+ component is large and conserved (the same for \vec{p}), and the p^- component is small and not conserved (the same for E). Furthermore, boosts along the $+z$ -direction (“+3”-direction) leave the transverse momenta unchanged. In leading order, $\tilde{Q}_{x(y)}$ can be replaced by Q , which is then the only large scale involved. The small scale of the system, called m in Eq. (1), does not enter the game explicitly (provided it is much smaller than Q); it nevertheless plays a crucial role in the determination of Φ and is the non-perturbative counterpart of the perturbative scale Λ_{QCD} . Physically, the existence of such a scale indicates that gluons with wavelengths larger than

m^{-1} do not “see” individual quarks and decouple. One should eventually be able to relate m with typical non-perturbative scales, like the average quark virtuality in the vacuum [59], mentioned in the Introduction, or the size of instantons [8,60].

Dispensing with the k_{\perp} -dependence in T_H , allows to integrate out this variable in the wave function parts up to the factorization scale μ^2 and replace the (renormalized) wave function by the distribution amplitude

$$\Phi(x_i, \mu^2) \equiv \left(\ln \frac{\mu^2}{\Lambda_{\text{QCD}}^2} \right)^{-c \gamma_F / \beta_0} \int \prod_{i=1}^n [d^2 \mathbf{k}_{\perp i}] \psi(x_i, \mathbf{k}_{\perp i}) \Theta(\mu^2 - |\mathbf{k}_{\perp i}|^2) , \quad (9)$$

where

$$[d^2 \mathbf{k}_{\perp i}] \equiv 16\pi^3 \delta^{(2)} \left(\sum_i^n \mathbf{k}_{\perp i} \right) \prod_j^n \frac{d^2 \mathbf{k}_{\perp j}}{16\pi^3} , \quad (10)$$

and γ_F is the anomalous dimension associated with quark self-energy in the light-cone gauge:

$$\gamma_F = C_F \left(1 + 4 \int_0^1 dx \frac{x}{1-x} \right) . \quad (11)$$

The logarithm in front of the integral in Eq. (9) stems from UV divergences due to gluon radiative corrections in the hard-scattering amplitude. Hence, all vertices and propagators have to be renormalized. However, Z_3^g , the gluon renormalization constant, and Z_1^{qg} , the quark-gluon renormalization constant, can be absorbed (removed) by replacing α_s by its renormalized value $\alpha_s^{\text{ren}} = (Z_2^q/Z_1^{qg})^2 Z_3^g \alpha_s$ so that the only renormalization constant to be determined is Z_2^q which renormalizes the quark propagator (or, by taking its square root, each incoming and outgoing quark line). But Z_2^q can be computed from the gluon radiative corrections to the quark-photon vertex by virtue of the QED Ward identity $Z_1^{q\gamma} = Z_2^q$. It is evident from our factorization prescription that only momenta $\tilde{Q} \lesssim Q$ are included in the wave function, meaning in turn that the virtual photon’s momentum probing it is also limited to \tilde{Q} . Hence, in computing the UV-divergent part of the photon-quark vertex, the photon momentum can be ignored, keeping only gluon loop momenta greater than \tilde{Q} . Then $Z_2^q \rightarrow Z_2^q(\tilde{Q})$ and as \tilde{Q} increases, $Z_2^q(\tilde{Q})$ (i.e., the probability to find a bare quark) decreases. The asymptotic result is

$$Z_2^q = \lim_{\mu^2 \rightarrow \infty} \ln \left(\frac{\mu^2}{\Lambda_{\text{QCD}}^2} \right)^{-c \gamma_F / \beta_0} , \quad (12)$$

where we have used the fact that in leading order $k_{\perp} \ll \tilde{Q}_x = \min\{x_i Q\}$, (or $k_{\perp} \ll \tilde{Q}_x = \min\{\bar{x}_i Q\}$) so that each individual “tilded” wave-function scales can be traded for a common factorization scale μ^2 . This renormalization procedure [83] yields $c = 1$ for mesons (two quark lines) and $c = 3/2$ for baryons (three quark lines).

The gauge-invariant distribution amplitude $\Phi^{(H)}(x_i, \mu^2)$ is intrinsically non-perturbative and – provided *the same factorization scheme is used to cast exclusive amplitudes for different processes in convolution form* [82] – universal. The large-momentum behavior of these functions can be analyzed either using operator product expansion techniques or, equivalently, by evolution equations analogous to DGLAP equations [84,85,86] in deep-inelastic

scattering. Following the second approach, one takes derivatives with respect to Q^2 of Eq. (9) to arrive at evolution equations of the generic form [21]

$$\frac{\partial \Phi^{(\text{H})}(x_i, Q^2)}{\partial \ln Q^2} = \int_0^1 [dy] V(x_i, y_i, \alpha_s(Q^2)) \Phi^{(\text{H})}(x_i, Q^2) \quad (13)$$

with distinct kernels $V(x_i, y_i, \alpha_s(Q^2))$ for each process at hand, which, to leading order in α_s , are computable from the single-gluon-exchange kernel.

To solve the evolution equation, $\Phi^{(\text{H})}$ for hadron H has to be expressed as an orthogonal expansion in terms of appropriate functions which constitute an eigenfunction basis of the particular gluon-exchange kernel, i.e.,

$$\Phi^{(\text{H})}(x_i, Q^2) = \Phi_{\text{as}}^{(\text{H})}(x_i) \sum_{n=0}^{\infty} B_n^{(\text{H})}(\mu^2) \tilde{\Phi}_n^{(\text{H})}(x_i) \exp \left\{ \int_{\mu^2}^{Q^2} \frac{d\bar{\mu}^2}{\bar{\mu}^2} \gamma_{\text{F}}(g(\bar{\mu}^2)) \right\}, \quad (14)$$

where $\Phi_{\text{as}}^{(\text{H})}$ is the renormalization group asymptotic distribution amplitude (see below) being proportional to the weight $w(x_i)$ of the particular orthogonal basis, and $\tilde{\Phi}_n^{(\text{H})}$ denotes the corresponding eigenfunctions. The coefficients $B_n^{(\text{H})}$ of this expansion are associated with matrix elements of composite lowest-twist operators with definite anomalous dimensions (after diagonalization of the evolution kernel) taken between the vacuum and the external hadron. They represent the non-perturbative input (integration constants of the renormalization group equation) in Eq. (14) and have to be determined at some initial scale of evolution μ^2 by non-perturbative techniques. The exponential factor in Eq. (14) takes care of momentum evolution according to the renormalization group and is governed by the quark anomalous dimension

$$\gamma_{\text{F}} = \frac{\mu}{Z_2^{\text{q}}} \frac{\partial Z_2^{\text{q}}}{\partial \alpha_s} \frac{\partial \alpha_s}{\partial \mu} \quad (15)$$

which in the axial gauge is [87]

$$\gamma_q = -\frac{\alpha_s}{\pi} + O(\alpha_{rms}^2). \quad (16)$$

2. Meson evolution equation

The advantage of using an eigenfunctions decomposition is that the evolution equation can be solved by diagonalization. Consider, for example, the meson evolution equation. Using the evolution “time” parameter [85,21]

$$\xi \equiv \frac{\beta_0}{4\pi} \int_{\mu^2}^{Q^2} \frac{dk_{\perp}^2}{k_{\perp}^2} \alpha_s(k_{\perp}^2) = \ln \frac{\alpha_s(\mu^2)}{\alpha_s(Q^2)} = \ln \frac{\ln Q^2 / \Lambda_{\text{QCD}}^2}{\ln \mu^2 / \Lambda_{\text{QCD}}^2}, \quad (17)$$

and the relation

$$\frac{\partial}{\partial Q^2} = \frac{\partial \xi}{\partial Q^2} \frac{\partial}{\partial \xi} = \frac{\beta_0}{4\pi} \frac{\alpha_s(Q^2)}{Q^2} \frac{\partial}{\partial \xi}, \quad (18)$$

the meson evolution equation reads

$$x_1 x_2 \left[\frac{\partial}{\partial \xi} \tilde{\Phi}(x_i, Q^2) + \frac{C_F}{\beta_0} \tilde{\Phi}(x_i, Q^2) \right] = \frac{C_F}{\beta_0} \int_0^1 [dy] V(x_i, y_i) \tilde{\Phi}(x_i, Q^2) , \quad (19)$$

where $\Phi(x_i, Q^2) = x_1 x_2 \tilde{\Phi}(x_i, Q^2)$. Expanding in terms of eigenfunctions Φ_n , or $x_1 x_2 \tilde{\Phi}_n$, one has

$$\frac{\partial}{\partial \xi} \Phi_n(x_i, Q^2) = -\gamma_n \Phi_n(x_i, Q^2) \quad (20)$$

from which one readily obtains

$$\begin{aligned} \Phi_n(x_i, Q^2) &= \Phi_n(x_i, \mu^2) e^{-\gamma_n \xi} \\ &= \Phi_n(x_i, \mu^2) \exp \left[-\gamma_n \ln \frac{\alpha_s(\mu^2)}{\alpha_s(Q^2)} \right] \\ &\simeq x_1 x_2 \tilde{\Phi}_n(x_i, \mu^2) \left(\ln \frac{Q^2}{\Lambda_{\text{QCD}}^2} \right)^{-\gamma_n} . \end{aligned} \quad (21)$$

Then the equation to be solved becomes

$$x_1 x_2 \left(\frac{C_F}{\beta_0} - \gamma_n \right) \tilde{\Phi}_n(x_i) = \frac{C_F}{\beta_0} \int_0^1 [dy] V(x_i, y_i) \tilde{\Phi}_n(y_i) , \quad (22)$$

where $V(x_i, y_i)$ is both real and symmetric, and $\{\tilde{\Phi}_n(x_i)\}$ form a set of orthogonal functions with respect to the weight $w(x_i) = x_1 x_2$:

$$\int_0^1 [dx] w(x_i) \Phi_n(x_i) \Phi_m(x_i) = K_n \delta_{nm} . \quad (23)$$

Within this basis of eigenfunctions, the pion distribution amplitude has a convergent expansion for all Q^2 , viz.:

$$\Phi^{(\pi)}(x_i, Q^2) = w(x_i) \sum_{n=0}^{\infty} B_n^{(\pi)} \left(\ln \frac{Q^2}{\Lambda_{\text{QCD}}^2} \right)^{-\gamma_n} \tilde{\Phi}_n(x_i) \quad (24)$$

with expansion coefficients

$$B_n^{(\pi)} \left(\ln \frac{Q^2}{\Lambda_{\text{QCD}}^2} \right)^{-\gamma_n} = K_n^{-1} \int_0^1 [dx] w(x_i) \tilde{\Phi}_n^{(\pi)}(x_i) \tilde{\Phi}_n^{(\pi)}(x_i, Q^2) . \quad (25)$$

To determine the anomalous dimensions γ_n and the corresponding eigenfunctions, it is convenient to introduce the relative coordinate $-1 \leq \zeta = x_1 - x_2 \leq 1$ and express the kernel V in terms of a matrix U_{jn} via a monomial basis $|\zeta^n\rangle$,

$$V(\zeta) |\zeta^n\rangle = w(\zeta) \sum_{j=0}^n |\zeta^j\rangle U_{jn} , \quad (26)$$

where $w(\zeta) = x_1 x_2 = \frac{1}{4}(1 - \zeta^2)$. The matrix U_{jn} turns out to be triangular [21]:

$$U_{jn} = 0 \quad j > n \quad (27)$$

$$U_{nn} = \frac{2\delta_{h_1\bar{h}_2}}{(n+1)(n+2)} - 4 \sum_{k=2}^{n+1} \frac{1}{k} \quad j = n \quad (28)$$

$$U_{jn} = \frac{1 + (-1)^{n-j}}{2} \left[\frac{2\delta_{h_1\bar{h}_2}}{(n+1)(n+2)} + \frac{4(j+1)}{(n-j)(n+1)} \right] \quad j < n. \quad (29)$$

Hence, the eigenvalues are just U_{nn} and the eigenfunctions are polynomials of finite order. The only polynomials in the interval $[-1, 1]$ orthogonal with respect to $w(\zeta) = \frac{1}{4}(1 - \zeta^2)$ are the Gegenbauer polynomials⁷ $C_n^{3/2}(\zeta)$ (see, e.g., [91]), normalized by

$$\int_{-1}^1 d\zeta w(\zeta) C_n^{3/2}(\zeta) C_m^{3/2}(\zeta) = K_n \delta_{nm}, \quad (30)$$

where

$$K_n = \frac{(2+n)(1+n)}{2(2n+3)}. \quad (31)$$

Then, on account of

$$\frac{C_F}{\beta_0} - \gamma_n = \frac{C_F}{\beta_0} U_{nn}, \quad (32)$$

the associated anomalous dimensions become

$$\gamma_n = \frac{C_F}{\beta_0} \left[1 + 4 \sum_{k=2}^{n+1} \frac{1}{k} - \frac{2\delta_{h_1\bar{h}_2}}{(n+1)(n+2)} \right] \geq 0 \quad (n \text{ even}), \quad (33)$$

where, for the pion, $\delta_{h_1\bar{h}_2} = 1$ (see Fig. 6). The corresponding eigenfunctions are $(\tilde{\Phi}_n^{(\pi)}(x_i) = C_n^{3/2}(x_i) = C_n^{3/2}(x_1 - x_2))$ so that

$$\Phi_n^{(\pi)}(x_i, Q^2) = x_1 x_2 C_n^{3/2}(x_1 - x_2) \left(\ln \frac{Q^2}{\Lambda_{\text{QCD}}^2} \right)^{-\gamma_n} \quad (34)$$

with coefficients going like (cf. Eq. (25))

$$\begin{aligned} B_n^{(\pi)} \left(\ln \frac{Q^2}{\Lambda_{\text{QCD}}^2} \right)^{-\gamma_n} &= \frac{2(2n+3)}{(2+n)(1+n)} \int_{-1}^1 d\zeta C_n^{3/2}(\zeta) \Phi^{(\pi)}(\zeta, Q^2), \\ &= \frac{\sqrt{2}(2n+3)}{(2+n)(1+n)} \frac{1}{\sqrt{N_c}} \langle 0 | \bar{\psi}(0) \gamma^+ \gamma_5 C_n^{3/2} \left(i \overleftrightarrow{D}^+ \right) \psi(0) | \pi \rangle_{(Q^2)}, \end{aligned} \quad (35)$$

⁷The Gegenbauer polynomials correspond to the conformally invariant operator product expansion for two spin- $\frac{1}{2}$ operators [23,88,89,90].

where in the last step we switched from the relative variable ζ back to x , and the matrix element of the local operator is evaluated with UV cutoff Q^2 . Here $\vec{D}_\mu = \vec{D} - \overleftarrow{D}$ with $\vec{D} = \partial_\mu - ig \sum_{i=1}^8 t^i A_\mu^i$ and $\overleftarrow{D} = \partial_\mu + ig \sum_{i=1}^8 t^i A_\mu^i$, and $D^+ = \partial^+$ in the light-cone gauge. From this equation one sees that the expansion coefficients $B_n^{(\pi)}$ are matrix elements of local operators and decrease like $1/n^2$, provided $\Phi^{(\pi)}(x_i, Q^2) \leq K x_i^\epsilon$ as $x_i \rightarrow 0$ for some $\epsilon > 0$ [21]. Thus to leading order the pion distribution amplitude becomes ($P_\pi^+ = 1$)

$$\begin{aligned} \Phi^{(\pi)}(x_i, Q^2) = & x(1-x) \sum_{n=0}^{\infty} \frac{\sqrt{2}(2n+3)}{(2+n)(1+n)} \frac{1}{\sqrt{N_c}} C_n^{3/2}(2x-1) \\ & \times \langle 0 | \bar{\psi}(0) \gamma^+ \gamma_5 C_n^{3/2} \left(i \vec{D}^+ \right) \psi(0) | \pi \rangle_{(Q^2)} . \end{aligned} \quad (36)$$

For asymptotic values of Q^2 only the leading logarithm in Eq. (35) with the least anomalous dimension $\gamma_0 = 0$ survives ($C_0^{3/2} = 1$), so that

$$\Phi^{(\pi)}(x_i, Q^2) \rightarrow \frac{3}{\sqrt{N_c}} f_\pi x(1-x) , \quad (37)$$

where $f_\pi = 93$ MeV is the pion weak decay constant. From this, one infers the normalization condition (sum rule)

$$\int_0^1 [dx] \Phi^{(\pi)}(x_i, Q^2) = \frac{f_\pi}{2\sqrt{N_c}} , \quad (38)$$

which, given the shape of $\Phi^{(\pi)}(x_i, Q^2)$, normalizes it for every value of Q^2 .

The above treatment can be readily used to provide information on the asymptotic behavior of the pion form factor as well. The electromagnetic pion form factor in the space-like region is defined by

$$\langle \pi^\pm(P') | J_\mu^{\text{em}}(0) | \pi^\pm(P) \rangle = (P' + P)_\mu F_\pi(Q^2) , \quad (39)$$

where $J_\mu^{\text{em}} = \sum_f e_f \bar{q}_f \gamma_\mu q_f$ is the electromagnetic current, and the index f denotes different flavors. To relate the pion form factor to the Fock state wave functions, discussed above, the $\mu = +$ component of this equation is taken.

With the spectrum of eigenfunctions and corresponding anomalous dimensions in hand, we can write Eq. (2) in the form (n even because of C -parity)

$$F_\pi(Q^2) = \frac{16\pi C_F \alpha_s(Q^2)}{Q^2} e_1 \left| \sum_n^\infty B_n^{(\pi)} \left(\ln \frac{Q^2}{\Lambda_{\text{QCD}}^2} \right)^{-\gamma_n} \int_0^1 dx_1 x_1 C_n^{3/2}(x_1 - x_2) \right|^2 + (1 \leftrightarrow 2) . \quad (40)$$

Recalling that for π^+ the charges of the struck quarks sum to one, and that for even Gegenbauer polynomials, $\int_0^1 dx_1 x_1 C_n^{3/2}(x_1 - x_2) = \frac{1}{2} \int_0^1 dx_1 (x_1 + x_2) C_n^{3/2}(x_1 - x_2) = \frac{1}{2}$, the pion form factor becomes (n even)

$$F_\pi(Q^2) = \frac{4\pi C_F \alpha_s(Q^2)}{Q^2} \left| \sum_n^\infty B_n^{(\pi)} \left(\ln \frac{Q^2}{\Lambda_{\text{QCD}}^2} \right)^{-\gamma_n} \right|^2 . \quad (41)$$

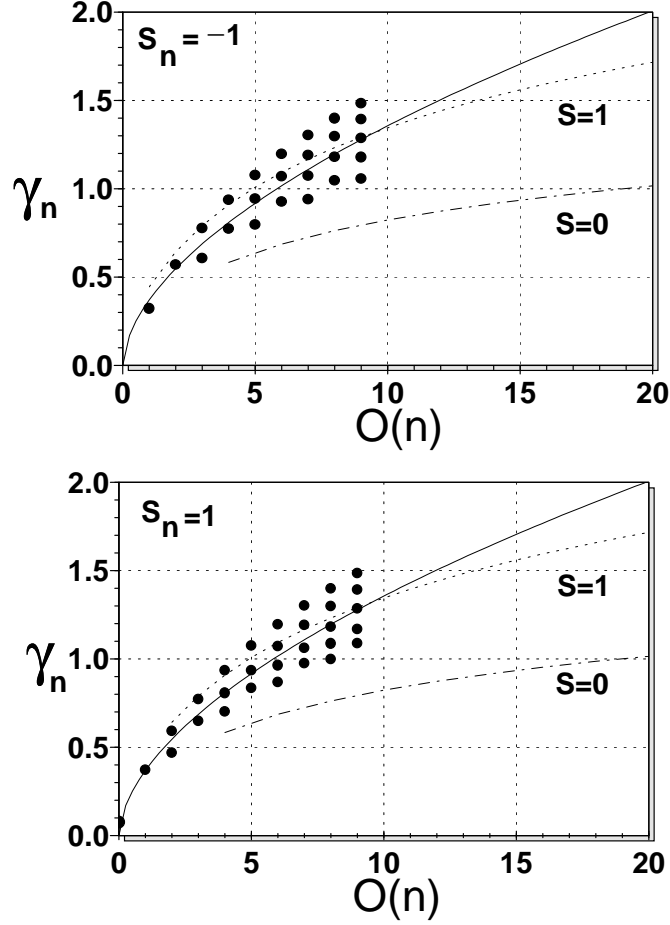


Figure 6. Anomalous dimensions of three-quark operators up to polynomial order $M = 9$ in comparison with those of two-quark (meson-like) operators. Curves are shown for antisymmetric ($S_n = -1$) and symmetric ($S_n = 1$) eigenfunctions of the diagonalized nucleon evolution equation. The solid line is an empirical fit which is compatible with power-law behavior.

In the limit of asymptotic values of momentum transfer, only the zeroth order term $C_0^{3/2} = 1$ contributes with anomalous dimension $\gamma_0 = 0$, so that

$$\lim_{Q^2 \rightarrow \infty} F_\pi(Q^2) = \frac{4\pi C_F \alpha_s(Q^2)}{Q^2} [B_0^{(\pi)}]^2. \quad (42)$$

This result can be couched in the final form [92]

$$\lim_{Q^2 \rightarrow \infty} F_\pi(Q^2) = \frac{16\pi f_\pi^2 \alpha_s(Q^2)}{Q^2} \quad (43)$$

by virtue of the decay process $\pi^+ \rightarrow l^+ \nu_l$, ($l = \mu^+, e^+$) which fixes $B_0^{(\pi)} = \frac{3f_\pi}{\sqrt{N_c}}$ in terms of the pion decay constant f_π , independent of the momentum variance. Unfortunately, the asymptotic prediction is not supported by the existing data [32]. Indeed, evaluating the above expression, say, at $Q^2 = 6 \text{ GeV}^2$ for $\Lambda_{\text{QCD}} = 0.2 \text{ GeV}$, one finds $Q^2 F_\pi(Q^2) = 0.12$ which is about a factor of three below the experimental value (and well below the error bars). The conclusion is that additional contributions of Gegenbauer terms in the expansion of the pion distribution amplitude have to be included, or that one has to take into account higher twist contributions (power corrections). In order to increase the value of the pion form factor at moderate Q^2 -values, a broader pion distribution amplitude, relative to $x_1 x_2 = \frac{1}{4}(1 - x^2)$, is needed with at least $B_2^{(\pi)}/B_0^{(\pi)} > 0$. This goal can be achieved using QCD sum rules [29,56,93]. The literature on this subject is vast and the selection of references [94,95,96,97,98,99,100] is by no means complete. We apologize to those authors whose works have not been included.

3. Nucleon evolution equation

Let us now turn to the nucleon case. The evolution equation is

$$x_1 x_2 x_3 \left[\frac{\partial}{\partial \xi} \tilde{\Phi}(x_i, Q^2) + \frac{3}{2} \frac{C_F}{\beta_0} \tilde{\Phi}(x_i, Q^2) \right] = \frac{C_F}{\beta_0} \int_0^1 [dy] V(x_i, y_i) \tilde{\Phi}(y_i, Q^2), \quad (44)$$

where $\Phi = x_1 x_2 x_3 \tilde{\Phi}$, C_F is defined below Eq. (4), and

$$V(x_i, y_i) = 2x_1 x_2 x_3 \sum_{i \neq j} \Theta(y_i - x_i) \delta(y_k - x_k) \frac{y_j}{x_j} \left[\frac{\delta_{h_i \bar{h}_j}}{x_i + x_j} + \frac{\Delta}{y_i - x_i} \right]. \quad (45)$$

Note that $V(x_i, y_i) = V(y_i, x_i)$ is the sum over single-gluon interactions between quark pairs $\{i, j\}$, and the subtraction prescription $\Delta \tilde{\Phi}(y_i, Q^2) \equiv \tilde{\Phi}(y_i, Q^2) - \tilde{\Phi}(x_i, Q^2)$ ensures IR finiteness at $x_i = y_i$, i.e., $V(x_i, y_i)$ is not a function but a distribution. For antiparallel spins $\delta_{h_i \bar{h}_j} = 1$ and for parallel spins it equals 0. Note also that if no gluon is exchanged, each x_k in the initial and final wave function is the same because no longitudinal momentum is introduced by q^μ ($q^+ = 0$).

We propose to solve the evolution equation by employing factorization of the dependence on longitudinal momentum from that on the external (large) momentum scale Q^2 (cf. Eq. (14)). The latter is renormalization group controlled according to

$$\frac{\partial}{\partial \xi} \tilde{\Phi}_n(x_i, Q^2) = -\gamma_n \tilde{\Phi}_n(x_i, Q^2) \quad (46)$$

with solutions

$$\tilde{\Phi}_n(x_i, Q^2) \simeq \tilde{\Phi}_n(x_i) \left(\ln \frac{Q^2}{\Lambda_{\text{QCD}}^2} \right)^{-\gamma_n}. \quad (47)$$

This allows us to write the full nucleon distribution amplitude in the form

$$\Phi(x_i, Q^2) \sim x_1 x_2 x_3 \sum_{n=0}^{\infty} B_n \tilde{\Phi}_n(x_i) \left(\ln \frac{Q^2}{\Lambda_{\text{QCD}}^2} \right)^{-\gamma_n}, \quad (48)$$

where $\tilde{\Phi}_n(x_i)$ are appropriate but not tabulated polynomials, and the expansion coefficients B_n encode the non-perturbative input of the bound-states dynamics at the factorization (renormalization) scale. Their determination will concern us in the next section.

From the factorized form of $\tilde{\Phi}_n(x_i, Q^2)$ in Eq. (47), it follows that the evolution equation for the x -dependence reduces to the characteristic equation

$$x_1 x_2 x_3 \left[\frac{3}{2} \frac{C_F}{\beta_0} - \gamma_n \right] \tilde{\Phi}(x_i) = \frac{C_B}{\beta_0} \int_0^1 [dy] \frac{V(x_i, y_i)}{w(x_i)} \tilde{\Phi}(y_i), \quad (49)$$

where $w(x_i) = x_1 x_2 x_3 = x_1(1 - x_1 - x_3)x_3$ is the weight function of the orthogonal basis and $C_B = (N_c + 1)/2N_c = 2/3$ the Casimir operator of the adjoint representation of $SU(3)_c$. To proceed, it is convenient to conceive of the kernel $V(x_i, y_i)$ as being an operator expanded over the polynomial basis [21] $|x_1^k x_3^l\rangle \equiv |k l\rangle$, (recall that because of momentum conservation, only two out of three x_i variables are linearly independent) i.e., to write

$$\hat{V} \equiv \int_0^1 [dy] V(x_i, y_i) \quad (50)$$

and convert Eq. (49) into the algebraic equation

$$\left[\frac{3}{2} \frac{C_F}{\beta_0} - 2 \frac{C_B}{\beta_0} \frac{\hat{V}}{2w(x_i)} \right] \tilde{\Phi}_n(x_i) = \gamma_n \tilde{\Phi}_n(x_i). \quad (51)$$

In this way, the action of the operator \hat{V} can be completely determined by a matrix, namely:

$$\frac{\hat{V} |k l\rangle}{2w(x_i)} = \frac{1}{2} \sum_{i,j}^{i+j \leq M} |i j\rangle U_{ij,kl}. \quad (52)$$

The corresponding eigenvalues are then determined by the roots η_n of the characteristic polynomial that diagonalizes the matrix U :

$$\hat{V} \tilde{\Phi}_n(x_i) = -\eta_n w(x_i) \tilde{\Phi}_n(x_i), \quad (53)$$

so that the anomalous dimensions for order M are given by

$$\gamma_n(M) = \frac{1}{\beta_0} \left(\frac{3}{2} C_F + 2\eta_n(M) C_B \right), \quad (54)$$

where the orthogonalization prescription

$$\int_0^1 [dx] w(x_i) \tilde{\Phi}_m(x_i) \tilde{\Phi}_n(x_i) = \frac{1}{N_m} \delta_{mn} \quad (55)$$

has been employed with N_m being appropriate normalization constants (see, Table 1).

The explicit form of the matrix U was derived by Lepage and Brodsky [21] and is reproduced in Appendix A. Within the basis $|k l\rangle$, the matrix U can be diagonalized to provide eigenfunctions, which are polynomials of degree $M = k + l = 0, 1, 2, 3 \dots$, with $M + 1$ eigenfunctions for each M . This was done in [21] by diagonalizing the $(M + 1) \times (M + 1)$ matrix $U_{ij,kl}$ with $i + j = k + l = M$ and results up to $M = 2$ were obtained. In our approach, reported in several meetings [49,101,102] and worked out in [103,104], we make use of another method that is based on symmetrized Appell polynomials [91].

Appell polynomials are special hypergeometric functions (see Appendix A) of the form

$$\mathcal{F}_{mn}^{(M)}(5, 2, 2; x_1, x_3) \equiv \mathcal{F}_{mn}(x_1, x_3) , \quad (56)$$

which constitute an orthogonal polynomial set on the triangle $T = T(x_1, x_3)$ with $x_1 > 0$, $x_3 > 0$, $x_1 + x_3 < 1$. They provide a suitable basis for solving the eigenvalue equations for the nucleon because within this basis \hat{V} is block diagonal for different polynomial orders. Moreover, introducing a “symmetrized” basis of such polynomials according to [103]

$$\begin{aligned} \tilde{\mathcal{F}}_{mn}(x_1, x_3) &= \frac{1}{2} [\mathcal{F}_{mn}(x_1, x_3) \pm \mathcal{F}_{nm}(x_1, x_3)] \\ &= \sum_{k,l=0}^{k+l \leq m+n} Z_{kl}^{mn} |k l\rangle \end{aligned} \quad (57)$$

(where $+$ refers to $m \geq n$ and $-$ to $m < n$), \hat{V} commutes with the permutation operator $P_{13} = [321]$ and thus becomes block diagonal within each sector of (definite) permutation-symmetry class of eigenfunctions for fixed order M . As a result, the kernel \hat{V} can be analytically diagonalized up to order seven. This is related to the fact that the characteristic polynomial of matrices with rank four can be solved analytically. Beyond that order, its roots have to be determined numerically. We present here results up to order $M = 4$. Still higher-order eigenfunctions (up to $M = 9$) were obtained by Bergmann [104]. The differential equation defining the symmetrized Appell polynomials is given in Appendix A.

To appreciate the usefulness of this type of approach, some historical remarks ought to be made before we proceed. The solution of the eigenvalue equations for the nucleon beyond leading order is a long-standing problem. As already mentioned, results up to order two were obtained by Lepage and Brodsky [21]. The anomalous dimensions they computed were subsequently confirmed by Peskin [105] who considered composite three-quark operators containing derivatives and having baryon quantum numbers. Such operators interpolate between the nucleon (or the Δ resonance) and the vacuum at leading twist-three. Their anomalous dimension was extracted from the divergent parts of their matrix elements by diagonalizing the renormalization matrix of these operators (see in this context also [106]). Then Tesima [107] analyzed the light-cone behavior of the Bethe-Salpeter wave functions of three-quark bound states with the use of the operator product expansion in terms of a conformally invariant operator basis. He presented results for twist-three operators up to

Table 1. Orthogonal eigenfunctions $\tilde{\Phi}_n(x_i) = \sum_{kl} a_{kl}^n x_1^k x_3^l$ of the nucleon evolution equation up to polynomial order $M = 4$ in terms of the coefficient matrix a_{kl}^n ($a_{kl}^n = S_n a_{lk}^n$ – no summation over n implied) and the corresponding anomalous dimensions γ_n defined in the text. The numerical results for $n \geq 12$ have been obtained with a much higher numerical accuracy than shown in this table.

n	M	S_n	γ_n	η_n	N_n	a_{00}^n
0	0	1	$\frac{2}{27}$	-1	120	1
1	1	-1	$\frac{26}{810}$	$\frac{2}{3}$	1260	0
2	1	1	$\frac{2}{27}$	1	420	-2
3	2	1	$\frac{38}{81}$	$\frac{5}{3}$	756	2
4	2	-1	$\frac{46}{81}$	$\frac{7}{3}$	34020	0
5	2	1	$\frac{81}{27}$	$\frac{2}{3}$	1944	2
6	3	1	$\frac{115-\sqrt{97}}{162}$	$\frac{-(-79+\sqrt{97})}{24}$	$\frac{4620(485+11\sqrt{97})}{97}$	1
7	3	1	$\frac{115+\sqrt{97}}{162}$	$\frac{79+\sqrt{97}}{24}$	$\frac{4620(485-11\sqrt{97})}{97}$	1
8	3	-1	$\frac{559-\sqrt{4801}}{810}$	$\frac{-(-379+\sqrt{4801})}{120}$	$\frac{27720(33607-247\sqrt{4801})}{4801}$	0
9	3	-1	$\frac{559+\sqrt{4801}}{810}$	$\frac{379+\sqrt{4801}}{120}$	$\frac{27720(33607+247\sqrt{4801})}{4801}$	0
10	4	-1	$\frac{346-\sqrt{1081}}{405}$	$\frac{-(-256+\sqrt{1081})}{60}$	$\frac{196560(7567-13\sqrt{1081})}{1081}$	0
11	4	-1	$\frac{346+\sqrt{1081}}{405}$	$\frac{256+\sqrt{1081}}{60}$	$\frac{196560(7567+13\sqrt{1081})}{1081}$	0
12	4	1	0.70204	3.23876	1	153.37061
13	4	1	0.80651	3.94397	1	332.500864
14	4	1	0.93589	4.81727	1	-137.11538

n	a_{10}^n	a_{20}^n	a_{11}^n	a_{30}^n	a_{21}^n	a_{40}^n	a_{31}^n	a_{22}^n
0	0	0	0	0	0	0	0	0
1	1	0	0	0	0	0	0	0
2	3	0	0	0	0	0	0	0
3	-7	8	4	0	0	0	0	0
4	1	$-\frac{4}{3}$	0	0	0	0	0	0
5	-7	$\frac{14}{3}$	14	0	0	0	0	0
6	-6	$\frac{41+\sqrt{97}}{4}$	$\frac{3(31-\sqrt{97})}{4}$	$\frac{-5(17+\sqrt{97})}{16}$	$\frac{-5(31-\sqrt{97})}{8}$	0	0	0
7	-6	$\frac{41-\sqrt{97}}{4}$	$\frac{3(31+\sqrt{97})}{4}$	$\frac{-5(17-\sqrt{97})}{16}$	$\frac{-5(31+\sqrt{97})}{8}$	0	0	0
8	1	-3	0	$\frac{601+\sqrt{4801}}{264}$	$\frac{59-\sqrt{4801}}{44}$	0	0	0
9	1	-3	0	$\frac{601-\sqrt{4801}}{264}$	$\frac{59+\sqrt{4801}}{44}$	0	0	0
10	1	-5	0	$\frac{379+\sqrt{1081}}{48}$	$\frac{61-\sqrt{1081}}{8}$	$\frac{-(159+\sqrt{1081})}{40}$	$\frac{-(61-\sqrt{1081})}{8}$	0
11	1	-5	0	$\frac{379-\sqrt{1081}}{48}$	$\frac{61+\sqrt{1081}}{8}$	$\frac{-(159-\sqrt{1081})}{40}$	$\frac{-(61+\sqrt{1081})}{8}$	0
12	-1380.33552	5232.86956	5006.42414	-8063.85349	-9178.44426	4345.63139	4926.80699	8503.27454
13	-2992.50778	9240.51876	17166.06044	-11695.76593	-31471.11081	5068.49438	19489.65169	23962.91822
14	1234.03849	-1843.05428	-12981.41464	-587.61051	23799.26017	1382.85660	-10302.90296	-26992.71442

order two which in general coincide with Peskin's results and also with those obtained by Lepage and Brodsky. In addition, he obtained results for higher orders, but published only the eigenvalues and eigenfunctions corresponding to order three. However, his higher-order results are not supported by our calculation. Moreover, it was shown by Ohrndorf [108] that collinear conformal covariance alone does not suffice to fix trilinear quark operators with derivatives uniquely.

We shall now give a brief description of our approach and present the main results. All nucleon eigenfunctions can be represented as linear combinations of (symmetrized) Appell polynomials of the same order M :

$$\tilde{\Phi}_k(x_i) = \sum_{m,n=0}^{m+n=M} c_{mn}^k \mathcal{F}_{mn}(5, 2, 2; x_1, x_3) \quad (58)$$

since Appell polynomials of the same order are not orthogonal to each other. For instance, for $M = 1$, one finds

$$\begin{aligned} \tilde{\Phi}_1(x_i) &= \mathcal{F}_{01}^{(1)}(5, 2, 2; x_1, x_3) - \mathcal{F}_{10}^{(1)}(5, 2, 2; x_1, x_3) \\ &= x_1 - x_3 \end{aligned} \quad (59)$$

and

$$\begin{aligned} \tilde{\Phi}_2(x_i) &= \mathcal{F}_{10}^{(1)}(5, 2, 2; x_1, x_3) + \mathcal{F}_{01}^{(1)}(5, 2, 2; x_1, x_3) \\ &= -2 + 3(x_1 + x_3) , \end{aligned} \quad (60)$$

where the notations and conventions of [35] are adopted.⁸ Before diagonalizing, it is convenient to rearrange $\tilde{\mathcal{F}}_{mn}$, which belongs to a definite symmetry class $S_n = \pm 1$ within order M , in the form of an (arbitrary) vector:

$$\tilde{\mathcal{F}}_{mn}(x_1, x_3) \mapsto \tilde{\mathcal{F}}_q(x_1, x_3) . \quad (61)$$

Then Hilbert-Schmidt orthogonalization yields a basis

$$|\tilde{\mathcal{F}}'_q\rangle = \sum_{k,l} Z_{kl}^q |k\ l\rangle \quad (62)$$

with

$$\int_0^1 [dx] w(x_i) \tilde{\mathcal{F}}'_q \tilde{\mathcal{F}}'_{q'} \propto \delta_{qq'} , \quad (63)$$

so that

$$\frac{\hat{V}|\tilde{\mathcal{F}}'_q\rangle}{2w(x_i)} = \frac{1}{2} \sum_{i,j,k,l} Z_{kl}^q U_{ij,kl} |i\ j\rangle . \quad (64)$$

⁸In particular, the coefficient B_2 has the opposite sign relative to [21].

Note that the construction of polynomials depending on two variables via the Hilbert-Schmidt method has no unique solution, but depends on the order in which the orthogonalization is performed. Since beyond order $M = 3$ neither the eigenvalues nor the normalization factors are rational numbers, one has to find which representation is more convenient for calculations.

The last step in determining the eigenfunctions and eigenvalues of \hat{V} is to define the matrix

$$\mathcal{M}_{q'q} = \int_0^1 [dx] w(x_1, (1 - x_1 - x_3), x_3) \tilde{\mathcal{F}}_{q'}'(x_1, x_3) \hat{V}(x_1, x_3) \tilde{\mathcal{F}}_q'(x_1, x_3) \quad (65)$$

and calculate the roots of the characteristic polynomial

$$\mathcal{P}(\eta) = \det [\mathcal{M}_{q'q} - \eta I_{q'q}] . \quad (66)$$

Consequently, in terms of the eigenvectors $\mathbf{m}_q = (m_q^1, \dots, m_q^{q'})$ of $\mathcal{M}_{q'q}$, the eigenfunctions of the evolution equation are given by

$$\begin{aligned} \tilde{\Phi}_q(x_1, x_3) &\propto \sum_{q'} m_q^{q'} \tilde{\mathcal{F}}_{q'}'(x_1, x_3) \\ &= \sum_{k,l} a_{kl}^q |k\ l\rangle . \end{aligned} \quad (67)$$

For every order M , there are $M + 1$ eigenfunctions of the same order with an excess of symmetric terms by one for even orders. The total number of eigenfunctions up to order M is $n_{\max}(M) = \frac{1}{2}(M + 1)(M + 2)$ and the corresponding $(M + 1)$ eigenvalues are obtained by diagonalizing the $(M + 1) \times (M + 1)$ matrix. A compendium of the results up to order $M = 4$, meaning a total of 15 eigenfunctions and associated anomalous dimensions, is given in Table 1. The precision of orthogonality is at least 10^{-8} . To get acquaintance with the use of Table 1, we write out explicitly one of the eigenfunctions contributing to order $M = 3$:

$$\begin{aligned} \tilde{\Phi}_9 &= a_{00}^9 + a_{10}^9 (x_1 - x_3) + a_{11}^9 x_1 x_3 + a_{20}^9 (x_1^2 - x_3^2) + a_{21}^9 x_1 x_3 (x_1 - x_3) + a_{30}^9 (x_1^3 - x_3^3) \\ &= (x_1 - x_3) - 3 (x_1^2 - x_3^2) + \frac{59 + \sqrt{4801}}{44} x_1 x_3 (x_1 - x_3) + \frac{601 - \sqrt{4801}}{264} (x_1^3 - x_3^3) . \end{aligned} \quad (68)$$

It turns out that the eigenfunctions $\{\tilde{\Phi}_k\}$ of the nucleon evolution equation satisfy a commutative algebra subject to the triangular condition $|\mathcal{O}(k) - \mathcal{O}(l)| \leq \mathcal{O}(m) \leq \mathcal{O}(k) + \mathcal{O}(l)$:

$$\tilde{\Phi}_k(x_i) \tilde{\Phi}_l(x_i) = \sum_{m=0}^{\infty} F_{kl}^m \tilde{\Phi}_m(x_i) \quad (69)$$

with structure coefficients F_{kl}^m given by

$$F_{kl}^m = N_m \int_0^1 [dx] x_1 x_3 (1 - x_1 - x_3) \tilde{\Phi}_m(x_i) \tilde{\Phi}_k(x_i) \tilde{\Phi}_l(x_i) , \quad (70)$$

$\mathcal{O}(k)$ being defined by

$$\mathcal{O}(k) = \begin{cases} 0 & k = 0 \\ 1 & 1 \leq k \leq 2 \\ 2 & 3 \leq k \leq 5 \\ 3 & 6 \leq k \leq 9 \\ 4 & k = 10, 11 \\ \vdots & \dots \end{cases} \quad (71)$$

The structure coefficients are symmetric, i.e., $F_{kl}^m = F_{lk}^m$. Furthermore, $F_{kk}^0 = \frac{N_0}{N_k}$. The utility of this algebra derives from the fact that once the structure coefficients have been computed, they can be used to express any function $f(x_1, x_3)$ in terms of the nucleon eigenfunctions. For example, one can calculate the Husini function

$$h \sim \int_0^1 [dx] \left| \tilde{\Phi}_m(x_i) \Phi^{(N)}(x_i) \right|^2 \quad (72)$$

which gives the probability for finding $\Phi^{(N)}$ in a particular solution $\tilde{\Phi}_m$. The values of F_{lk}^m up to $\mathcal{O}(k) = 11$ are tabulated in [104].

The obtained results for the exponents (anomalous dimensions) governing the scaling behavior of the nucleon distribution amplitude (cf. Eqs. (47), (48)) are shown in a series of four figures associated with successively increasing order M .⁹ As outlined above, the eigenfunctions correspond to trilinear quark operators with definite anomalous dimension. Such operators can be renormalized in a multiplicative way. But as the order M increases, so increases also the number of derivatives in these operators entailing a strong amount of mixing owing to the fact that they carry the same quantum numbers. As a consequence, the anomalous dimensions are degenerate within fixed symmetry classes and hence a “multiplet” structure emerges. Because all γ_n are positive fractional numbers increasing with n (i.e., order M), higher terms in the eigenfunctions decomposition are gradually suppressed. Fig. 6 displays the anomalous dimensions γ_n up to order $M = 9$, distinguishing between symmetric and antisymmetric eigenfunctions. The trend line of this pattern seems to follow the empirical law (solid line) $\gamma_n = 0.37\mathcal{O}(n)^{0.565}$. The illustration of the spectrum up to order 20 is displayed in Fig. 7.

The next two figures, Fig. 8 and Fig. 9, address the large-order behavior of the anomalous dimensions. Also here, both symmetry classes under the permutation P_{13} are shown in unison: open circles for values belonging to $S_n = 1$ and black dots for those belonging to $S_n = -1$. As the order of eigenfunctions increases, a different picture for the large-order behavior of the spectrum of anomalous dimensions develops, namely, one of logarithmic increase. Indeed, in the limit of very high polynomial orders, symmetric eigenfunctions tend to degenerate with their antisymmetric partners as one observes from Figs. 7 and 8, where, with increasing order, the dots tend to enter the centers of the circles. At the same time, the eigenvalues γ_n increase logarithmically. Hence, to order 20, the spectrum of anomalous dimensions as a whole is better described by a logarithmic fit (solid line) of the form $\gamma_n = 1.25[\log_{10}(\mathcal{O}(n) + 1.37)]^{1.32}$. The dotted curve shows the power-law fit $\gamma_n = 0.52\mathcal{O}(n)^{0.417}$ which is no more supported by the higher-order values. A more accurate prediction for the

⁹This part was done in collaboration with Michael Bergmann.

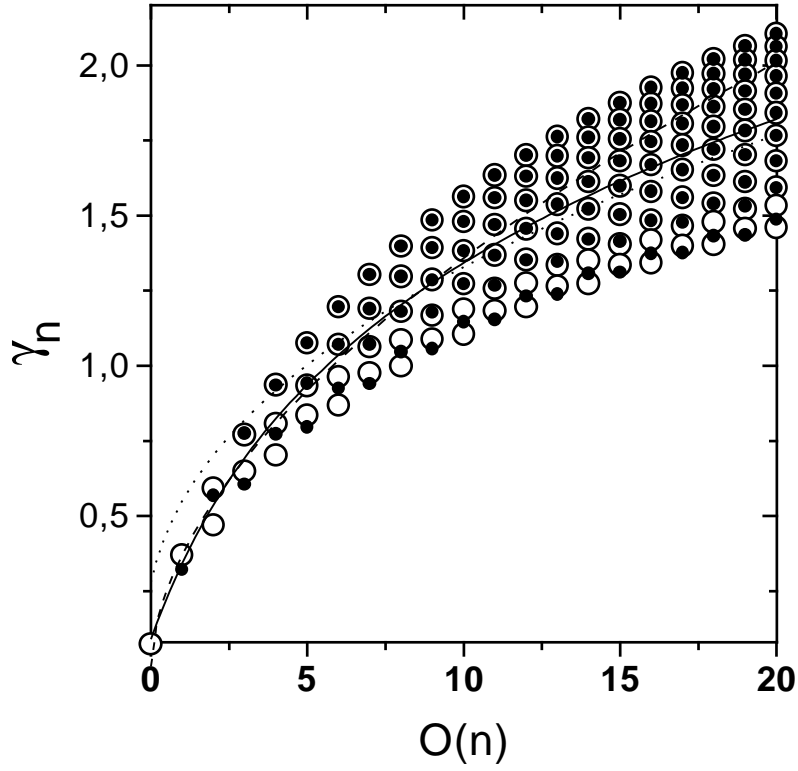


Figure 7. Pattern of anomalous dimensions of three-quark operators up to $M = 20$. Values associated with symmetric eigenfunctions are denoted by open circles. Those corresponding to antisymmetric eigenfunctions are marked by black dots.

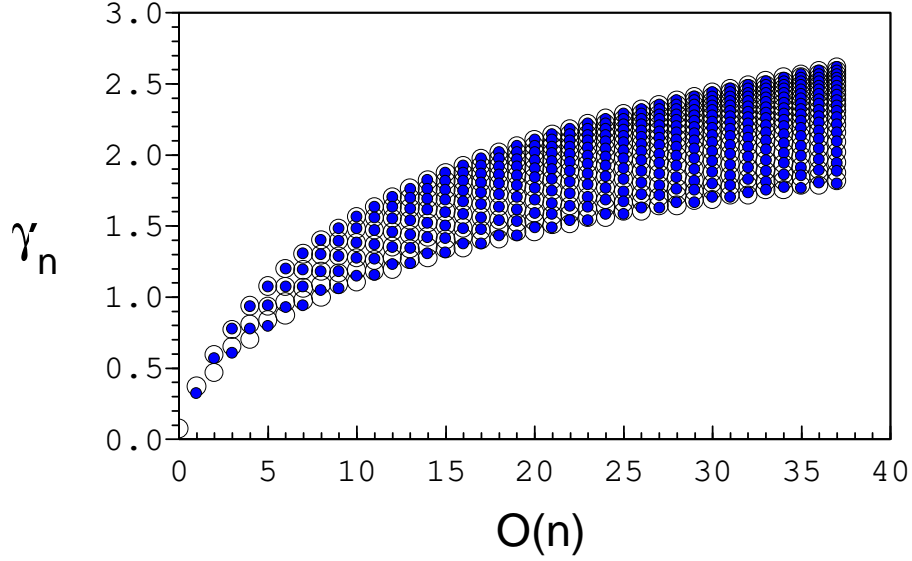


Figure 8. Pattern of anomalous dimensions of three-quark operators up to $M = 37$. Values associated with symmetric eigenfunctions are denoted by open circles. Those associated with antisymmetric eigenfunctions are marked by black dots. The solid line is an empirical fit already compatible with logarithmic behavior.

asymptotic behavior of γ_n is provided by Fig. 9 where the upper envelope of the spectrum is well-described by $\gamma_n = [\log_{10}(2.13\mathcal{O}(n) + 1.4)]^{1.48}$. These findings, presented here for the first time, confirm expectations based on exponentiation assumptions of leading-loop contributions [62,109,110,111]. Physically, the logarithmic rise is due to enhanced emission of soft gluons, reflecting the fact that the probability for finding bare quarks decreases. However, in order to establish this trend, still higher orders have to be computed, at least up to $M = 10^3$ (three points on a logarithmic plot).

D. LARGE DISTANCE PART: NON-PERTURBATIVE ASPECTS

Given the eigenfunctions and associated anomalous dimensions of the nucleon evolution equation, the only unknown quantities entering the description of the nucleon distribution amplitude are the expansion coefficients B_n , i.e., the set of matrix elements of tri-local operators interpolating between the one-nucleon state and the vacuum. The QCD sum rules method is presently the best approach for extracting these quantities, albeit there are conceptual limitations. We do not discuss the pion here since it has been studied extensively elsewhere [17,31,94,112].

Specifically, we consider the following gauge-invariant proton wave function

$$\langle 0 | [C(z_1, z_3 | A) u_\alpha(z_1)]^a [C(z_2, z_3 | A) u_\beta(z_2)]^b d_\gamma^c(z_3) | P \rangle \frac{1}{\sqrt{N_c!}} \epsilon^{abc}, \quad (73)$$

where a, b, c and α, β, γ are color and spinor labels, respectively, $A_\mu(x) = \sum_{i=1}^8 A_\mu^i(x) t^i$ are the Lie-algebra valued gluon fields (t^i being the generators of $SU(3)_c$). The operator

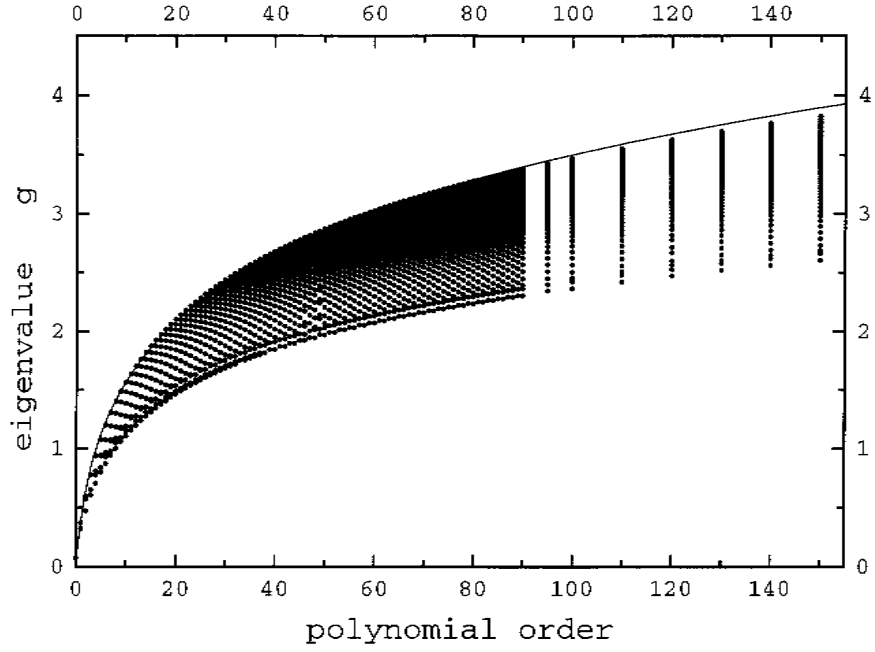


Figure 9. Pattern of anomalous dimensions of three-quark operators up to $M = 150$. For technical reasons, antisymmetric eigenfunctions are included only up to order $M = 37$. This has no substantial influence on the large-order structure. The obstruction at order $M = 45$ is caused by a change in the numerical precision. The solid line is a logarithmic fit to the upper envelope of the spectrum up to order $M = 90$.

$$C(z_i, z_j|A) = \mathcal{P} \exp \left[ig \int_{z_i}^{z_j} d\omega_\mu A_\mu(\omega) \right] \quad (74)$$

denotes a path-dependent phase factor (“connector” [113]) in which the expansion of the exponential along a contour C joining the points z_i and z_j is controlled by the path-ordering prescription \mathcal{P} . For a short-distance expansion, the connector can be evaluated along straight lines with lengths $\propto |z_i - z_j|^{1/2} \approx |z_{\perp i} - z_{\perp j}|^{1/2} \rightarrow 0$ as $Q^2 \rightarrow \infty$. Working in the light cone frame, one can use the axial gauge $A^+ = 0$ by virtue of which the connector at short distances can be replaced by unity since all inter-quark separations along the light cone are short. A covariant gauge in which the connector can also be neglected is provided by using the gauge parameter $a = -3$ [113,114]. By virtue of the light-cone gauge, the contour factors reduce to unity and the path-dependent matrix element simplifies to a tri-local quantity of leading twist-three which can be written in terms of three Lorentz invariant functions of positive parity V (vector $\leftrightarrow \gamma_\mu C$), A (axial vector $\leftrightarrow \gamma_\mu \gamma_5 C$), and T (tensor $\leftrightarrow \sigma_{\mu\nu} C$) [115]:

$$\langle 0 | u_\alpha^a(z_1) u_\beta^b(z_2) d_\gamma^c(z_3) | P, + \rangle \frac{\epsilon^{abc}}{\sqrt{N_c!}} = \frac{1}{4\sqrt{N_c!}} f_N [(\not{p}C)_{\alpha\beta} (\gamma_5 N)_\gamma V(z_i \cdot p) + (\not{p}\gamma_5 C)_{\alpha\beta} N_\gamma A(z_i \cdot p) - (\sigma_{\mu\nu} p_\nu C)_{\alpha\beta} (\gamma_\mu \gamma_5 N)_\gamma T(z_i \cdot p)] . \quad (75)$$

Here $|P, +\rangle$ is the proton state with momentum P and positive helicity, N denotes the proton spinor, and $C = i\gamma_0\gamma_2$ is the charge-conjugation matrix. The “proton decay constant” f_N is a dimensionful quantity determining the value of the nucleon distribution amplitude at the origin [30,31].

To perform the actual calculations of the nucleon distribution amplitudes, it is convenient to define the functions V , A , and T in the space of longitudinal momentum fractions:

$$F(x_1, x_2, x_3) = \prod_{i=1}^3 \frac{d(z_i \cdot P)}{2\pi} \exp \left[i \sum_{j=1}^3 x_j (z_j \cdot P) \right] F(z_i \cdot P) . \quad (76)$$

Note that these functions depend implicitly on the factorization scale which is supposed to serve as the starting point of evolution. Furthermore, renormalization group controlled evolution fixes the asymptotic limits of these functions to be $\lim_{\mu^2 \rightarrow \infty} V = \lim_{\mu^2 \rightarrow \infty} T = \phi_{\text{as}} = 120x_1x_2x_3$, and $\lim_{\mu^2 \rightarrow \infty} A = 0$, the latter because of the Pauli principle. The next step is to obtain solutions for these functions at finite evolution scales by determining the coefficients B_n and then to represent them as a series expansion over a finite number of their eigenfunctions.

Before we proceed, let us first discuss the symmetry properties of these functions in the infinite momentum frame. Because of the identity of the two u -quarks in the nucleon, the functions V and T transform under the scalar symmetric representation and the function A under the scalar antisymmetric representation of the permutation group S_3 . Then one has (in obvious shorthand notation [116]: $P_{123} \equiv [123]$, etc.)

$$\begin{aligned} [213]V(1, 2, 3) &= V(1, 2, 3) \\ [213]T(1, 2, 3) &= T(1, 2, 3) \\ [213]A(1, 2, 3) &= -A(1, 2, 3) . \end{aligned} \quad (77)$$

On the other hand, the requirement that the total isospin of the three-quark bound state should equal 1/2 yields one more relation:

$$2T(1, 2, 3) = V(1, 3, 2) - A(1, 3, 2) + V(2, 3, 1) - A(2, 3, 1) . \quad (78)$$

Thus the system of the functions V , A , and T is redundant and the whole information they contain can be expressed by a single function, termed Φ_N [116,30]:

$$\Phi_N(x_i) \equiv V(x_i) - A(x_i) . \quad (79)$$

This function is mixed symmetric, i.e., it transforms under the 2-dimensional (matrix) representation of S_3 . Knowing Φ_N it is sufficient to determine all other nucleon distribution amplitudes. For the time being, there is actually no method of computing hadron distribution amplitudes as a *whole*.¹⁰ Hence, we must content ourselves with descriptions in terms of truncated eigenfunctions series demanding that they (1) comply with theoretical constraints, set for example by QCD sum rules or lattice calculations, (2) are renormalization group controlled, i.e., satisfy the nucleon evolution equation at every order of truncation, and (3) eventually match the available experimental data.

In the following exposition the nucleon distribution amplitudes will be determined via their moments

$$F^{(n_1 n_2 n_3)} = \int_0^1 [dx] x_1^{n_1} x_2^{n_2} x_3^{n_3} F(x_1, x_2, x_3) , \quad (80)$$

where $F(x_i)$ stands for one of the amplitudes V , T , A , or linear combinations of them. These moments are related to the covariant derivatives of the invariant functions with respect to the light-cone positions $z_i \cdot p$. The latter are the Fourier conjugate variables to the longitudinal momenta x_i . Hence we have

$$\begin{aligned} \prod_{i=1}^3 \left(iz \cdot \frac{\partial}{\partial z_i} \right)^{n_i} \hat{F}(z_i \cdot p)|_{z_i=0} &= \prod_{i=1}^3 \left(iz \cdot \frac{\partial}{\partial z_i} \right)^{n_i} \int_0^1 [dx] \exp \left[-i \sum_{j=1}^3 x_j (z_j \cdot P) \right] \hat{F}(x_i) \\ &= (z \cdot P)^{n_1+n_2+n_3} \int_0^1 [dx] x_1^{n_1} x_2^{n_2} x_3^{n_3} \hat{F}(x_i) \\ &= (z \cdot P)^{n_1+n_2+n_3} \hat{F}^{(n_1 n_2 n_3)} , \end{aligned} \quad (81)$$

where z is an arbitrary auxiliary vector ($z^2 = 0$) and the caret, $\hat{}$, serves to distinguish operators from scalar functions. Taking matrix elements between the proton state and the vacuum, we get

$$\langle 0 | \hat{F}_\gamma^{(n_1 n_2 n_3)}(0) | P \rangle = f_N (z \cdot P)^{n_1+n_2+n_3+1} N_\gamma F^{(n_1 n_2 n_3)} , \quad (82)$$

where the moments on the rhs are defined in Eq. (80). More precisely, we consider matrix elements (moments) of the following operators:

$$\hat{V}_\gamma^{(n_1 n_2 n_3)}(0) \equiv (iz \cdot D)^{n_1} u(0) [C \gamma_\mu z_\mu] (iz \cdot D)^{n_2} u(0) (iz \cdot D)^{n_3} \gamma_5 d_\gamma(0) , \quad (83)$$

¹⁰A promising approach, applied so far only to the pion, was recently presented in [93].

$$\hat{A}_\gamma^{(n_1 n_2 n_3)}(0) \equiv (iz \cdot D)^{n_1} u(0) [C \gamma_5 \gamma_\mu z_\mu] (iz \cdot D)^{n_2} u(0) (iz \cdot D)^{n_3} d_\gamma(0) , \quad (84)$$

$$\hat{T}_\gamma^{(n_1 n_2 n_3)}(0) \equiv (iz \cdot D)^{n_1} u(0) [C (-\sigma_{\mu\nu}) z_\nu] (iz \cdot D)^{n_2} u(0) (iz \cdot D)^{n_3} \gamma_5 \gamma_\mu d_\gamma(0) . \quad (85)$$

The determination of the moments of these operators derives from correlators of the generic form

$$\begin{aligned} I^{(n_1 n_2 n_3, m)}(q, z) &= i \int d^4 x e^{iq \cdot x} \langle 0 | T(F_\gamma^{(n_1 n_2 n_3)}(0) \hat{J}_{\gamma'}^{(m)}(x)) | 0 \rangle (z \cdot \gamma)_{\gamma\gamma'} \\ &= (z \cdot q)^{n_1 + n_2 + n_3 + m + 3} I^{(n_1 n_2 n_3, m)}(q^2) , \end{aligned} \quad (86)$$

where z is again a light-like auxiliary vector and the factor $(z \cdot \gamma)_{\gamma\gamma'}$ serves to project out the leading-twist structure of the correlator. The computation of the Wilson coefficients on the quark side of the correlator amounts to the perturbative evaluation of diagrams involving local quark/gluon condensates [30]. It yields the theoretical side of the sum rule. The hadronic (phenomenological) side of the sum rule is obtained by saturating the correlator by the lowest-mass baryon state(s) via a dispersion relation. Reconciliation of the two sides of the sum rule with respect to the Borel parameter within a continuous interval as large as possible determines the variation of permissible values for a particular moment. We do not derive sum rules here. For more details we refer to the original works [30,37,35,38] and the review article [31]. We merely use them as theoretical constraints imposed on the moments of the nucleon distribution amplitude. However, these constraints cannot fix the shape of the nucleon distribution amplitude uniquely and one has to impose additional *global* constraints as opposed to the moment sum rules which constitute *local* constraints.¹¹

The moments of the nucleon distribution amplitude Φ_N in terms of the expansion coefficients B_n are displayed in Table 2.

Because of longitudinal momentum conservation, $x_1 + x_2 + x_3 = 1$, not all the moments at a given order $M = n_1 + n_2 + n_3$ are linearly independent. This implies [37]

$$\Phi_N^{(n_1, n_2, n_3)} = \Phi_N^{(n_1+1, n_2, n_3)} + \Phi_N^{(n_1, n_2+1, n_3)} + \Phi_N^{(n_1, n_2, n_3+1)} . \quad (87)$$

For instance, at order $M = 3$ there are 20 moments out of which only 10 are strict. Which combinations are actually taken, depends on the choice of the polynomial basis in which the eigenfunctions are finally expressed. We use throughout this report the powers of the monomial $x_1 x_3$, i.e., the basis $|k l\rangle$. In terms of this basis, the moments of Φ_N read

$$\Phi_N^{(n_1 n_2 n_3)} = \int_0^1 dx_1 \int_0^{1-x_1} dx_3 \left[\sum_{i=0}^{n_2} \sum_{j=0}^i (-1)^i \binom{n_2}{i} \binom{i}{j} x_1^{n_1+i-j} x_3^{n_3+j} \right] \Phi_N(x_1, x_3) . \quad (88)$$

It was first shown in [49,50,101] and then outlined in [103] that it is possible to derive a *closed-form* relation between the expansion coefficients B_n and the strict moments of Φ_N , defined by

¹¹One can always add some oscillating function which vanishes at the points fixed by the local constraints but which contributes outside.

Table 2. Analytical expressions for the moments of the nucleon distribution amplitude $\Phi_N^{(n_1 n_2 n_3)} \equiv \Phi_N^{[k]}$ in terms of the expansion coefficients B_n up to order $M = n_1 + n_2 + n_3 = 3$.

k	$\Phi_N^{[k]}$	Moments
0	$\Phi_N^{(000)}$	B_0
1	$\Phi_N^{(100)}$	$\frac{7 B_0 + B_1 + B_2}{21}$
2	$\Phi_N^{(010)}$	$\frac{7 B_0 - 2 B_2}{21}$
3	$\Phi_N^{(001)}$	$\frac{7 B_0 - B_1 + B_2}{21}$
4	$\Phi_N^{(200)}$	$\frac{108 B_0 + 27 B_1 + 27 B_2 + 9 B_3 - B_4 - B_5}{756}$
5	$\Phi_N^{(020)}$	$\frac{18 B_0 - 9 B_2 + B_3 + B_5}{126}$
6	$\Phi_N^{(002)}$	$\frac{108 B_0 - 27 B_1 + 27 B_2 + 9 B_3 + B_4 - B_5}{756}$
7	$\Phi_N^{(110)}$	$\frac{72 B_0 + 9 B_1 - 9 B_2 - 3 B_3 + B_4 - 3 B_5}{756}$
8	$\Phi_N^{(101)}$	$\frac{36 B_0 + 9 B_2 - 3 B_3 + 2 B_5}{378}$
9	$\Phi_N^{(011)}$	$\frac{72 B_0 - 9 B_1 - 9 B_2 - 3 B_3 - B_4 - 3 B_5}{756}$
10	$\Phi_N^{(300)}$	$\frac{87120 B_0 + 29040 B_1 + 29040 B_2 + 17424 B_3 - 1936 B_4 - 1936 B_5}{1219680}$
11	$\Phi_N^{(030)}$	$\frac{-33 B_6 - 33 \sqrt{97} B_6 - 33 B_7 + 33 \sqrt{97} B_7 + 146 B_8 + 2 \sqrt{4801} B_8 + 146 B_9 - 2 \sqrt{4801} B_9}{1219680}$
12	$\Phi_N^{(003)}$	$\frac{165 B_0 - 110 B_2 + 22 B_3 + 22 B_5 + B_6 + B_7}{2310}$
13	$\Phi_N^{(210)}$	$\frac{87120 B_0 - 29040 B_1 + 29040 B_2 + 17424 B_3 + 1936 B_4 - 1936 B_5}{1219680}$
14	$\Phi_N^{(201)}$	$\frac{-33 B_6 - 33 \sqrt{97} B_6 - 33 B_7 + 33 \sqrt{97} B_7 - 146 B_8 - 2 \sqrt{4801} B_8 - 146 B_9 + 2 \sqrt{4801} B_9}{1219680}$
15	$\Phi_N^{(120)}$	$\frac{5940 B_0 + 1320 B_1 + 88 B_4 - 440 B_5 + 15 B_6 + 3 \sqrt{97} B_6 + 15 B_7 - 3 \sqrt{97} B_7 - 12 B_8 - 12 B_9}{166320}$
16	$\Phi_N^{(102)}$	$\frac{130680 B_0 + 14520 B_1 + 43560 B_2 - 8712 B_3 - 968 B_4 + 10648 B_5}{3659040}$
17	$\Phi_N^{(021)}$	$\frac{-231 B_6 + 33 \sqrt{97} B_6 - 231 B_7 - 33 \sqrt{97} B_7 - 174 B_8 - 6 \sqrt{4801} B_8 - 174 B_9 + 6 \sqrt{4801} B_9}{3659040}$
18	$\Phi_N^{(012)}$	$\frac{495 B_0 + 55 B_1 - 165 B_2 - 11 B_3 + 11 B_4 - 11 B_5 - 3 B_6 - 3 B_7 + B_8 + B_9}{13860}$
		$\frac{130680 B_0 - 14520 B_1 + 43560 B_2 - 8712 B_3 + 968 B_4 + 10648 B_5}{3659040}$
		$\frac{-231 B_6 + 33 \sqrt{97} B_6 - 231 B_7 - 33 \sqrt{97} B_7 + 174 B_8 + 6 \sqrt{4801} B_8 + 174 B_9 - 6 \sqrt{4801} B_9}{3659040}$
		$\frac{495 B_0 - 55 B_1 - 165 B_2 - 11 B_3 - 11 B_4 - 11 B_5 - 3 B_6 - 3 B_7 - B_8 - B_9}{13860}$
		$\frac{5940 B_0 - 1320 B_1 - 88 B_4 - 440 B_5 + 15 B_6 + 3 \sqrt{97} B_6 + 15 B_7 - 3 \sqrt{97} B_7 + 12 B_8 + 12 B_9}{166320}$

$$\Phi_N^{(i0j)} = \int_0^1 [dx] x_1^i x_2^0 x_3^j \Phi_N(x_k, \mu^2), \quad (89)$$

to arrive at

$$\frac{B_n(Q^2)}{\sqrt{N_n}} = \frac{\sqrt{N_n}}{120} \left[\frac{\ln(Q^2/\Lambda_{QCD}^2)}{\ln(\mu^2/\Lambda_{QCD}^2)} \right]^{-\gamma_n} \sum_{i,j=0}^{\infty} a_{ij}^n \Phi_N^{(i0j)}(\mu^2), \quad (90)$$

where the normalization constants N_n , the matrix coefficients a_{ij}^n , and the anomalous dimensions γ_n (up to $M = 4$) are those tabulated in Table 1. This expression enables the *analytical* calculation of the coefficients to any desired order of polynomial expansion. The utility of Eq. (90) is twofold: (1) As repeatedly stated, the moments of hadron distribution amplitudes are not accurately determined. Thus, without such an *explicit* relation between expansion coefficients and strict moments, one has to perform a simultaneous and self-consistent fit to the moment sum rules constraints, a procedure which obviously becomes increasingly tedious as the moment-order grows. (2) As already outlined in the previous chapter, the Hilbert-Schmidt orthogonalization procedure of polynomials with more than one variable is not unique, and one is well-advised to look for higher-order eigenfunctions which are as simple as possible, absorbing numerical coefficients into the normalization constants. This non-uniqueness entails that one can compare expansion coefficients B_n , obtained in different approaches, only if they are *normalized*. Without the knowledge of the normalization constants N_n , the values of B_n are of no significance or practical usefulness. However, having derived Eq. (90), the knowledge of the specific normalization used in different approaches becomes superfluous. The coefficients B_n can be self-consistently computed on the basis of the strict moments alone, which are universal quantities, modulo an overall normalization through the value of $\Phi_N^{(000)}$. In the following,

$$\int_0^1 [dx] \Phi_N(x_i, \mu^2) = 1 \quad (91)$$

is used. Hence, evaluating the strict moments of the nucleon distribution amplitude up to a given order, one can determine the corresponding expansion coefficients of the same order and vice versa. All these advantages will become successively apparent through the applications of the formalism in subsequent chapters. The link between B_n and the strict moments of Φ_N is exemplified below (see also [41,51]):

$$\begin{aligned} B_1(\mu^2) &= \frac{1260}{120} \left[\Phi_N^{(100)} - \Phi_N^{(001)} \right] \Big|_{\mu^2} \\ B_2(\mu^2) &= \frac{420}{120} \left[2\Phi_N^{(000)} - 3\Phi_N^{(100)} - 3\Phi_N^{(001)} \right] \Big|_{\mu^2} \\ B_3(\mu^2) &= \frac{756}{120} \left[2\Phi_N^{(000)} - 7\Phi_N^{(100)} - 7\Phi_N^{(001)} + 8\Phi_N^{(200)} + 4\Phi_N^{(101)} + 8\Phi_N^{(002)} \right] \Big|_{\mu^2} \\ B_4(\mu^2) &= \frac{34020}{120} \left[\Phi_N^{(100)} - \Phi_N^{(001)} - \frac{4}{3}\Phi_N^{(200)} + \frac{4}{3}\Phi_N^{(002)} \right] \Big|_{\mu^2} \\ B_5(\mu^2) &= \frac{1944}{120} \left[2\Phi_N^{(000)} - 7\Phi_N^{(100)} - 7\Phi_N^{(001)} + \frac{14}{3}\Phi_N^{(200)} + 14\Phi_N^{(101)} + \frac{14}{3}\Phi_N^{(002)} \right] \Big|_{\mu^2}. \end{aligned} \quad (92)$$

Note that B_0 is fixed to unity by the normalization of Φ_N (cf. Eq. (91)). Furthermore, recall once again that the notations of [35] are used. The next-to-leading order expansion coefficients ($M = 3$) are:

$$\begin{aligned}
B_6(\mu^2) &= \frac{4620}{120} \frac{485 + 11\sqrt{97}}{97} \left[\Phi_N^{(000)} - 6 \left(\Phi_N^{(100)} + \Phi_N^{(001)} \right) + \frac{41 + \sqrt{97}}{4} \left(\Phi_N^{(200)} + \Phi_N^{(002)} \right) \right. \\
&\quad \left. + 3 \frac{31 - \sqrt{97}}{4} \Phi_N^{(101)} - 5 \frac{17 + \sqrt{97}}{16} \left(\Phi_N^{(300)} + \Phi_N^{(003)} \right) \right. \\
&\quad \left. - 5 \frac{31 - \sqrt{97}}{8} \left(\Phi_N^{(201)} + \Phi_N^{(102)} \right) \right] \Big|_{\mu^2} \\
B_7(\mu^2) &= \frac{4620}{120} \frac{485 - 11\sqrt{97}}{97} \left[\Phi_N^{(000)} - 6 \left(\Phi_N^{(100)} + \Phi_N^{(001)} \right) + \frac{41 - \sqrt{97}}{4} \left(\Phi_N^{(200)} + \Phi_N^{(002)} \right) \right. \\
&\quad \left. + 3 \frac{31 + \sqrt{97}}{4} \Phi_N^{(101)} - 5 \frac{17 - \sqrt{97}}{16} \left(\Phi_N^{(300)} + \Phi_N^{(003)} \right) \right. \\
&\quad \left. - 5 \frac{31 + \sqrt{97}}{8} \left(\Phi_N^{(201)} + \Phi_N^{(102)} \right) \right] \Big|_{\mu^2} \\
B_8(\mu^2) &= \frac{27720}{120} \frac{33607 - 247\sqrt{4801}}{4801} \left[\Phi_N^{(100)} - \Phi_N^{(001)} - 3 \left(\Phi_N^{(200)} - \Phi_N^{(002)} \right) \right. \\
&\quad \left. + \frac{601 + \sqrt{4801}}{264} \left(\Phi_N^{(300)} - \Phi_N^{(003)} \right) \right. \\
&\quad \left. + \frac{59 - \sqrt{4801}}{44} \left(\Phi_N^{(201)} - \Phi_N^{(102)} \right) \right] \Big|_{\mu^2} \\
B_9(\mu^2) &= \frac{27720}{120} \frac{33607 + 247\sqrt{4801}}{4801} \left[\Phi_N^{(100)} - \Phi_N^{(001)} - 3 \left(\Phi_N^{(200)} - \Phi_N^{(002)} \right) \right. \\
&\quad \left. + \frac{601 - \sqrt{4801}}{264} \left(\Phi_N^{(300)} - \Phi_N^{(003)} \right) \right. \\
&\quad \left. + \frac{59 + \sqrt{4801}}{44} \left(\Phi_N^{(201)} - \Phi_N^{(102)} \right) \right] \Big|_{\mu^2}. \tag{93}
\end{aligned}$$

The values of the moments of Φ_N are extracted from the correlator in Eq. (86) for $n_1 + n_2 + n_3 \leq 3$ and $m = 1$ at some self-consistently determined normalization point $\mu = \mu_F$ of order 1 GeV (see, e.g., [30,35]) at which a short-distance operator product expansion can be safely performed and quark-hadron duality is supposed to be valid. Table 3 shows the range of values obtained by COZ [38] up to order $M = 3$ together with those calculated by KS [37] for the first- and second-order moments.

This exposition completes our discussion of the expansion coefficients and the brief review of the conceptual essentials underlying their non-perturbative determination. Before moving on in the next chapter to the actual models for the nucleon distribution amplitude, we briefly discuss now the momentum evolution of the normalized expansion coefficients B_n (recall Eq. 90) against the order of expansion in terms of eigenfunctions. The result is illustrated in Fig. 10. One observes that the ratio $\frac{B_n(Q^2)}{B_n(\mu^2)}$ decreases both with increasing polynomial order and increasing momentum transfer so that a truncation at low orders seems, in principle, justifiable. However, in order that the truncation of the infinite eigenfunctions expansion, given by Eq. (14), is computationally useful, we have to ensure dominance of the lowest-order contributions. Given this premise, the guiding principle is to minimize the influence of higher-order terms which we have discarded. This procedure is in some sense analogous to the optimization of the renormalization-scheme dependence of physical quan-

Table 3. Numerical values of the moments $M = n_1 + n_2 + n_3 \leq 3$ of the heterotic nucleon distribution amplitude in comparison with those of previous models versus the QCD sum-rule constraints derived by Chernyak, Ogloblin, and Zhitnisky [38], and King and Sachrajda [37].

$(n_1 n_2 n_3)$	COZ-SR	KS-SR	$\Phi_{N/het}^{(n_1 n_2 n_3)}$	$\Phi_{N/COZ}^{(n_1 n_2 n_3)}$	$\Phi_{N/CZ}^{(n_1 n_2 n_3)}$	$\Phi_{N/GS}^{(n_1 n_2 n_3)}$	$\Phi_{N/KS}^{(n_1 n_2 n_3)}$
(000)	1	1	1	1	1	1	1
(100)	0.54—0.62	0.46—0.59	0.5721	0.5790	0.630	0.6269	0.550
(010)	0.18—0.20	0.18—0.21	0.1837	0.1920	0.150	0.1371	0.210
(001)	0.20—0.25	0.22—0.26	0.2442	0.2290	0.220	0.2359	0.240
(200)	0.32—0.42	0.27—0.37	0.3380	0.3690	0.397	0.2879	0.350
(020)	0.065—0.088	0.08—0.09	0.0661	0.0680	0.0233	0.0321	0.090
(002)	0.09—0.12	0.10—0.12	0.1696	0.0890	0.080	0.0079	0.120
(110)	0.08—0.10	0.08—0.10	0.1386	0.0970	0.110	0.1080	0.100
(101)	0.09—0.11	0.09—0.11	0.0955	0.1130	0.123	0.2309	0.100
(011)	-0.03—0.03	unreliable	-0.0210	0.0270	0.017	-0.0029	0.020
(300)	0.21—0.25		0.2101	0.2445	0.257	0.1281	0.2333
(030)	0.028—0.04		0.0392	0.0381	0.0013	0.0169	0.0573
(003)	0.048—0.056		0.1392	0.0485	0.0413	-0.0515	0.0813
(210)	0.041—0.049		0.0789	0.0587	0.068	0.0463	0.0593
(201)	0.044—0.055		0.0490	0.0658	0.0713	0.1135	0.0573
(120)	0.027—0.037		0.0504	0.0243	0.0253	0.0278	0.030
(102)	0.037—0.043		0.0372	0.0331	0.0353	0.0836	0.0320
(021)	-0.004—0.007		-0.0235	0.0056	-0.003	-0.0127	0.0027
(012)	-0.005—0.008		-0.0068	0.0073	0.003	-0.0241	0.0067

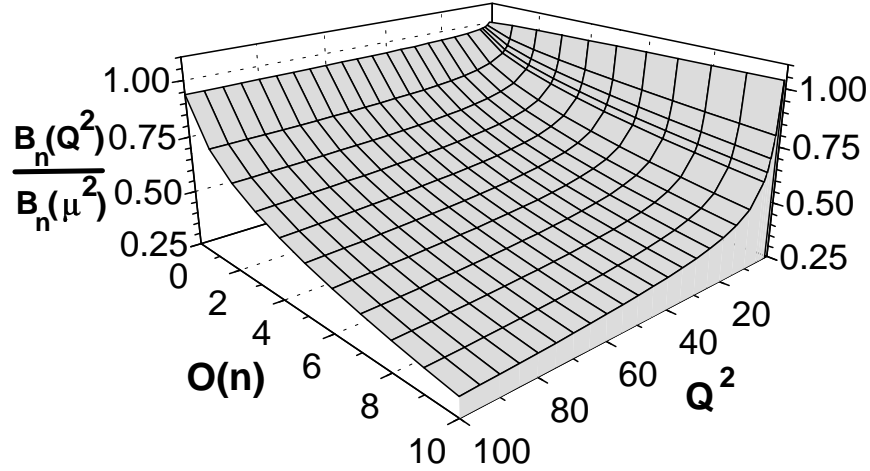


Figure 10. Evolution behavior of the normalized expansion coefficients B_n versus the tradeoff with the order of expansion in eigenfunctions.

tities computed in a perturbative scheme (*principle of minimum sensitivity* [117]). Without enough understanding of the underlying non-perturbative dynamics, it remains a challenge to develop a method of computing hadron distribution amplitudes as a *whole*. For the time being, we must content ourselves with an *effective* description in which the *local* low-order moment constraints are supplemented by additional *global* constraints to impose restrictions on the shape of the nucleon distribution amplitude as a whole. This may be achieved by means of a *hierarchical* (with respect to moment order) χ^2 -criterion (see next section) or by demanding, for instance, smoothness of the nucleon distribution amplitude [40]. In this way, one can enforce the dominance of the lowest-order contributions and minimize the influence of the disregarded higher-order terms. Since the extraction of reliable estimates of higher-order moments from QCD sum rules is severely limited [31] (the accuracy of the moment values one can extract decreases as the moment order increases), there is actually no other pragmatic alternative to this type of approach. So, if one is satisfied with a given accuracy (of observables calculated with these nucleon distribution amplitudes) relative to existing data, reconstructing an analytic representation of the nucleon distribution amplitude in terms of higher and higher eigenfunctions is unnecessary – maybe even irrelevant.

E. NUCLEON DISTRIBUTION AMPLITUDES

It is evident from the discussion in the previous chapter that the method of QCD sum rules enables the determination of the basic characteristics of the nucleon distribution amplitude, namely: (1) its value at the origin, f_N , and (2) a model representation over longitudinal momenta via a finite number of moments. However, the reliability of this procedure depends crucially on the particular way of using the QCD sum-rule constraints. The basic assumptions in truncating the infinite series of eigenfunctions should be:

- A truncated representation at relatively low orders provides a reasonable approximation of the true nucleon distribution amplitude, given that the normalized expansion

coefficients decrease with the (moment) order, albeit slowly.

- The intrinsic inaccuracy of the sum rules for higher-order moments is taken into account.
- The evolution equation is always satisfied.

The first premise says nothing about the convergence of the eigenfunctions series. We know that this series converges for very large values of Q^2 to the asymptotic solution ϕ_{as} , but only logarithmically. Nevertheless, it seems reasonable to believe that the characteristic properties of the nucleon distribution amplitude belong to the *entire* series and that they do not first show up in higher orders. On the contrary, the polynomial structure of the eigenfunctions (comprising not only symmetric but also antisymmetric Appell polynomials) will inevitably introduce oscillations (“wiggles”) at every step of truncation because of the normalization condition imposed on Φ_N (cf. Eq. (91)). These wiggles are unphysical and should be washed out by destructive interference at subsequent steps of truncation. Hence, it is evident that the trial nucleon distribution amplitude at every step of truncation should be chosen to have a shape as smooth as the sum-rule constraints on its moments allow. This procedure has close resemblance to the Tamm-Dancoff method [118] of truncating time-ordered products in quantum field theory in seeking for a ground-state solution.¹² In this method, as in our approach, the parameters of the low order solutions are *effective*, meaning that they incorporate by construction crucial high-order effects.

Following this strategy, we introduce a χ^2 -criterion which not only parameterizes deviations from the sum rules *laterally*, i.e., within some fixed moment order, but – in addition – which weighs the quality of sum rules *vertically*, i.e., according to their order [41,42,51,52,103]. This can be realized by defining

$$\chi_k^2 = \left(\chi_{k,(a)}^2 + \chi_{k,(b)}^2 \right) \left[1 - \Theta \left(m_k - M_k^{\min} \right) \Theta \left(M_k^{\max} - m_k \right) \right] \quad (94)$$

with

$$\chi_{k,(a)}^2 = \min \left(\left| M_k^{\min} - m_k \right|, \left| m_k - M_k^{\max} \right| \right) N_k^{-1} \quad (95)$$

(m_k ($k = 1, 2, \dots, 18$) denoting collectively the moments), where $N_k = \left| M_k^{\min} \right|$ or $\left| M_k^{\max} \right|$, whether m_k lies on the left- or on the right-hand side of the corresponding sum-rule interval ($\chi_{\text{tot}}^2 = \sum_k \chi_k^2$) and

$$\chi_{k,(b)}^2 = \begin{cases} 100, & 1 \leq k \leq 3 \\ 10, & 4 \leq k \leq 9 \\ 1, & 10 \leq k \leq 18. \end{cases} \quad (96)$$

Let us consider a concrete example in order to make this criterion and its use more transparent. Suppose a trial distribution amplitude corresponds to $\chi_{\text{tot}}^2 = 132.85$. This means

¹²I wish to thank Prof. D. Shirkov for discussions on this point.

Table 4. Theoretical parameters to classify the nucleon distribution amplitudes discussed in the text. The samples shown refer to the COZ sum rules.

Model	B_1	B_2	B_3	B_4	B_5	$\vartheta[deg]$	R	χ^2	Symbol
Het	3.4437	1.5710	4.5937	29.3125	-0.1250	-1.89	.104	33.48	●
Het'	4.3025	1.5920	1.9675	-19.6580	3.3531	24.44	.448	30.63	●
COZ^{opt}	3.5268	1.4000	2.8736	-4.5227	0.8002	9.13	.465	4.49	■
COZ^{up}	3.2185	1.4562	2.8300	-17.3400	0.4700	5.83	.4881	21.29	+
COZ	3.6750	1.4840	2.8980	-6.6150	1.0260	10.16	.474	24.64	□
CZ	4.3050	1.9250	2.2470	-3.4650	0.0180	13.40	.487	250.07	◆
KS^{low}	3.5818	1.4702	4.8831	31.9906	0.4313	-0.93	.0675	36.27	○
KS/COZ^{opt}	3.4242	1.3644	3.0844	-3.2656	1.2750	9.47	.453	5.66	○
KS^{up}	3.5935	1.4184	2.7864	-13.3802	2.0594	13.82	.482	40.38	○
KS	3.2550	1.2950	3.9690	0.9450	1.0260	2.47	.412	116.35	◇
GS^{opt}	3.9501	1.5273	-4.8174	3.4435	8.7534	80.87	.095	54.95	▲
GS^{min}	3.9258	1.4598	-4.6816	1.1898	8.0123	80.19	.035	54.11	▼
GS	4.1045	2.0605	-4.7173	5.0202	9.3014	78.87	.097	270.82	△
Samples									
0	3.3125	1.4644	3.1438	-1.0000	0.8750	7.67	.441	4.63	+
1	3.2651	1.4032	3.5466	2.8685	1.7954	8.94	.405	5.11	+
2	3.4026	1.4917	3.0629	7.3430	0.6719	8.75	.385	16.07	+
3	3.7225	1.5030	3.6592	10.7265	1.5154	9.29	.355	17.78	+
4	3.8407	1.4968	3.2142	14.4093	0.8757	10.49	.325	19.41	+
5	3.6544	1.4000	3.0993	15.5614	-0.1329	6.35	.305	18.15	+
6	3.8607	1.4000	3.2375	19.8571	-0.1635	6.32	.255	20.57	+
7	3.9783	1.4000	3.2706	22.4194	-0.4805	5.29	.225	21.69	+
8	4.1547	1.4000	3.3756	26.1305	-0.5855	5.02	.175	23.52	+
9	3.4044	1.5387	4.3094	25.5625	0.0625	.01	.153	30.80	+

that it breaks one first-order sum rule, three second-order sum rules, and two third-order sum rules, whereas the total breaking is 85%.

This “hierarchical” treatment of the sum rules (1) accounts for the higher stability of the lower-level moments relative to the higher ones [35], and (2) does not overestimate the significance of the unverified constraints [38] for the third-order moments. Consequently, our parameterization in Eq. (96) favors solutions that satisfy best the lowest-order moments and gives (arbitrary) penalty points to those solutions which violate them. This relegates third-order terms to contribute only marginally, i.e., to merely *refine* (if at all) the shape of the nucleon distribution amplitude determined in the first step solely on the basis of the second-order moment constraints. It goes without saying that this procedure intrinsically suppresses solutions with unphysical oscillations. A physical analog of truncating the representation of the nucleon distribution amplitude this way is perhaps provided by a holographic image which is not destroyed when cut into smaller pieces (corresponding here to a lower order of truncation) but becomes rather less sharp [41]. In contrast, a series truncation according to a simple (i.e., lateral) χ^2 -criterion corresponds to a conventional image which is really destroyed when cut into smaller pieces.

Table 5. Theoretical parameters to classify the nucleon distribution amplitudes discussed in the text. The samples shown refer to a combined use of the COZ and KS sum rules.

Model	B_1	B_2	B_3	B_4	B_5	$\vartheta[deg]$	R	χ^2	Symbol
Samples									
0	3.7520	1.3845	2.7000	-10.5000	1.8500	14.24	.480	28.77	○
1	3.7065	1.3298	2.9000	- 8.0500	1.1500	10.15	.475	18.28	○
2	3.4075	1.4191	3.3813	- 7.6500	1.4750	7.82	.465	9.02	○
3	3.6695	1.3186	2.8375	- 5.8875	1.1125	10.62	.470	16.90	○
4	3.4120	1.3906	3.2375	- 5.5875	1.3625	8.51	.460	6.76	○
5	3.4242	1.3644	3.0844	- 3.2656	1.2750	9.47	.453	5.66	○
6	3.3500	1.3710	3.1192	- 0.9556	1.2995	9.48	.440	5.75	○
7	3.3501	1.4045	3.3004	0.2513	1.4203	8.95	.430	5.86	○
8	3.3536	1.4327	3.4787	4.8241	1.5609	8.97	.395	15.11	○
9	3.3500	1.3303	3.1262	8.8918	1.3173	10.75	.360	15.19	○
10	2.9067	1.3664	4.0326	12.0701	1.0180	2.46	.300	26.37	○
11	2.9300	1.3899	4.4263	16.4589	0.8764	-0.019	.250	28.91	○
12	3.1760	1.4491	4.6009	22.9637	0.5213	-1.016	.180	31.06	○
13	3.2912	1.4545	4.6802	25.5161	0.4903	-1.014	.150	32.96	○
14	3.4017	1.4595	4.7558	27.9607	0.4594	-1.014	.120	34.20	○
15	3.5078	1.4638	4.8284	30.3070	0.4310	-1.012	.090	35.39	○

All told, let us present the results. They are gathered in Tables 4 and 5 in correspondence with Figs. 11 and 12. We can see the utility of this procedure of fitting the sum rules as follows: the parameter space of the decomposition coefficients (“Appell” coefficients) that project on to the nucleon eigenfunctions, derived in the previous chapter, is systematically scanned seeking for evolving morphologies of geometric features such as the peak pattern of the amplitudes V , A , and T . Quantification of a feature or region involves its isolation, extraction, and stability. Next, one tracks features corresponding to particular solutions to determine how they change their form and how they compare with features in other regions. By testing the effects of various combinations of symmetric versus antisymmetric components of the distribution amplitudes, the whole parameter space can be systematically explored with respect to local minima of χ^2 and a complete picture of their distribution pattern can be pieced together. Using for the first- and second-order moments either the COZ or the KS sum-rule constraints in conjunction with those of COZ for the third-order moments, a simple *scaling relation* between the ratio $R \equiv |G_M^n|/G_M^p$ and the expansion coefficient B_4 emerges as one progresses through the generated solutions. That smooth scaling behavior is inherent in the particular set of sum rules used in the fit and does not rely on additional assumptions.

Fig. 12 illustrates the χ^2 quality of the COZ samples. Depending on the degree of matching with the corresponding sum rule, a solution found this way appears as a local minimum of the χ^2 criterion. We have plotted in the (B_4, R) plane interpolating solutions to the COZ sum rules (+ labels) and such to a combined set of KS/COZ sum rules (○ labels). The latter set is not quite consistent because the typical sum-rule parameters, such as Borel intervals, energy thresholds, etc., are treated differently in the two approaches. Nevertheless,

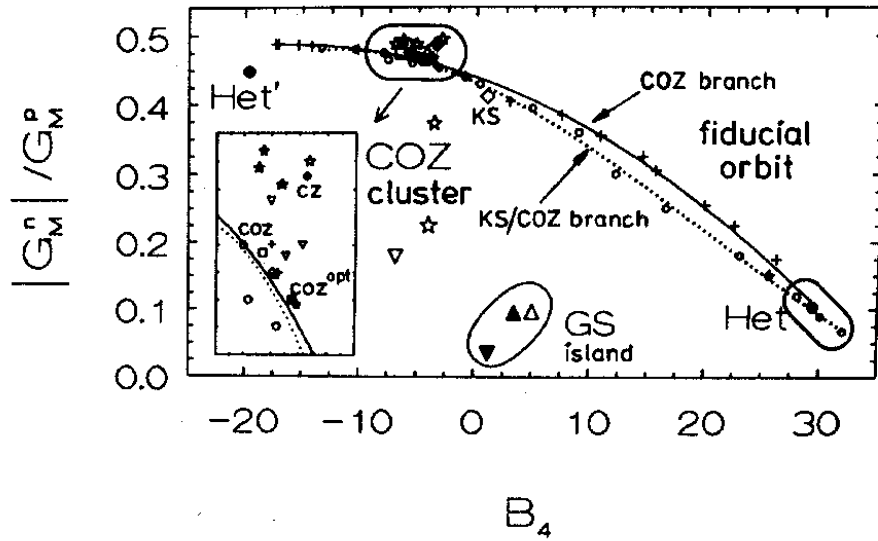


Figure 11. Pattern of nucleon distribution amplitudes matching the COZ sum-rule constraints (crosses) and such to a combined set of KS/COZ sum rules (open circles). A striking scaling relation between the ratio R of the magnetic nucleon form factors and the coefficient B_4 that projects on to the corresponding eigenfunction is revealed. The various models of nucleon distribution amplitudes discussed in the text are compiled in Table 4. Interpolating samples of distribution amplitudes with respect to the COZ sum rules are denoted by crosses (see Table 4); those referring to the combined set of the KS/COZ sum rules, by circles (see Table 5). The inset at the lower left expands the vertical scale between 0.455 and 0.495 (corresponding to the B_4 interval $[-10, 0]$) to exhibit the close agreement between the fiducial orbit and a variety of proposed amplitudes with third-order Appell polynomials, *not* included in the fit. Significantly, those model amplitudes which appear as isolated points are exactly the ones which possess unphysical features, namely, either in the form of spurious oscillations, or because they violate the renormalization group equation, leading this way to a wrong QCD evolution behavior of form factors (see [51]). The curves are fits to the local minima of the COZ sum rules (solid line) and the KS/COZ sum rules (dotted line). They constitute a *fiducial orbit* with respect to χ^2 beginning in the heterotic region (small R and large positive B_4) and terminating past the COZ cluster (large R and large negative B_4).

it is instructive to examine what changes the inclusion of the KS sum rules may cause. As it turns out, there is no significant difference between the two treatments (see Fig. 11), and this insensitivity justifies the whole approach and promotes the orbit structure to a key element of the analysis.

The solutions to the sum rules agree within less than 1% with the empirical fits :

$$R = 0.437338 - 0.006016B_4 - 0.000176B_4^2 \quad (97)$$

(only COZ constraints) or

$$R = 0.431303 - 0.00752B_4 - 0.000241B_4^2 + 3.851221 \times 10^{-6}B_4^3 \quad (98)$$

(combined KS and COZ constraints), represented by the solid and dotted curves, respectively. For simplicity, we use the term “orbit” to refer to both characteristic curves.

Furthermore, we find that the magnitude of the ratio R is restricted at both ends of the orbit. For the first discussed case, the upper bound is 0.4881 and for the second one, 0.482. The corresponding lower bounds are 0.104 and 0.0675. In the course of this analysis [51,52], optimized versions – with respect to the sum rules – of all previous models [30,33,37,38] have been determined. These amplitudes, denoted by the superscript “opt”, are shown in Fig. 13. [The assignments of models to symbols are given in Table 4.]

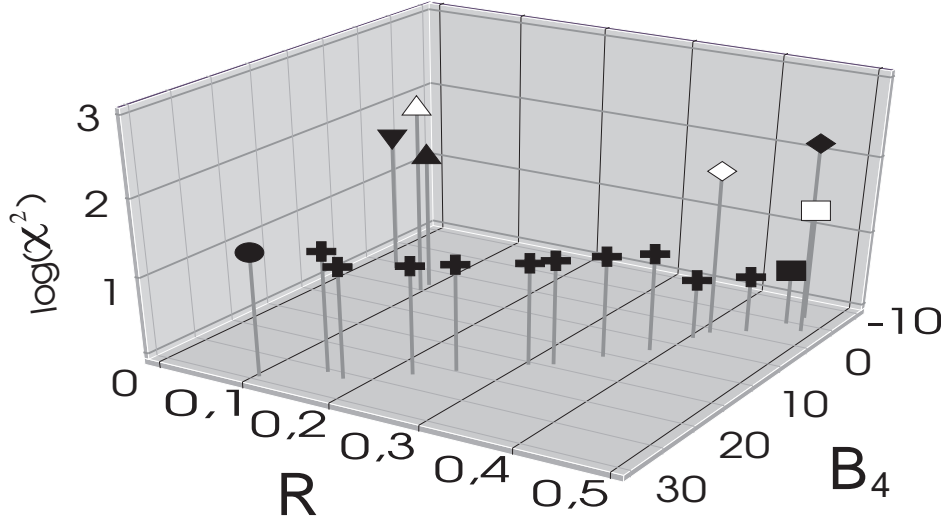


Figure 12. Two-dimensional view on solutions to the QCD sum rules as successive local minima in the plane spanned by $R \equiv |G_M^n|/G_M^p$ and B_4 with respect to the “hierarchical” χ^2 -criterion discussed in the text. Referring to the previous figure, only the COZ branch of the “fiducial orbit” is shown.

As mentioned previously, the lower part of the orbit is associated with the heterotic solution [42] which gives the smallest possible ratio still compatible with the sum-rule constraints. This solution, although degenerated with respect to R , is *distinct* from the GS one. As we shall see in the next chapters, the predictions extracted from the heterotic model are dramatically different compared to those following from the GS model. The upper region of the orbit controls COZ-type amplitudes and contains a cluster of solutions densely populating the orbit in the R -interval $0.455 \div 0.495$ (see the inset in Fig. 11). This cluster contains the amplitude denoted COZ^{opt} (see Table 4), which is associated with the absolute minimum of χ^2 and plays the role of an attractor for all other solutions with similar features. Strictly speaking, also the CZ model and the KS one, although in the vicinity of the orbit, are actually isolated points because they correspond to much larger χ^2 values (cf. Fig. 12) in correspondence with Table 4) than the proper solutions on the orbit. The heterotic amplitude and the original COZ amplitude correspond to similar χ^2 values. It is remarkable that the heterotic solution matches the KS [37] sum-rule constraints better than the original COZ amplitude. This is worth noting because the KS results have been independently verified in [45].

Analogously, the solution with the smallest χ^2 value on the KS/COZ branch of the orbit is the amplitude denoted KS/COZ^{opt} (see Table 4). GS-type amplitudes constitute an isolated region in the (B_4, R) plane and are separated from the characteristic orbit by a large χ^2 barrier. There is yet another type of solutions (we termed *Het'*) past the upper end of the orbit – first discussed in [51]. *Het'* belongs to a secondary-branch of the main orbit which can be reached by coercing the amplitudes V and T to have a particular symmetry pattern of maxima and minima, corresponding to the reversed combination as compared to the heterotic solution. Remarkably, each of the discussed categories of solutions has unique geometric characteristics specific for its class. One has to exercise a certain amount of care

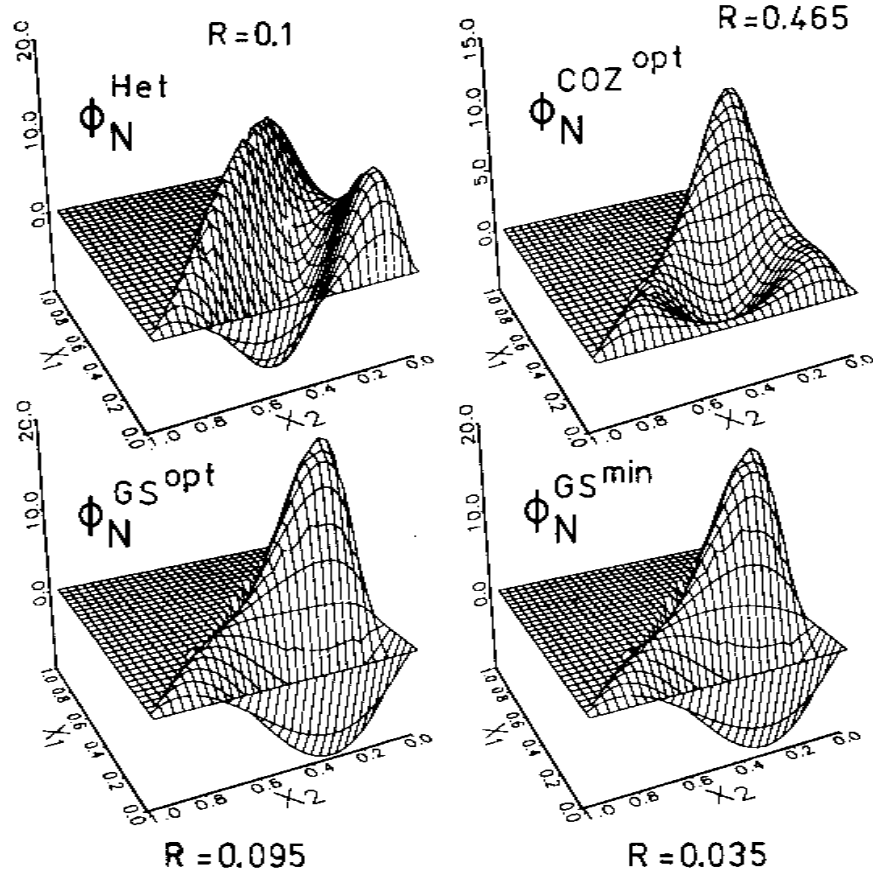


Figure 13. Profiles of the optimized versions of model distribution amplitudes, commonly discussed in the literature, shown together with the heterotic one.

to be sure that these are indeed the only regions in the parameter space contributing to the sum rules at the desired level of accuracy.

Having completed the classification of distribution amplitudes rendering the degree of Appell polynomials $M \leq 2$, let us now turn to models with functional representations which attempt to include third-order eigenfunctions, in connection with additional cutoff-parameters [40,119]. The inset in Fig. 11 shows how such models [40] (marked by stars) and [119] (marked by light upside-down triangles) group around the optimum amplitudes COZ^{opt} and KS/COZ^{opt} , thus establishing the scaling relation between R and B_4 in a much more general context. This result suggests that the inclusion of higher-order eigenfunctions (Appell polynomials) in the nucleon distribution amplitude is indeed a marginal effect, as argued above. If so, the antisymmetric content of the nucleon distribution amplitude is sufficiently accounted for by the eigenfunction $\tilde{\Phi}_4(x_i)$ since higher antisymmetric components are offset by this term. On the other hand, those model amplitudes proposed in [40,119] which appear as isolated points scattered toward the GS “island” are unacceptable on physical grounds, either because they exhibit unrealistic large oscillations in the longitudinal momentum fractions [40] or because they entail a wrong evolution behavior for the nucleon form factors [119]. In addition, as was pointed out in [41], models which use cutoffs, like

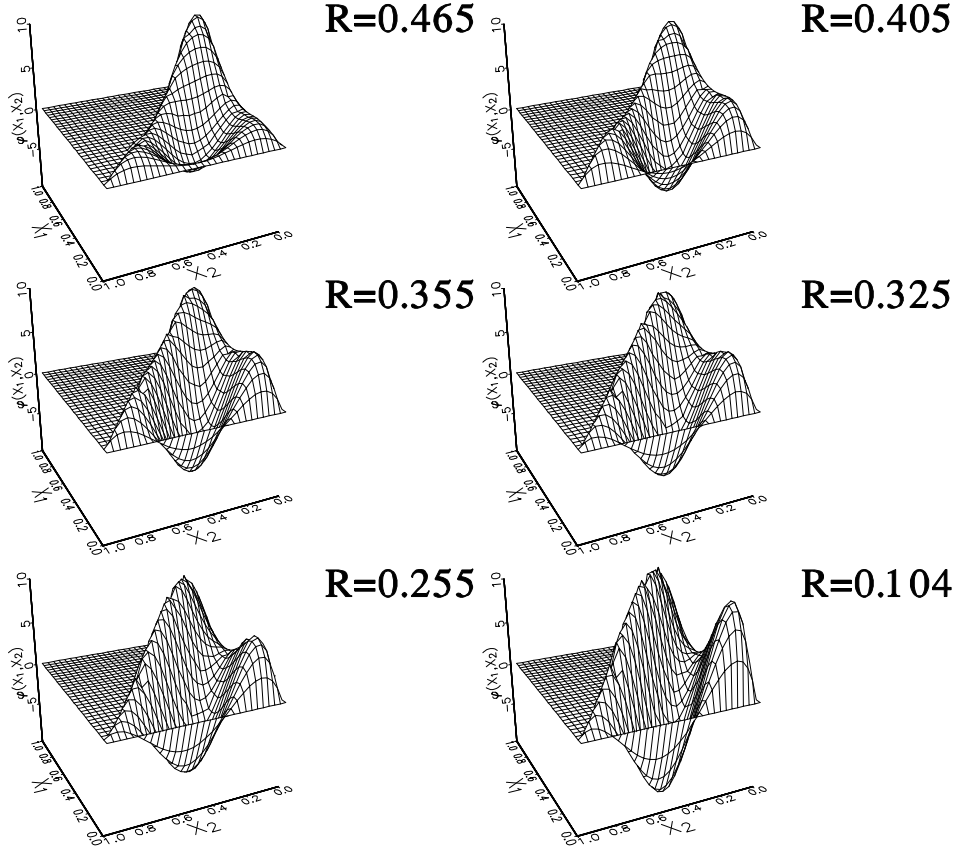


Figure 14. A two-dimensional example showing how the profile of the nucleon distribution amplitude Φ_N changes along the χ^2 orbit. The amplitudes are labeled by the corresponding R value.

those in [119], have difficulties in preserving the validity of the evolution equation.

The general picture emerging from the presented analysis is a pattern of nucleon distribution amplitudes which develops into several regions of the (B_4, R) plane. The main sector is characterized by an orbit which shows a striking scaling behavior between the ratio R (a measurable quantity) and the (theoretical) expansion parameter B_4 . For a variety of amplitudes this result is unique, irrespective of their functional representation. Isolated samples in this plane are relegated to spurious solutions owing to their unphysical features. The profiles of the distribution amplitudes across the orbit change in an orderly sequence of gradations with some mixture of COZ and GS characteristics until the COZ amplitude is transmuted into the heterotic solution. The variation with shape of the nucleon distribution amplitude with R is shown graphically in Fig. 14.

Despite differing functional representations of the nucleon distribution amplitudes (use of higher-order eigenfunctions with or without cutoffs), the results plotted in Fig. 11 show that all nucleon distribution amplitudes complying with the sum-rule constraints actually collapse to the fiducial orbit, thereby providing convincing evidence that the scaling relation between the ratio R and the expansion parameter B_4 reflects a genuine non-perturbative feature of the true nucleon distribution amplitude. To underline the hybrid character of the heterotic distribution amplitude, we show in Fig. 15 the invariant functions V , A , and

T associated with it in comparison with their counterparts for the optimized versions of the COZ and the GS models. To leading order $M = 2$, the algebraic expressions for these functions in terms of the expansion coefficients B_n are [35]:

$$\begin{aligned} V(x_i) = \phi_{\text{as}}(x_i) & \left[(B_0 + B_2 - 5B_3 - 5B_5) + \frac{1}{2} (B_1 - 3B_2 + 11B_3 + B_4 + 21B_5) (x_1 + x_2) \right. \\ & - (B_1 + B_4) x_3 - (4B_3 + 14B_5) x_1 x_2 + \frac{1}{6} (12B_3 - 4B_4 - 28B_5) (x_1^2 + x_2^2) \\ & \left. + \frac{1}{3} (24B_3 + 4B_4 + 14B_5) x_3^2 \right], \end{aligned} \quad (99)$$

$$\begin{aligned} A(x_i) = \phi_{\text{as}}(x_i) & \left[\frac{1}{2} (-B_1 - 3B_2 + 3B_3 - B_4 - 7B_5) (x_1 - x_2) \right. \\ & \left. + \frac{1}{6} (-12B_3 + 4B_4 + 28B_5) (x_1^2 - x_2^2) \right], \end{aligned} \quad (100)$$

$$\begin{aligned} T(x_i) = \phi_{\text{as}}(x_i) & \left[(B_0 + B_2 - 5B_3 - 5B_5) + (-3B_2 + 7B_3 + 7B_5) x_3 \right. \\ & \left. + (4B_3 + 14B_5) x_1 x_2 + \left(8B_3 + \frac{14}{3} B_5 \right) (x_1^2 + x_2^2) \right], \end{aligned} \quad (101)$$

where the appropriate coefficients for every model have to be inserted.¹³ While V_{Het} has a symmetry pattern similar to that of V_{GS} (one main maximum in the central region), T_{Het} is characterized by two maxima, much the same as T_{COZ} . The inverse heterotic combination is realized by the “mirror” solution $\Phi_N^{\text{Het}'}$ (see Table 4).

These remarks can be put on more mathematical grounds by considering a classification scheme of the various nucleon distribution amplitudes based on the observation that the optimized versions of the COZ-type and GS-type amplitudes, we derived, are almost orthogonal to each other with respect to the weight $w(x_i) = \phi_{\text{as}}(x_i)/120$. Their normalized inner product $\langle \text{COZ}^{\text{opt}} | \text{GS}^{\text{opt}} \rangle$ yields 0.1607, which corresponds to an angle of 80.8° . Thus these functions form a quasi-orthogonal basis that can be used to continuously parameterize the nucleon distribution amplitudes in terms of a “hybridity” angle ϑ , defined by

$$\vartheta = \arctan \left(\frac{\langle \text{GS}^{\text{opt}} | i \rangle}{\langle \text{COZ}^{\text{opt}} | i \rangle} \right), \quad (102)$$

where the index i denotes collectively any of the nucleon distribution amplitudes listed in Tables 4 and 5. Here the bracket denotes the normalized inner product

¹³Note that at the central point $x_i = 1/3$,

$$V(x_i) = T(x_i) = \Phi_N(x_i) = \frac{120}{729} (27 - 12B_3 - 2B_5)$$

to leading order $M = 2$.

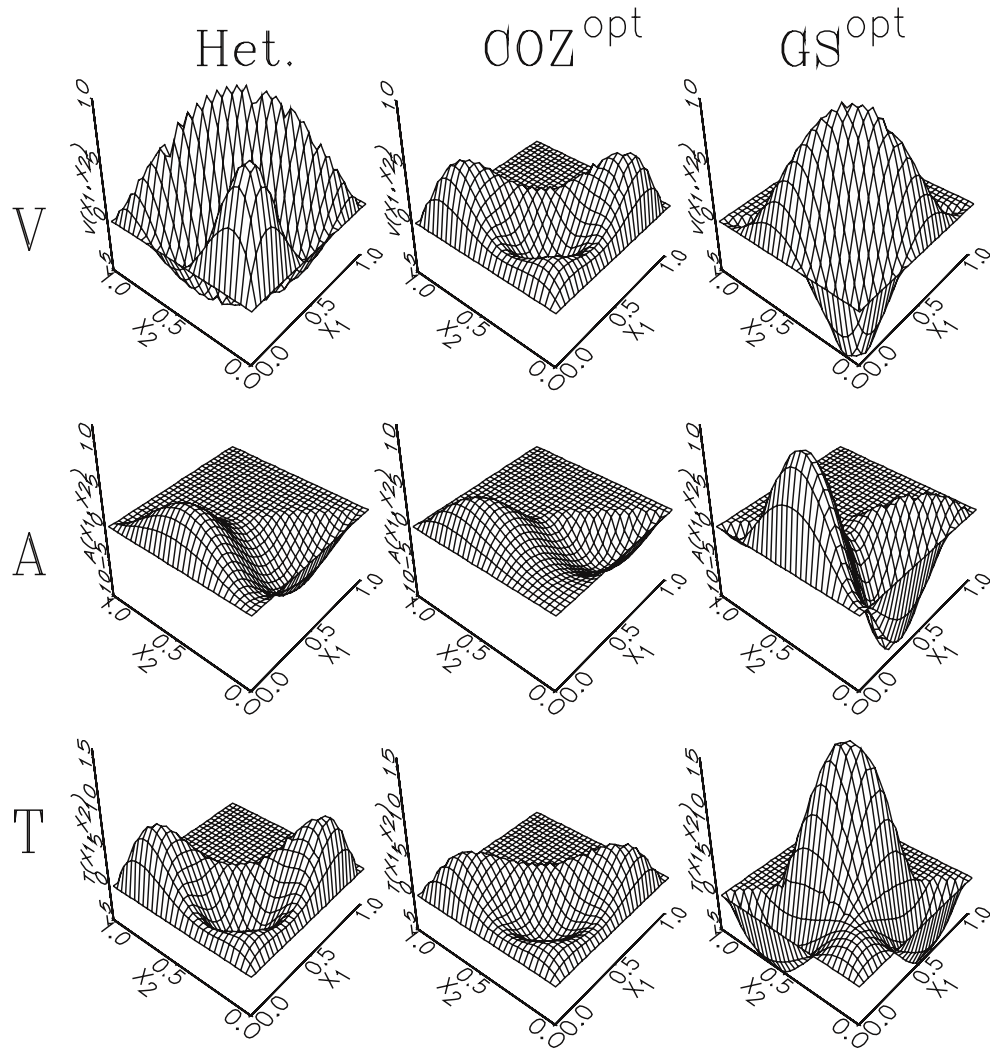


Figure 15. Invariant distribution amplitudes V , A , and T associated with the optimized versions of the COZ and GS models in comparison with the heterotic model.

$$\langle i|j \rangle \equiv \frac{(i,j)}{\|i\| \|j\|}, \quad (103)$$

where

$$(i,j) = \int_0^1 [dx] w(x_i) \Phi_i(x_k) \Phi_j(x_k) \quad (104)$$

and

$$\|i\| = \sqrt{(i,i)}. \quad (105)$$

The hybridity angle parameterizes the mingling of geometrical characteristics attributed to COZ-like and GS-like amplitudes and provides a quantitative measure for their presence in any solution conforming with the sum-rule constraints (see Fig. 16). The superimposed dashed line in Fig. 16(c) is a fit given by $\vartheta/[deg] = 8.5693 + 0.0160B_4 + 0.0073B_4^2 - 0.00067B_4^3$. The dashed line in Fig. 16(a) represents the empirical fit $R = 0.436415 - 0.005374B_4 - 0.000197B_4^2$. An improvement of this fit was presented above in connection with the orbit structure of the nucleon distribution amplitudes (cf. Fig. 11). The mixing of different geometrical characteristics is particularly relevant for the heterotic solution, which generically amalgamates features of both types of amplitudes (cf. Fig. 15). In this role, the heterotic model has the special virtue of simultaneously fitting the twin hopes for making reliable predictions with respect to the experimental data while being in agreement with the sum-rule constraints. The other models can be tuned to fit some aspects of the data, but never all aspects simultaneously.

To conclude this chapter, we remark that fixing the value of the ratio R by experiment, one could use the presented classification scheme to identify the corresponding nucleon distribution amplitude determined by theory.

F. DELTA DISTRIBUTION AMPLITUDES

The heterotic concept developed for the nucleon distribution amplitude can be extended to derive an optimal distribution amplitude for the $\Delta^+(1232)$ resonance as well [43]. The quark structure of this particle and the $N - \Delta$ transition form factor were investigated within the method of QCD sum rules by Farrar et al. “FZOZ” [44] (denoted by the acronyms of the authors), and independently by Carlson and Poor (CP) [45]. Both groups derived sum-rule constraints on the moments of the Δ distribution amplitude and used them to construct model distribution amplitudes in terms of low-order eigenfunctions ($M = 2$). Note that only symmetric eigenfunctions under permutations $x_1 \leftrightarrow x_3$ can contribute to the Δ distribution amplitude, so that $B_1 = B_4 = 0$. Thus the general form of the distribution amplitude for $M = 2$ is

$$\begin{aligned} \Phi_\Delta(x_i) = \phi_{as}(x_i) & \left[\left(8B_3^\Delta + \frac{14}{3}B_5^\Delta \right) (x_1^2 + x_3^2) + (-3B_2^\Delta + 7B_3^\Delta + 7B_5^\Delta) x_2 \right. \\ & \left. + (4B_3^\Delta + 14B_5^\Delta) x_1 x_3 + (B_0^\Delta + B_2^\Delta - 5B_3^\Delta - 5B_5^\Delta) \right]. \end{aligned} \quad (106)$$

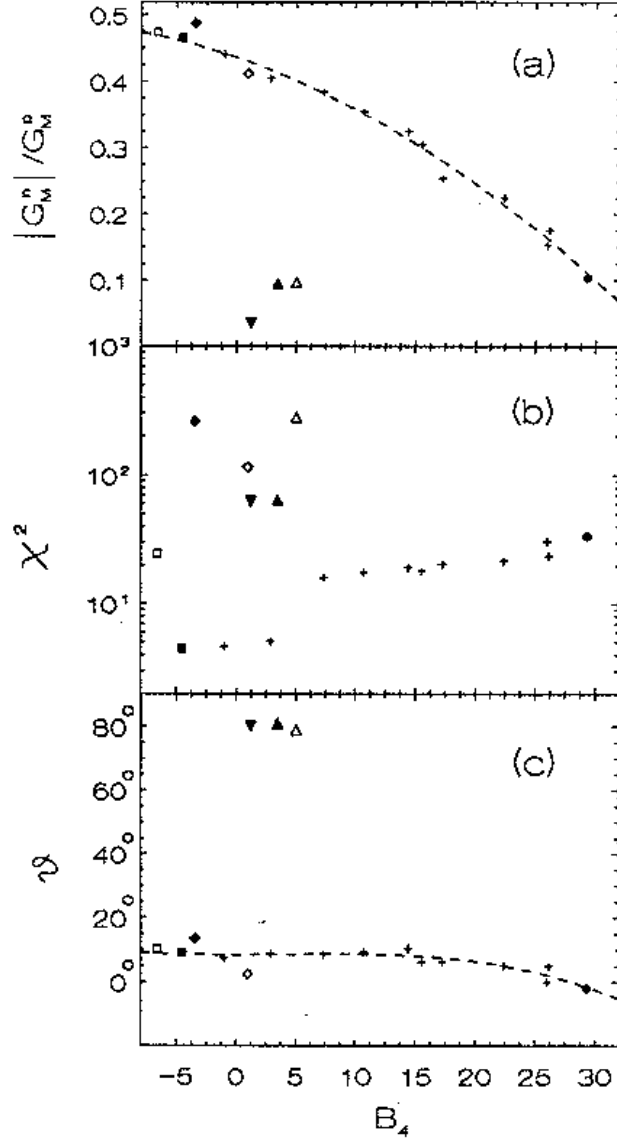


Figure 16. Classification scheme of nucleon distribution amplitudes complying with the constraints set by QCD sum rules (Table 3). (a) The ratio $R = |G_M^n|/G_M^p$ as a function of the expansion coefficient B_4 . The positions of the χ^2 minima are indicated (see Fig. 12). (b) Distribution of local minima of χ^2 (on a logarithmic scale) plotted vs B_4 . (c) Pattern of nucleon distribution amplitudes parameterized by the hybridity angle ϑ , defined in Eq. (102), vs B_4 . The dashed curves are the fits described in the text.

Table 6. Numerical values of the moments $n_1 + n_2 + n_3 \leq 3$ of model distribution amplitudes for the Δ^+ -isobar in comparison with the sum-rule constraints of Carlson and Poor (CP) [45] and those of Farrar, Zhang, Ogloblin, and Zhitnitsky (FZOZ) [44]. The numbers in parentheses are those published by FZOZ.

Moments ($n_1 n_2 n_3$)	Sum rules	Models			
	$T_\Delta(\text{FZOZ})$	CP	FZOZ	heterotic	FZOZ ^{opt}
(000)	1	1	1	1	1
(100)	0.31—0.35	0.350	0.325 (0.32)	0.321	0.325
(001)	0.35—0.40	0.300	0.350 (0.36)	0.357	0.350
(200)	0.14—0.16	0.160	0.150	0.140	0.156
(002)	0.15—0.18	0.123	0.160	0.151	0.154
(110)	0.07—0.1	0.101	0.080 (0.07)	0.078	0.071
(101)	0.09—0.13	0.089	0.095 (0.1)	0.103	0.098
(300)	0.06—0.09	0.085	0.083 (0.085)	0.073	0.090
(003)	0.06—0.10	0.060	0.085 (0.081)	0.071	0.078
(210)	0.025—0.04	0.039	0.030 (0.025)	0.027	0.026
(201)	0.04—0.06	0.035	0.037 (0.04)	0.040	0.040
(102)	0.035—0.06	0.031	0.037 (0.039)	0.040	0.038
$V_\Delta(\text{CP})$					
(001)	0.33—0.37	0.350	0.325	0.321	0.325
(002)	0.14—0.18	0.160	0.150	0.140	0.156
(101)	0.072—0.12	0.095	0.088	0.091	0.085

Note also that $T_\Delta(x_1, x_2, x_3) = [\Phi_\Delta(132) + \Phi_\Delta(231)]$ and that in addition $T_\Delta(x_1, x_2, x_3) = \Phi_\Delta(231)$ because $\Phi_\Delta(132) = \Phi_\Delta(231)$. The shapes of these two model distribution amplitudes look quite different, and also the predictions one can extract from them are different (see for details in subsequent chapters). While the CP amplitude has almost asymptotic profile, the FZOZ one exhibits two maxima. The corresponding sum rule estimates are compiled in Table 6. The same table contains also the moments of the proposed model distribution amplitudes.

Following again similar ideas of “heteroticity”, as in the nucleon case, one can attempt to combine the CP sum rules with those of FZOZ in order to obtain an amplitude that is capable to satisfy both sets simultaneously. The incentive is to obtain an amplitude that is optimized with respect to the sum-rule constraints as well as to improve its phenomenological capabilities. Both hopes can be satisfied by an amplitude termed again “Het”, derived in [43], and shown in Fig. 17. This amplitude satisfies all FZOZ moment constraints while providing the best possible compliance with those of CP (only one of their sum rules is violated). Concerning its shape, one sees that it is, nevertheless, close to the CP amplitude, though its maximum is somehow shifted towards the center of phase space.

There is yet another specific Δ amplitude [49], denoted “FZOZ^{opt}”, which was derived by demanding that the nucleon-Delta transition form factor, which involves in the nucleon

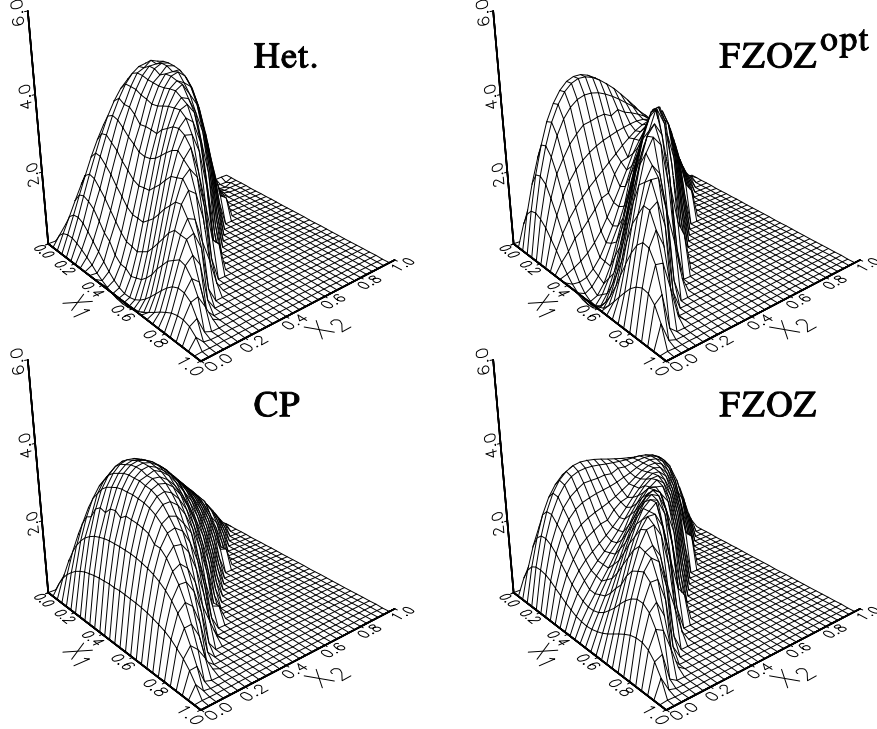


Figure 17. Profiles of model distribution amplitudes, defined in Table 7, for the Δ^+ -isobar, derived from QCD sum rules.

channel the COZ^{opt} distribution amplitude, is at least positive.¹⁴ Unfortunately, it turns out that this amplitude cannot reproduce any data (see below), though it is perfectly acceptable from the point of view of the sum rules. Thus we reiterate that optimum agreement with the moment sum rules – provided by COZ^{opt} – does not necessarily entail best phenomenological behavior. The expansion coefficients for all considered distribution amplitudes are listed in Table 7.

¹⁴All COZ-like distribution amplitudes yield N- Δ transition form factors compatible with zero.

Table 7. Expansion coefficients for Δ -isobar distribution amplitudes derived from QCD sum rules within a truncated expansion of eigenfunctions. Note that $B_0^\Delta = 1$ by normalization and that only eigenfunctions symmetric under $x_1 \leftrightarrow x_3$ contribute, i.e., $B_1^\Delta = B_4^\Delta \equiv 0$. As in the nucleon case, the notation of [35] is adopted.

Expansion coefficients	Models			
	CP	FZOZ	heterotic	FZOZ^{opt}
B_2^Δ	0.350	-0.175	-0.2499	-0.175
B_3^Δ	0.4095	1.071	0.3297	1.4117
B_5^Δ	0.1755	-0.486	-1.6205	-1.620

IV. ELECTROWEAK FORM FACTORS

The technical apparatus discussed in the previous chapters can now be used to calculate several electroweak form factors of the nucleon.

The standard differential inclusive cross section for electron-nucleon scattering in terms of directly measured quantities is

$$\frac{d^2\sigma}{d\Omega dE'} = \frac{\alpha_e^2}{4E^2 \sin^4 \frac{\theta}{2}} \left[2W_1(Q^2, \nu) \sin^2 \frac{\theta}{2} + W_2(Q^2, \nu) \cos^2 \frac{\theta}{2} \right], \quad (107)$$

where $E' = E - Q^2/2M_N^2$ and W_1 and W_2 are Lorentz-invariant structure functions of the target nucleon expressed in terms of Q^2 , $\nu = Q^2/2M_N = (E - E')$ is the energy loss of the incident lepton, and $q^2 = (P' - P)^2 = -4EE' \sin^2 \frac{\theta}{2} \leq 0$ ($Q^2 = -q^2 > 0$) is the four-momentum transfer. If the nucleon (with mass M_N) were a point-like particle like the electron, say, we would have $P^2 = P'^2 = M_N^2$ and $P \cdot q = M_N \nu$ so that $\nu = Q^2/2M_N$; furthermore, $W_1(Q^2)$ and $W_2(Q^2)$ would reduce respectively to $Q^2/4M_N$ and 1. Then Eq. (107) would simply be:

$$\frac{d^2\sigma}{d\Omega dE'} = \frac{4\alpha_e^2 E'^2}{Q^4} \left[\cos^2 \frac{\theta}{2} + \frac{Q^2}{2M_N^2} \sin^2 \frac{\theta}{2} \right] \delta \left(\nu - \frac{Q^2}{2M_N} \right). \quad (108)$$

Integrating over dE' one gets the familiar formula

$$\frac{d\sigma}{d\Omega} = \left(\frac{d\sigma}{d\Omega} \right)_{\text{Mott}} \frac{E'}{E} \left(1 + \frac{Q^2}{2M_N} \tan^2 \frac{\theta}{2} \right), \quad (109)$$

where the Mott differential cross section for a singly-charged point-like target, assumed to have an infinite mass, is $\alpha_e^2 \cos^2 \frac{\theta}{2} / 4E^2 \sin^4 \frac{\theta}{2}$. However, because of the internal (quark) structure of the nucleon, this differential cross section does not describe the elastic scattering of an electron off the nucleon. Hence, one has to assume that the incident electron is scattered elastically by a nucleon with a “diffuse” structure which can be revealed by increasing the momentum transfer. Then we can write Eq. (108) in the form

$$\begin{aligned} \frac{d^2\sigma}{d\Omega dE'} &= \frac{4\alpha_e^2 E'^2}{Q^4} \delta \left(\nu - \frac{Q^2}{2M_N} \right) \\ &\times \left\{ \left[\frac{G_E^2(Q^2) + (Q^2/4M_N^2) G_M^2(Q^2)}{1 + Q^2/4M_N^2} \right] \cos^2 \frac{\theta}{2} + \frac{G_M^2(Q^2)}{2M_N^2} \sin^2 \frac{\theta}{2} \right\}, \end{aligned} \quad (110)$$

where $G_E^2(Q^2)$ and $G_M^2(Q^2)$ are the electric and magnetic (“Sachs”) form factors of the nucleon, respectively, parameterizing in some sense our ignorance about its non-perturbative (binding) structure. A phenomenologically successful parameterization is provided by the empirical “dipole” form factor, *viz*:

$$\frac{G_E^2(Q^2)}{G_E^2(0)} = \frac{G_M^2(Q^2)}{G_M^2(0)} = \left(1 + \frac{Q^2}{0.71 \text{ GeV}^2} \right)^{-2}. \quad (111)$$

Obviously, the finite-size (“diffuse”) nucleon causes the elastic scattering cross section to decrease rapidly as Q^2 grows – in contrast to the behavior of a point-like nucleon described by Eq. (108). Hence, as long as there is a single hadron in the final state, there is an extremely rapid drop-off of the cross section for $Q^2 \gg 0.7 \text{ GeV}^2$. Clearly, the challenge is to calculate the nucleon’s form factors within QCD, employing for the intact nucleon wave functions of the sort we discussed in the previous sections.

A. NUCLEON FORM FACTORS

From Lorentz covariance, charge conservation, and invariance under space reflections there exist two electromagnetic form factors for a spin-1/2 particle. Then, in the Sachs parameterization, we have

$$\langle P' | J_\mu^{\text{em}}(0) | P \rangle = \frac{\tau}{2M_N} \bar{u}'(P') \left[G_E(q^2) K_\mu + \frac{i}{2M_N} G_M(q^2) R_\mu \right] u(P), \quad (112)$$

where $\tau = \left(1 + \frac{q^2}{4M_N^2}\right)^{-1}$, $K_\mu = (P_\mu + P'_\mu)$, and $R_\mu = \frac{-i}{2} (\gamma_\mu \not{P} \not{q} - \not{q} \not{P} \gamma_\mu)$ with normalizations as $G_E(0) = e_N$ ($e_p = 1, e_n = -1$); $G_M(0) = \mu$ being the total magnetic moment in units $e/2M_N$: $\mu_p = 2.7928$, $\mu_n = -1.9131$, and with the threshold condition $G_E(4M_N^2) = G_M(4M_N^2)$. The connection to the Dirac parameterization is established by the on-shell relation

$$\bar{u}'(P') i R_\mu u(P) = \bar{u}'(P') (2iM_N \sigma_{\mu\nu} q^\nu + q^2 \gamma_\mu) u(P) \quad (113)$$

with

$$\begin{aligned} F_1 &= \tau \left(G_E + \frac{q^2}{4M_N^2} G_M \right) && \text{Dirac form factor} \\ F_2 &= \tau (G_M - G_E) && \text{Pauli form factor} \\ G_E &= F_1 - \frac{q^2}{4M_N^2} F_2 && \text{electric form factor} \\ G_M &= F_1 + F_2 && \text{magnetic form factor} \end{aligned} \quad (114)$$

so that the on-shell nucleon current in the Dirac parameterization is given by

$$\langle P' | J_\mu^{\text{em}}(0) | P \rangle = \bar{u}'(P') \left[F_1(q^2) \gamma_\mu + \frac{i}{2M_N} F_2(q^2) \sigma_{\mu\nu} q^\nu \right] u(P). \quad (115)$$

Recalling Eq. (2), the nucleon helicity-conserving form factor can be written in convolution form as

$$G_M(Q^2) = \int_0^1 [dx] \int_0^1 [dy] \Phi^*(y_i, \tilde{Q}_y^2) T_H(x_i, y_i, Q^2, \alpha_s(\mu^2)) \Phi(x_i, \tilde{Q}_x^2). \quad (116)$$

In the evaluation of this expression one may encounter singularities owing to the fact that the gluon virtualities should enter the arguments of the strong coupling constant in T_H , i.e., $\alpha_s(\mu^2 = Q^2 x_i y_j)$. These virtualities depend on the longitudinal momentum fractions, and as a result, α_s becomes singular in the endpoint region. Several options have been suggested to avert this singularity:

- The simplest choice is to assume that one can use two *collective* scales, one for the hard and another for the soft gluon propagator, and then take the geometric average of both couplings in the form factor. In this way the dependence of α_s on the fractional momenta is avoided and α_s can be taken outside the integral, amounting to a rescaled Q^2 -dependent pre-factor (“peak approximation”). It seems reasonable to fix

the gluon scales by the gluon virtualities from that Feynman graphs which contribute most for each particular nucleon distribution amplitude by substituting the longitudinal momenta at the position of the main maximum of the corresponding nucleon distribution amplitude. Then one has $\bar{\alpha}_s(Q^2) = [\alpha_s(Q^2 v_{\text{hard}}) \alpha_s(Q^2 v_{\text{soft}})]^{1/2}$, where typically $v_{\text{hard}} = \bar{x}_i \bar{y}_i$ and $v_{\text{soft}} = x_j y_j$. This technique was used in several works, like [30,33,53,35,42], and the results are quite reasonable.

- A refined version of this approximation was proposed by Stefanis in [35]. Recalling that there are in total 8 topologically distinct diagrams which give non-zero contributions to the form factor, one can use the virtualities of the hard and soft gluon propagators in each individual diagram to calculate the corresponding α_s values. This procedure improves the predictions, though this improvement depends on the specific nucleon distribution amplitude used; for example, the effect when using the CZ-distribution amplitude is negligible [35].
- In both cases considered above, one can only change the absolute value of the form factor but not its slope. This can only be improved if α_s can be retained inside the integral. To this end, one can either cutoff α_s explicitly – typically between 0.5 to 07 – or saturate its momentum dependence by introducing, say, an effective gluon mass. Such an analysis was performed in [120], having recourse to a modified expression for α_s , proposed by Cornwall [121] (see also [122]):

$$\alpha_s(Q^2) = \frac{4\pi}{\beta_0 \ln \left[\left(Q^2 + 4m_g^2 \right) / \Lambda_{\text{QCD}}^2 \right]}. \quad (117)$$

Here m_g stands for the effective gluon mass with values in the range (500 ± 200) MeV. Technically, m_g is an IR-cutoff serving implicitly to regularize that gluon propagator which becomes soft (compared to the large external momentum) in the endpoint region. It is evident that such a nonzero gluon mass will “freeze” the value of the running coupling constant for $Q^2 \leq 4m_g^2$. Since a dynamically generated (gluon) mass is not a constant but vanishes at large momentum, the asymptotic behavior is not affected. Strictly speaking, one should use to saturate α_s a scale-dependent gluon mass which is governed by the renormalization group equation with an appropriate anomalous dimension [121]. Such a saturation procedure was adopted in [43] and will be presented below. Physically, the IR regularization of α_s connects to our previous discussion concerning the existence of a fundamental IR scale in the non-perturbative regime. This scale may be thought of as being the average transverse momentum of vacuum partons and is of order 300 MeV to 600 MeV, but cannot be reliably computed at present. Within the framework of quark/gluon condensates, this scale separates hard from soft momentum flows of gluon (or quark) propagators which go into the corresponding condensates. It is also worth noting that according to Cornwall, m_g and Λ_{QCD} are interrelated by the consistency relation $m_g/\Lambda_{\text{QCD}} \approx 1.5 - 2.0$. It was warned in [35] that the treatment in [120] violates this relation, handling m_g as an additional fit parameter for improving the slope of the form factors.

- Another, theoretically more appealing, possibility is provided by including in the calculation of the form factor gluon radiative corrections in the form of Sudakov-type

damping exponentials [76]. This procedure is technically more complicated though theoretically more sound than, more or less plausible, cutoff or saturation prescriptions. The “Sudakov option” will be discussed in detail in the second main part of this report.

In the remainder of this chapter we shall present results obtained within the peak approximation. In this case, the nucleon form factor can be cast in the form [30]

$$Q^4 G_M^N(Q^2) = \frac{1}{54} \left[4\pi \bar{\alpha}_s(Q^2) \right]^2 |f_N|^2 \int_0^1 [dx] \int_0^1 [dy] \left[2 \sum_{i=1}^7 e_i T_i(x_j, y_j) + \sum_{i=8}^{14} e_i T_i(x_j, y_j) \right], \quad (118)$$

where the amplitudes $T_i(x_j, y_j) = \Phi_i(x_j) T_H(x_j, y_j) \Phi_i(y_j)$ represent convolutions of T_H with the appropriate distribution amplitudes evaluated term by term for each contributing diagram (marked by the index “i”). Inputting

$$\begin{aligned} \Phi_N(x_i) = & \phi_{as}(x_i) \left[(B_0 + B_2 - 5B_3 - 5B_5) + (B_1 + B_4)(x_1 - x_3) + (-3B_2 + 7B_3 + 7B_5)x_2 \right. \\ & \left. + (4B_3 + 14B_5)x_1x_3 + (8B_3 - \frac{4}{3}B_4 + \frac{14}{3}B_5)x_1^2 + (8B_3 + \frac{4}{3}B_4 + \frac{14}{3}B_5)x_3^2 \right] \end{aligned} \quad (119)$$

and integrating over variables x_i and y_i , the proton and neutron form factors acquire the following form

$$Q^4 G_M^p(Q^2) = \frac{1}{54} \left[4\pi \bar{\alpha}_s(Q^2) \right]^2 |f_N|^2 I^p, \quad (120)$$

$$Q^4 G_M^n(Q^2) = \frac{1}{54} \left[4\pi \bar{\alpha}_s(Q^2) \right]^2 |f_N|^2 I^n, \quad (121)$$

where I^p and I^n are functions of the coefficients B_n . Analytic expressions for I^p and I^n up to order $M = 2$ ($n = 0, 1, 2, \dots, 5$) were published in [35]; such up to order $M = 3$ ($n = 0, 1, 2, \dots, 9$) are given in Appendix B.

The results for the main models in use are shown in Fig. 18 in comparison with existing data [34] (for the proton) and [123] (for the neutron). Note that the Q^2 -evolution of the coefficients B_n has been neglected and that the average value $\bar{\alpha}_s(Q^2) = [\alpha_s(Q^2 \bar{x}_i \bar{y}_i) \alpha_s(Q^2 x_j y_j)]^{1/2}$ has been used to account for the different virtualities of the involved gluon propagators. For instance, for the heterotic amplitude we use $\bar{\alpha}_s(Q^2) = [\alpha_s(Q^2 \times 0.427) \alpha_s(Q^2 \times 0.178)]^{1/2}$. Here and below the values $\Lambda_{\text{QCD}} = 180$ MeV [124] and $|f_N| = 5.0 \times 10^{-3}$ GeV² [37,38] are taken.

Since there are no direct data on G_M^n beyond, say, 5 GeV², it is virtually impossible to extract experimental values of the neutron form factors in a model-independent way. Therefore, we show in Fig. 18 the theoretical predictions along with G_M^n -data, extracted under the proviso of two extreme, albeit reasonable assumptions: (1) assuming that the electric neutron form factor is at least of the order of the magnetic one (open circles), and (2) assuming $G_E^n = 0$ (black dots).

The main conclusion to be inferred from these results is twofold: (1) The heterotic model yields the best relative agreement with the experimental data, though the prediction for the

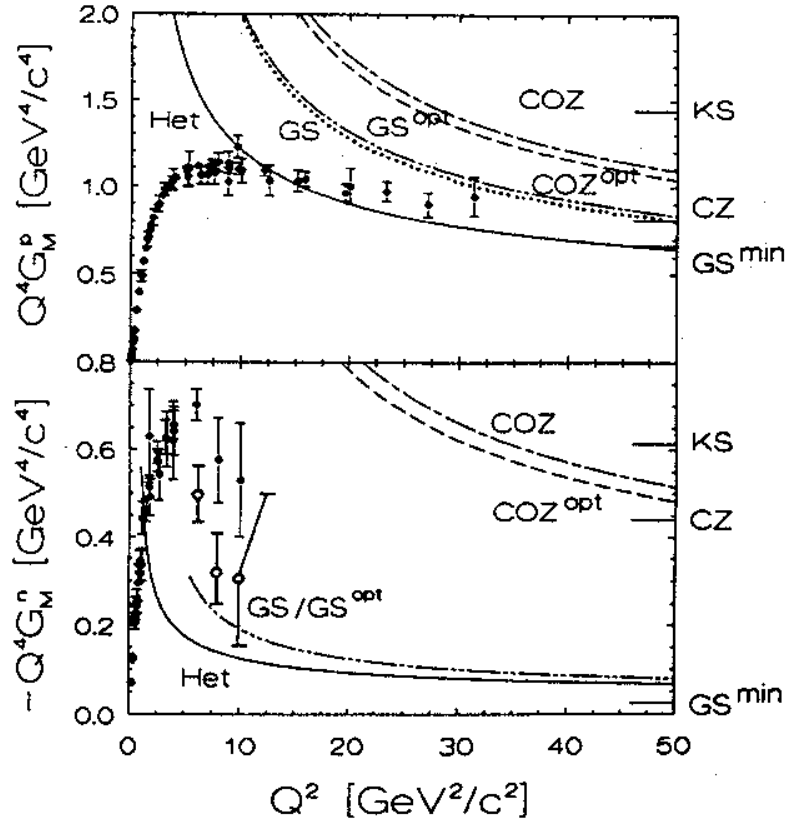


Figure 18. Comparison with available data of the magnetic form factor of the proton and the neutron for the heterotic and other model distribution amplitudes, labeled by the acronyms of the corresponding authors.

neutron form factor is too small to account for the observed form factor. (2) The COZ^{opt} amplitude – designed to yield optimum agreement with the COZ sum rules – fails in both cases to describe the experimental data.

Another place to test these results is in the data for the elastic cross sections σ_p and σ_n . For small scattering angles, where the terms $\propto \tan^2(\theta/2)$ can be neglected, there are two main possibilities for the ratio σ_n/σ_p . If the Dirac form factor F_1^n is zero, or small compared to the Pauli form factor F_2^n [125], then σ_n should be due only to the higher-order term F_2^n . At large Q^2 the ratio would become

$$\frac{\sigma_n}{\sigma_p} \Rightarrow \left(\frac{C_2^n}{C_1^p} \right)^2 \frac{1}{4M_N^2 Q^2} \quad (122)$$

(modulo logarithmic corrections due to anomalous dimensions) and would decrease with increasing Q^2 due to the extra power of $1/Q^2$ of the Pauli form factor. Alternatively, if F_1^n is comparable to F_2^n , then σ_n would eventually be due to F_1^n at large Q^2 . Then the ratio σ_n/σ_p would be given by some constant determined by the nucleon wave functions

$$\frac{\sigma_n}{\sigma_p} \Rightarrow \left(\frac{C_1^n}{C_1^p} \right)^2. \quad (123)$$

In the above expressions, the wave-function characteristics are parameterized by the (dimensionful) coefficients C_i , which are functions of the expansion coefficients B_n and the “proton decay constant” $|f_N| = (5.0 \pm 0.3) \times 10^{-3} \text{ GeV}^2$ [38,37].

From this analysis it follows that in the Q^2 domain where the helicity-flipping parts of the form factors can be ignored, σ_n/σ_p should be within the range 0.238 and 0.01. If the results of the combined KS/COZ sum rules are taken seriously, then this range is somewhat shifted: $0.232 \div 0.005$. Comparing with available data [123], we see that the measured value of σ_n/σ_p enters the estimated range already at $Q^2 \approx 8 \text{ GeV}^2/c^2$ (see Fig. 19). Here two concluding remarks are in order: (1) The present accuracy of QCD sum rules (modulo technicalities) is sufficient to provide bounds on σ_n/σ_p within the observed region. (2) The available data in the range $Q^2 \approx (8 \div 10) \text{ GeV}^2/c^2$ are well below the calculated upper bound and still decreasing. This indicates that distribution amplitudes which give $|G_M^n|/G_M^p \approx 0.5$ may be in contradiction to experiment because they yield a Dirac form factor F_1^n which starts to overestimate the data already at $Q^2 \approx 8 \text{ GeV}^2/c^2$. In particular, there is no room for contributions due to the Pauli form factor. On the contrary, models which give a small value of $|G_M^n|/G_M^p$ can explain the data only under the assumption that in this Q^2 region the Pauli contribution is still dominant. For instance, the heterotic model requires at $Q^2 = 10 \text{ GeV}^2/c^2$ a Pauli contribution to the neutron form factor approximately three times as large as that from the Dirac form factor. The principal result from this discussion is that in the intermediate Q^2 domain, σ_n/σ_p should be within the range 0.238 and 0.001.

We close this section by presenting results for the axial-vector and isoscalar axial-vector form factors of the nucleon. These form factors were analyzed with perturbative QCD by Carlson and Poor in [126] and [127]. The axial-vector currents in question are:

$$A_\mu = \bar{d}\gamma_\mu\gamma_5 u, \quad A_\mu^{(3)} = \frac{1}{2} \left(\bar{u}\gamma_\mu\gamma_5 u - \bar{d}\gamma_\mu\gamma_5 d \right), \quad (124)$$

$$A_\mu^{(S)} = \frac{1}{2} \left(\bar{u}\gamma_\mu\gamma_5 u + \bar{d}\gamma_\mu\gamma_5 d \right). \quad (125)$$

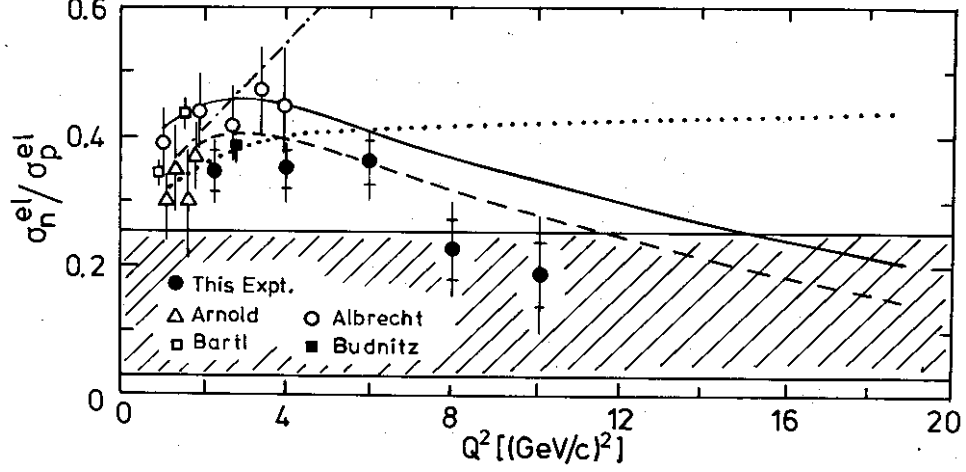


Figure 19. Bounds on the elastic cross sections σ_n/σ_p obtained from QCD sum rules (shaded area). The data are taken from [123].

The first two currents are related by an isospin rotation. Then the axial-vector form factor g_A and the pseudoscalar form factor g_P are defined by the matrix element with nucleon states as follows

$$\langle n(P', \lambda') | A^\mu p(P)(P, \lambda) \rangle = \bar{u}_\lambda(P') \left[g_A(Q^2) \gamma^\mu \gamma^5 + g_P(Q^2) q^\mu \gamma^5 \right] u_\lambda(P) , \quad (126)$$

where $q = P' - P$, and $Q^2 = -q^2$. The axial-vector form factor can be isolated by taking the A^+ component and working in a frame with $q^+ = 0$. Then

$$\langle n | A^+ | p \rangle = 2P^+ g_A , \quad (127)$$

and

$$\begin{aligned} \langle p | A^{+(3)} | p \rangle &= 2P^+ G_A^{(3)} , \\ \langle p | A^{+(S)} | p \rangle &= 2P^+ G_A^{(S)} . \end{aligned} \quad (128)$$

The first two form factors are related by isospin invariance to give

$$G_A^{(3)} = \frac{1}{2} g_A \quad (129)$$

while the last one is the non-leading isoscalar form factor. Both form factors can be cast in convolution form to read

$$g_A(Q^2) = \int_0^1 [dx] \int_0^1 [dy] \Phi(y_i, Q^2) T_{H5}(x_i, y_i, Q^2) \Phi(x_i, Q^2) , \quad (130)$$

$$G_A^{(S)}(Q^2) = \int_0^1 [dx] \int_0^1 [dy] \Phi(y_i, Q^2) T_{H5}^{(S)}(x_i, y_i, Q^2) \Phi(x_i, Q^2) . \quad (131)$$

Assuming, as previously, constant arguments of the strong coupling constants and expanding the nucleon distribution amplitudes in terms of their eigenfunctions within the basis of Appell polynomials, the integrals over the fractional momenta can be carried out to arrive at the following expressions

$$Q^4 g_A(Q^2) = \left(\frac{4\pi}{27}\right)^2 [\alpha_s(Q^2)]^2 I_A, \quad (132)$$

$$Q^4 G_A^{(S)}(Q^2) = \left(\frac{4\pi}{27}\right)^2 [\alpha_s(Q^2)]^2 I_S, \quad (133)$$

where I_A and I_S are functions of the non-perturbative expansion coefficients B_n . Carlson and Poor truncate the eigenfunctions decomposition at leading order $M = 2$. A more general expression for g_A which includes the next-to-leading order eigenfunctions ($M = 3$) is given in Appendix B.

Let us now present some results for the heterotic model. The calculation for the nucleon axial form factor $g_A(Q^2)$ according to [126] yields at $Q^2 \approx 10 \text{ GeV}^2$, $Q^4 g_A(Q^2) = 0.90 \text{ GeV}^4$ for $\Lambda_{\text{QCD}} = 100 \text{ MeV}$, and $Q^4 g_A(Q^2) = 1.44 \text{ GeV}^4$ for $\Lambda_{\text{QCD}} = 180 \text{ MeV}$. These results compare fairly well with the value $Q^4 g_A(Q^2) \approx 1.5 \text{ GeV}^4$ extrapolated from the data [128]. Also the ratio $g_A(Q^2)/G_M^p(Q^2) \approx 1.19$, in the region where the calculations can still be trusted, is consistent with the (extrapolated) experimental value $g_A(Q^2)/G_M^p(Q^2) \approx 1.35$. As for the isoscalar nucleon form factor [127], we find at $Q^2 \approx 10 \text{ GeV}^2$, $Q^4 G_A^{(S)}(Q^2) = 0.83 \text{ GeV}^4$ for $\Lambda_{\text{QCD}} = 100 \text{ MeV}$ and $Q^4 G_A^{(S)}(Q^2) = 1.34 \text{ GeV}^4$ for $\Lambda_{\text{QCD}} = 180 \text{ MeV}$. Assuming isospin invariance, we combine these results with those for g_A to obtain $G_A^{(S)}/G_A^{(3)} \approx 1.85$, where $G_A^{(3)}$ is the isovector axial-vector nucleon form factor. If a dipole form

$$G_A^{(S)}(Q^2) = \frac{G_A^{(S)}(0)}{(1 + Q^2/M_{AS}^2)^2}, \quad (134)$$

with $G_A^{(S)}(0) = 0.38$ from $SU(6)$, is used to describe the Q^2 dependence of $G_A^{(S)}$ [127], then, in the high- Q^2 region, the heterotic model yields $M_{AS} = (1.15 - 1.22) \text{ GeV}$ for $\Lambda_{\text{QCD}} = 100 \text{ MeV}$ and $M_{AS} = (1.27 - 1.37) \text{ GeV}$ for $\Lambda_{\text{QCD}} = 180 \text{ MeV}$. These values comply with the experimental value $M_A = (1.032 \pm 0.036) \text{ GeV}$. More systematic results are compiled in Table 8.

B. NUCLEON-DELTA TRANSITION FORM FACTOR

The electromagnetic $N - \Delta$ transition is another exclusive process which offers the possibility to test the quality of the model distribution amplitudes for the nucleon and the Δ resonance, obtained in the previous chapters. This process involves only interactions mediated by vector bosons so that, neglecting quark masses, quark helicity is conserved. Hence, analogously to the elastic electron-nucleon scattering, one can define a helicity-conserving form factor $G_M^{N \rightarrow \Delta}$ which according to perturbative QCD should fall off like $1/Q^2$ when Q^2 becomes large. On the experimental side, there are no exclusive data for Q^2 above 3 GeV^2 , though there are inclusive results, obtained in SLAC experiment E133 spanning the Q^2 range $2.5 - 10.0 \text{ GeV}^2$ [48].

Table 8. Values of the axial-vector form factor g_A and the isoscalar axial-vector form factor $G_A^{(S)}$ at $Q^2 = 10 \text{ GeV}^2/c^2$ for $\Lambda_{\text{QCD}} = 180 \text{ MeV}$. The estimated empirical dipole masses M_A , M_{AS} are also shown for some selected model distribution amplitudes for the nucleon.

Model	$Q^4 g_A$	M_A	$Q^4 G_A^{(S)}$	M_{AS}	$G_A^{(S)}/G_A^{(3)}$	g_A/G_M^p
Het	1.4374	1.0347	1.3379	1.3700	1.862	1.195
COZ^{opt}	4.1185	1.3462	1.6104	1.4348	0.782	1.531
GS^{opt}	2.2419	1.2236	2.4376	1.5915	2.175	1.111
CZ	3.5349	1.2957	1.2152	1.3373	0.688	1.529
COZ	4.2747	1.3588	1.6404	1.4414	0.768	1.536
KS	6.1508	1.4882	2.8808	1.6593	0.937	1.489
GS	2.2130	1.1526	2.2436	1.5588	2.028	1.119

The form factor $G_M^{N \rightarrow \Delta}$ was calculated within perturbative QCD by Carlson [129]. Starting from the convolution form

$$G_M^{N \rightarrow \Delta}(Q^2) = \int_0^1 [dx] \int_0^1 [dy] \Phi_\Delta(y_i, \tilde{Q}_y) T_H(x_i, y_i, Q) \Phi_N(x_i, \tilde{Q}_x), \quad (135)$$

the result after integrating over longitudinal momenta can be expressed in the following form

$$Q^4 G_M^*(Q^2) = \left[\frac{4\pi\alpha_s(Q^2)}{27} \right]^2 \frac{\sqrt{2}}{3} I^{(\Delta)}, \quad (136)$$

where it is assumed that the argument of α_s depends on Q^2 only, and $I^{(\Delta)}$ is a function of the expansion coefficients B_n^Δ which project the Δ distribution amplitude on to the eigenfunctions of the interaction kernel:

$$I^\Delta \simeq \sum E_{ij} B_i^{(\Delta)} B_j^{(N)}. \quad (137)$$

The hard part of the process derives from T_H , encountered in the calculation of the nucleon form factor, so that Φ_Δ can be expanded over the same eigenfunctions basis, i.e., the Appell polynomials. The difference here is that, as stated in Subsection III F, only symmetric terms under $x_1 \leftrightarrow x_3$, contribute. The coefficients E_{ij} in Eq. (137) are calculable with perturbative QCD. Their values for $i, j = 0, 1, \dots, 5$ are tabulated in [129]. The non-perturbative expansion coefficients $B_n^{(N)}$ can be taken from Table 4, those for $B_n^{(\Delta)}$ from Table 7. Several options are possible, depending on the favored choice among the various distribution amplitudes. In Fig. 20 we show predictions (solid lines) for $\gamma p \Delta^+$, calculated with the heterotic distribution amplitude for the nucleon and various Δ distribution amplitudes, in comparison with existing experimental data (see [48,130]). The short horizontal lines on the right margin are predictions for the absolute value of G_M^* at $Q^2 = 15 \text{ GeV}^2$ from other nucleon distribution amplitudes, listed in Table 4. In all considered cases the CP value $|f_\Delta| = 11.5 \times 10^{-3} \text{ GeV}^2$ has been used, which is within the spread of the FZOZ estimate. We emphasize that the sign of G_M^* predicted by CZ [30], COZ [38], and GS [33] comes out negative for all Δ distribution amplitudes discussed here, except for the amplitude FZOZ^{opt} which yields for COZ^{opt} a small positive form factor by construction. In contrast, convolution of FZOZ^{opt} with the

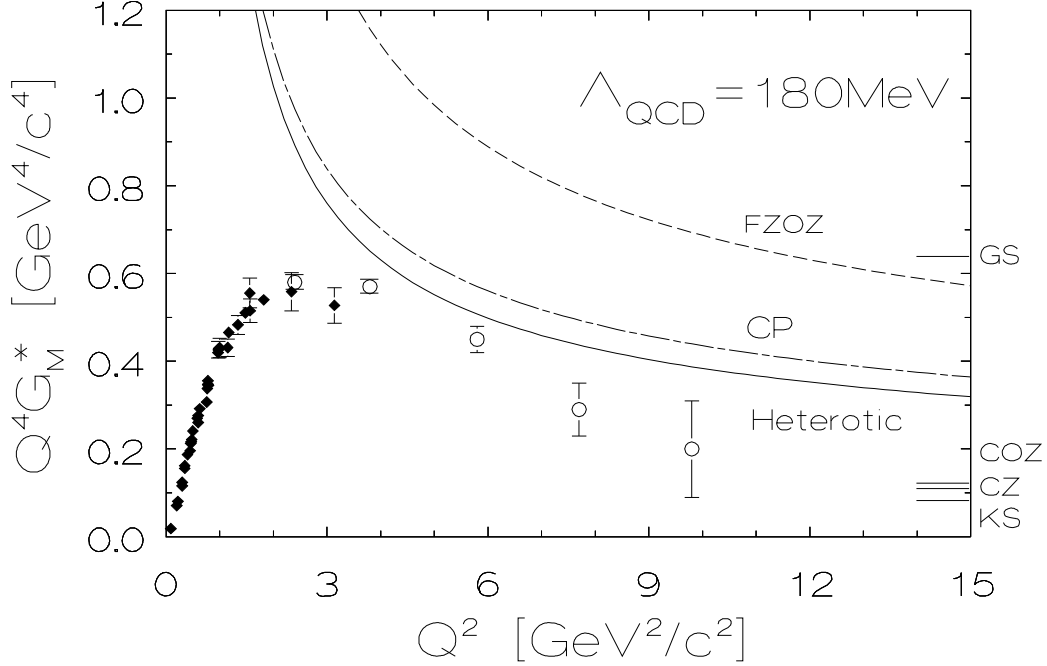


Figure 20. Transition form factor $\gamma p \Delta^+$, calculated with the heterotic distribution amplitude for the nucleon [42,43] and various Δ^+ distribution amplitudes in comparison with existing experimental data (see [130]). The dashed-dotted line shows a calculation [43] which takes into account a dynamical gluon mass to saturate α_s at low Q^2 . The dashed line illustrates the effect of evolution of the coefficients B_n^Δ . Predictions from previous nucleon distribution amplitudes are indicated on the right margin. The open circles denote the data from Stoler's [48] analysis. Note that for all curves the value $|f_\Delta| = 11.5 \times 10^{-3} \text{ GeV}^2$ from [45] has been used.

heterotic nucleon distribution amplitude yields a form factor which overshoots the data by orders of magnitude. Only the heterotic nucleon distribution amplitude and the KS [37] one yield a positive sign for G_M^* and only the heterotic Δ distribution amplitude comes close to the data.

This agreement can be significantly improved. In order to account for (unknown) confinement effects at low Q^2 , we saturate α_s in the one-loop approximation by introducing an effective gluon mass [121]: $\alpha_s(Q^2) \mapsto \alpha_s(Q^2 + 4m_g^2(Q^2))$. In contrast to other approaches of this type [120,119], we use a dynamical, i.e., scale-dependent gluon mass derived by Cornwall [121]:

$$m_g^2(Q^2) = m_g^2 \left[\ln \left(\frac{Q^2 + 4m_g^2}{\Lambda_{QCD}^2} \right) / \ln \left(\frac{4m_g^2}{\Lambda_{QCD}^2} \right) \right]^{-12/11}. \quad (138)$$

Due to the positivity of the anomalous dimension of the mass operator, this gluon mass vanishes asymptotically. This soft behavior at short distances leaves the validity of form-factor evolution at large momentum transfer virtually unaffected (as it should, if the dynamical mass generation is to be consistent with the renormalization group). In the fit represented by the dashed-dotted line (Fig. 20) we use $m_g = 380 \text{ MeV}$, which matches Cornwall's consistency relation, mentioned previously. Referring to the same figure, we see that including

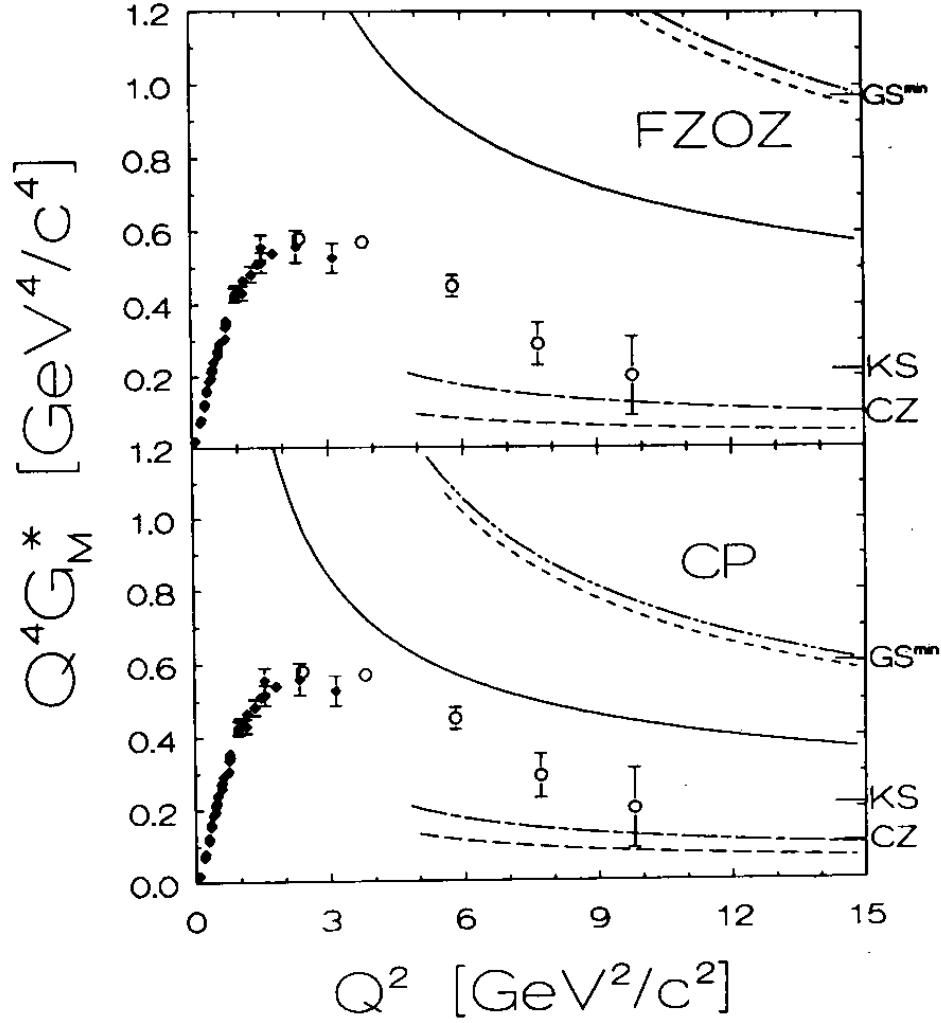


Figure 21. Transition form factor $\gamma p \Delta^+$, calculated with the FZOZ (top figure) and the CP distribution amplitude (lower figure) for the Δ resonance, and various nucleon distribution amplitudes in comparison with existing experimental data (see [130]). The dashed-dotted line shows the calculation with the COZ distribution amplitude; the dashed line that one with the COZ^{opt} distribution amplitude. Predictions from previous nucleon distribution amplitudes are again indicated on the right margin. The open circles denote the data from Stoler's [48] analysis. Note that for all curves the value $|f_\Delta| = 11.5 \times 10^{-3} \text{ GeV}^2$ from [45] has been used.

the perturbative Q^2 evolution of the coefficients B_n^Δ , it is sufficient to provide a good fit to the data above $Q^2 \approx 3 \text{ GeV}^2/c^2$ (dashed line) (see, the recent data analysis in [46,47]). At lower Q^2 values, additional non-perturbative parameters have to be introduced, e.g., parton transverse momenta, effective parton masses, higher-twist contributions, quark clustering, etc. to account for the limitations of the leading-order formalism. In a recent analysis [131] Belyaev and Radyushkin calculated on the basis of local quark-hadron duality the purely non-perturbative soft contribution to the $\gamma^* p \rightarrow \Delta$ form factor and showed that their result can account for the observed behavior of the form factor at Q^2 values as low as 3 GeV^2 . They also argued that this contribution remains leading up to the highest laboratory Q^2 values without any need for the contribution due to hard-gluon exchange (embedded in T_H). It is clear that experimental efforts to measure G_M^* beyond $10 \text{ GeV}^2/c^2$ would be extremely helpful to discriminate among these options.

To complete our discussion, we show in Fig. 21 the form-factor predictions for G_M^* obtained from other nucleon distribution amplitudes in convolution with the model Δ distribution amplitudes of CP (top figure) and FZOZ (lower figure). One may interpret these figures as indicating that none of the shown amplitudes neither for the nucleon nor for the Δ can account for the observed behavior of the form factor. COZ-type distribution amplitudes for the nucleon exhibit strong cancellation of symmetric vs antisymmetric contributions [132], while GS-type distribution amplitudes yield unrealistically large negative contributions.

V. CHARMONIUM DECAYS

The last phenomenological application we consider here within the standard convolution scheme here deals with exclusive decays of charmonium states to $p\bar{p}$ and $\Delta\bar{\Delta}$. Such decays are sensitive to the nucleon (Δ) distribution amplitude and hence may serve to discriminate among proposed models. Calculations of charmonium decays have been performed by many authors [36,133,134,135] within the QCD convolution framework. We follow [36]. We consider first the 3P_J states with $J = 1, 2$. The branching ratio for the decay of the χ_{c1} state ($J^{PC} = 1^{++}$) into $p\bar{p}$ is given by¹⁵

$$\text{BR} \left(\frac{{}^3P_1 \rightarrow p\bar{p}}{{}^3P_1 \rightarrow \text{all}} \right) \approx \frac{0.75}{\ln(\bar{M}/\Delta)} (\pi\alpha_s)^3 \frac{16\pi^2}{729} \left| \frac{f_N}{\bar{M}^2} \right|^4 M_1^2, \quad (139)$$

where $\bar{M} \approx 2m_c \approx 3 \text{ GeV}$ and $\Delta = 0.4 \text{ GeV}$ (the last value from [136]). The non-perturbative content of Eq. (139) is due to f_N and the decay amplitude for the process $^3P_1 \rightarrow p\bar{p}$, denoted M_1 , which involves Φ_N . Inserting expression (119), in connection with Table 4, the decay amplitude M_1 for each model is computed with an elaborate integration routine which properly takes account of contributions near singularities [104]. The results for different model distribution amplitudes are compiled in Table 9.

The analogous expression to (139) for the χ_{c2} state ($J^{PC} = 2^{++}$) has the form

¹⁵I wish to thank Victor Chernyak for bringing to my attention that the factor $(\pi\alpha_s)^3$ was missing in [36,42,103].

Table 9. Exclusive charmonium decays into $p\bar{p}$ for a variety of nucleon distribution amplitudes. The data are taken from [137]. The numbers in parentheses are those given in [36]. The decay amplitudes termed M_0 were independently verified by Bolz [138].

Models	$M(^3P_1 \rightarrow p\bar{p}) = M_1$	$M(^3P_2 \rightarrow p\bar{p}) = M_2$	$M(^3S_1 \rightarrow p\bar{p}) = M_0$
heterotic	99849.6	515491.2	13726.8
CZ	28310.4 (0.63 $\times 10^5$)	246052.8 (2.87 $\times 10^5$)	7545.6 (0.72 $\times 10^4$)
COZ	53625.6 (0.88 $\times 10^5$)	298123.2 (3.4 $\times 10^5$)	8758.8 (0.79 $\times 10^4$)
COZ ^{opt}	55137.6	289728.0	8499.6
GS	26366.4	232632.0	928.8 (0.7 $\times 10^3$)
GS ^{opt}	19915.2	230659.2	986.4
GS ^{min}	17193.6	210729.6	964.8
KS	94723.2 (1.35 $\times 10^5$)	416937.6 (4.84 $\times 10^5$)	11484.0 (1.15 $\times 10^4$)
rm asympt.	20086.6 (0.2 $\times 10^5$)	43099.2 (0.43 $\times 10^5$)	1517.4 (0.14 $\times 10^4$)
Observables	$\text{BR}\left(\frac{^3P_1 \rightarrow p\bar{p}}{^3P_1 \rightarrow \text{all}}\right)$ in %	$\text{BR}\left(\frac{^3P_2 \rightarrow p\bar{p}}{^3P_2 \rightarrow \text{all}}\right)$ in %	$\Gamma(^3S_1 \rightarrow p\bar{p})$ [eV]
heterotic	0.22×10^{-2}	0.89×10^{-2}	138.37
CZ	0.017×10^{-2}	0.20×10^{-2}	41.81
COZ	0.06×10^{-2}	0.30×10^{-2}	56.34
COZ ^{opt}	0.066×10^{-2}	0.28×10^{-2}	53.07
GS	0.014×10^{-2}	0.18×10^{-2}	0.63
GS ^{opt}	0.086×10^{-3}	0.18×10^{-2}	0.71
GS ^{min}	0.066×10^{-3}	0.15×10^{-2}	0.68
KS	0.198×10^{-2}	0.59×10^{-2}	96.84
asympt.	0.086×10^{-3}	0.01×10^{-2}	1.69
E760	$(0.78 \pm 0.10 \pm 0.11) \times 10^{-2}$	$(0.91 \pm 0.08 \pm 0.14) \times 10^{-2}$	$180 \pm 16 \pm 26$

$$\text{BR} \left(\frac{{}^3P_2 \rightarrow p\bar{p}}{{}^3P_2 \rightarrow \text{all}} \right) \approx 0.85(\pi\alpha_s)^4 \frac{16}{729} \left| \frac{f_N}{\bar{M}^2} \right|^4 M_2^2, \quad (140)$$

which is Eq. (20) of [36] with an obvious minor correction. The results for the branching ratio of this process, shown in Table 9, have been calculated with $\alpha_s(m_c) = 0.210 \pm 0.028$ (see third paper of [136]).

Similar considerations apply also to the charmonium decay into $p\bar{p}$ of the level 3S_1 with $J^{PC} = 1^{--}$. The partial width of J/ψ (i.e., χ_{c0}) into $p\bar{p}$ is defined by

$$\Gamma({}^3S_1 \rightarrow p\bar{p}) = (\pi\alpha_s)^6 \frac{1280}{243\pi} \frac{|f_\psi|^2}{\bar{M}} \left| \frac{f_N}{\bar{M}^2} \right|^4 M_0^2, \quad (141)$$

where f_ψ determines the value of the 3S_1 -state wave function at the origin, *viz*,

$$\langle 0 | \bar{c}(0) \gamma_\mu c(0) | {}^3S_1 \rangle = \psi_\mu f_\psi M_\psi, \quad (142)$$

where ψ_μ is the J/ψ polarization vector. The value of f_ψ can be extracted from the leptonic width $\Gamma({}^3S_1 \rightarrow e^+e^-) = (5.36 \pm 0.29) \text{ keV}$ [139] via the Van Royen-Weisskopf formula:

$$\Gamma({}^3S_1 \rightarrow e^+e^-) = \frac{64}{9} \pi \alpha_s^2 |\psi_{J/\psi}(0)|^2 \frac{1}{\bar{M}^2}. \quad (143)$$

The result is $|f_\psi| = 409 \text{ MeV}$ with $m_{J/\psi} = 3096.93 \text{ MeV}$. (Note that $\bar{M} \approx M_{J/\psi}$.) Then, using the same values of parameters as before, we obtain the results shown in Table 9. One sees from this table that the agreement between the predictions of the heterotic model and the recent high-precision data of the E760 experiment at Fermilab [137] is quite good. The only exception is the branching ratio for the process ${}^3P_1 \rightarrow p\bar{p}$ which comes out too small, though the heterotic amplitude yields the largest value, compared to all other models. The experimental result can be reproduced using $\alpha_s \simeq 0.32$.

In a completely analogous way, one can calculate the corresponding exclusive decays of (helicity-conserving) charmonium states in $\Delta\bar{\Delta}$. The branching ratios follow by replacing f_N by $f_\Delta/\sqrt{3}$. The results of this calculation are summarized in Table 10. As regards the branching ratio of the 3S_1 state, the heterotic distribution amplitude yields $BR({}^3S_1 \rightarrow \Delta\bar{\Delta}/{}^3S_1 \rightarrow \text{all}) = 0.30 \times 10^{-2}\%$, where $\Gamma_{\text{tot}} = 85.5^{+6.1}_{-5.8} \text{ keV}$ is used. Note that in all considered decays $\alpha_s(m_c) = 0.210 \pm 0.028$ as before.

VI. MODIFIED CONVOLUTION SCHEME

In casting the hadron form factors in convolution form (cf. Eq. (116)), we tacitly assumed that the k_\perp -dependence of the quark and gluon propagators in T_H can be ignored. This is tantamount to factorizing the k_\perp -dependence into the distribution amplitudes which are the wave functions integrated over k_\perp up to the factorization scale. Thus, in the limit $Q^2 \rightarrow \infty$, the only gluon radiative corrections remaining uncanceled are those giving rise to wave-function renormalization. Indeed, recalling Eqs. (24), (48), one sees that asymptotically the most likely configurations are those in which the valence quarks share longitudinal momentum in a uniform way, i.e., $x_i = 1/2$ for the pion and $x_i = 1/3$ for the nucleon.

Table 10. Exclusive charmonium decays in $\Delta\bar{\Delta}$ for the models discussed in the text.

Amplitudes	CP	FZOZ	Heterotic
$M^\Delta(^3P_1)$	11418.23	21585.99	11651.26
$M^\Delta(^3P_2)$	30924.07	48233.23	26277.40
$M^\Delta(^3S_1)$	1480.67	1882.31	1134.94
Observables			
$BR\left(\frac{^3P_1 \rightarrow \Delta\bar{\Delta}}{^3P_1 \rightarrow all}\right)$	$0.089 \times 10^{-3}\%$	$0.3196 \times 10^{-3}\%$	$0.093 \times 10^{-3}\%$
$BR\left(\frac{^3P_2 \rightarrow \Delta\bar{\Delta}}{^3P_2 \rightarrow all}\right)$	$0.100 \times 10^{-3}\%$	$0.106 \times 10^{-3}\%$	$0.072 \times 10^{-3}\%$
$\Gamma(^3S_1 \rightarrow \Delta\bar{\Delta})$	$0.439 \times 10^{-2} \text{ keV}$	$0.709 \times 10^{-2} \text{ keV}$	$0.258 \times 10^{-2} \text{ keV}$

When confinement sets in, a quark is not able to venture too far from the anti-quark (in the pion) or the other two valence quarks (in the nucleon), and this poses constraints on the off-shellness of the involved propagators (see lhs of Fig. 22). However, in the end-point region, the parton transverse momenta in T_H cannot be *a priori* ignored, since, say, for the pion, $(\mathbf{k}_{\perp i} + \mathbf{k}'_{\perp j})^2 \gg x_i x'_j Q^2$. As a result, the transverse distance between the quark and the anti-quark becomes large compared to $1/Q$ and the corresponding gluon line is no more part of the hard-scattering process but should be counted to its soft part. This is in contrast to the perturbative QCD treatment in which the struck quark connects to the other valence quarks via highly off-shell gluon propagators, meaning that the transverse inter-quark distances are rather small, *viz.* of order $1/Q$ and that *all* partons share comparable fractions of longitudinal momentum. In other words, the mechanism of hard-gluon exchange becomes inapplicable and should be replaced by that of Feynman [140]. According to the latter mechanism, almost all of the hadron's momentum is carried off by a single parton, the others being “wee”. This picture is consistent with a configuration in which only the struck quark is within an impact distance $1/Q$ of the electron while all other partons have rather random positions in the transverse direction, building a soft “cloud” with transverse size $\gg 1/Q$ [141]. Once the elastic scattering has happened, rearrangements are necessary to change quarks and gluons into an unscathed hadron. This conversion procedure (visualized on the rhs of Fig. 22) is controlled by the overlap of the initial and final state wave functions and cannot be computed within pQCD.

A. MODIFIED FACTORIZATION

The physical basis of the modified convolution scheme is to dissect the process in such a way as that for transverse distances large compared to $1/Q$ (the latter being the playground of the hard-scattering mechanism) but still small relative to the true confinement regime – characterized by $1/\Lambda_{\text{QCD}}$ – the hadron wave function is modified to exhibit the effect of Sudakov enhancements *explicitly* up to the transverse scale retained in T_H (see Fig. 23). Going over to the transverse configuration space, the modified wave function in the axial gauge $A^+ = 0$ reads

$$\hat{\Psi}_{(\text{mod})}^{(H)}(x_i, 1/\tilde{b}_i, Q^2, \mu_{\text{ren}}^2) = e^{-S} \hat{\Psi}^{(H)}(x_i, Q^2, 1/\tilde{b}_i). \quad (144)$$

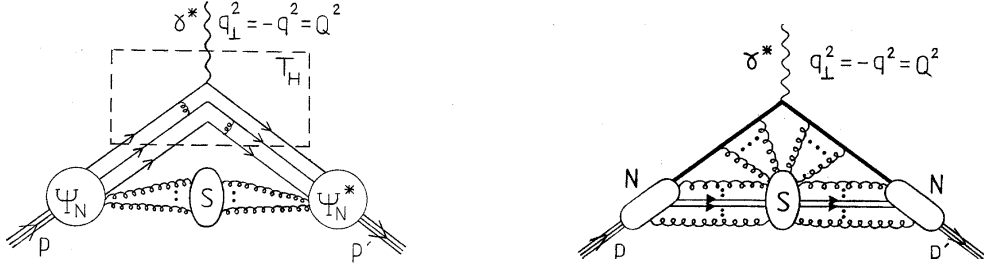


Figure 22. Mechanisms for momentum transfer during elastic scattering. The lhs shows hard-gluon exchange within pQCD. The blob S containing soft gluon lines (and an analogous one with soft quark-anti-quark lines not shown here) spoils factorization but is power-suppressed, i.e., non-leading. The (rhs) shows the Feynman mechanism using, for purposes of illustration, quark and gluon lines. The leading quark is denoted by a heavy line, while all other lines represent wee quarks and soft gluons.

The Sudakov exponential factor re-sums contributions from two-particle reducible diagrams (giving rise to double logarithms), whereas two-particle irreducible diagrams (giving rise to single logarithms) are absorbed into the hard scattering amplitude T_H [76]. Hence, e^{-S} can be conceived of as being a *finite* IR renormalization factor to the hadron's wave function [25], encoding the exponentiation of the probability for no-emission of soft gluons. This factor renormalizes the wave function in addition to the conventional renormalization factor Z_2^q due to UV divergences, encountered before. While Z_2^q contains single logarithms in leading order, the Sudakov renormalization factor is dominated by double logarithms. The leading double logarithms derive from those momentum regions where soft gluons (all four-momentum components small) and collinear gluons to the external quark lines overlap. These contributions are numerically dominated by the term

$$\exp \left\{ -\frac{2C_F}{\beta_0} \ln \frac{\xi_i Q}{\sqrt{2}\Lambda_{\text{QCD}}} \ln \frac{\ln(\xi_i Q/\sqrt{2}\Lambda_{\text{QCD}})}{\ln(1/\tilde{b}_i\Lambda_{\text{QCD}})} \right\}, \quad (145)$$

where ξ_i is one of the fractions $x_i, \bar{x}_i \equiv 1 - x_i$ (for incoming valence quarks) or $x'_i, \bar{x}'_i \equiv 1 - x'_i$ (for outgoing valence quarks), and β_0 is the first-order term of the Gell-Mann and Low function encountered before. The single logarithm in Eq. (eq:doublelog) stems from the running of the coupling constant, and the double logarithm contains the exponentiated higher-order corrections – required by the renormalization group – rendered finite by the *inherent* IR-cutoff $1/\tilde{b}_i$. This issue marks the crucial difference between the modified convolution scheme and previous approaches dealing with *isolated* quarks where such IR-cutoff parameters had to be introduced as *external* regulators. Here IR regularization is provided *in situ* without additional assumptions. For small transverse distances (or equivalently, $1/\tilde{b}_i \gg \xi_i Q$), gluonic radiative corrections are treated as being part of T_H and are excluded from the Sudakov form factor. Consequently, for $\xi_i \leq \sqrt{2}/\tilde{b}_i Q$ the Sudakov functions $s(\xi_i, \tilde{b}_i, Q)$ are set equal to zero. On the other hand, as \tilde{b}_i increases, e^{-S} decreases, reaching zero at $\tilde{b}_i\Lambda_{\text{QCD}} = 1$.

The full expression for the Sudakov exponent was calculated by Botts and Sterman [76].

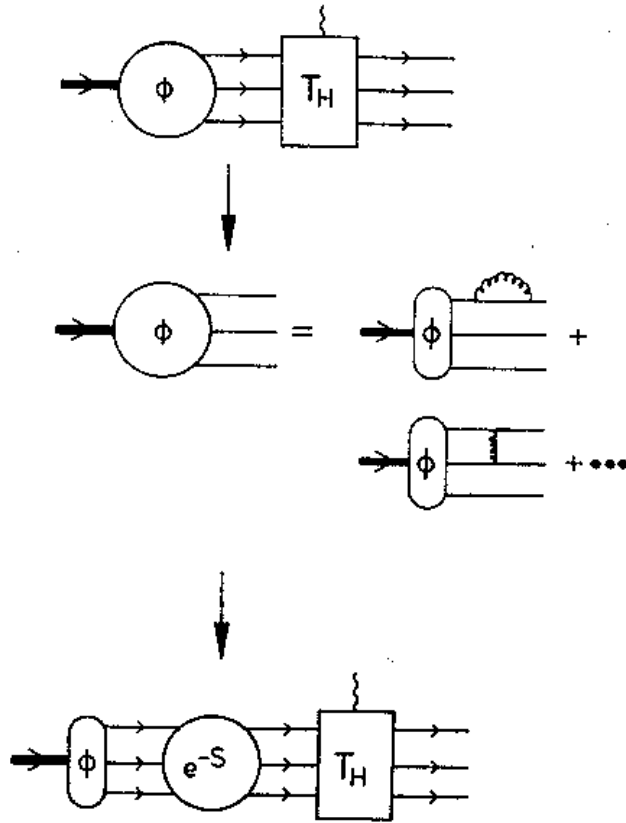


Figure 23. Modified factorization of soft-gluon contributions tantamount to a finite renormalization of the nucleon wave function.

It is given by¹⁶

$$S_j = \sum_{l=1}^3 \left[s(x_l, \tilde{b}_l, Q) + \int_{1/\tilde{b}_l}^{t_{j1}} \frac{d\bar{\mu}}{\bar{\mu}} \gamma_q(g(\bar{\mu}^2)) \right] \\ + \sum_{l=1}^3 \left[s(x'_l, \tilde{b}_l, Q) + \int_{1/\tilde{b}_l}^{t_{j2}} \frac{d\bar{\mu}}{\bar{\mu}} \gamma_q(g(\bar{\mu}^2)) \right] , \quad (146)$$

wherein the Sudakov functions $s(\xi_l, \tilde{b}_l, Q)$ are given by

$$s(\xi_l, \tilde{b}_l, Q) = \frac{A^{(1)}}{2\beta_1} \hat{q}_l \ln\left(\frac{\hat{q}_l}{\hat{b}_l}\right) + \frac{A^{(2)}}{4\beta_1^2} \left(\frac{\hat{q}_l}{\hat{b}_l} - 1\right) - \frac{A^{(1)}}{2\beta_1} (\hat{q}_l - \hat{b}_l) \\ - \frac{A^{(1)}\beta_2}{16\beta_1^3} \hat{q}_l \left[\frac{\ln(2\hat{b}_l) + 1}{\hat{b}_l} - \frac{\ln(2\hat{q}_l) + 1}{\hat{q}_l} \right] \\ - \left[\frac{A^{(2)}}{4\beta_1^2} - \frac{A^{(1)}}{4\beta_1} \ln(e^{2\gamma-1}/2) \right] \ln\left(\frac{\hat{q}_l}{\hat{b}_l}\right) \\ - \frac{A^{(1)}\beta_2}{32\beta_1^3} [\ln^2(2\hat{q}_l) - \ln^2(2\hat{b}_l)] . \quad (147)$$

Here $\xi_l = x_l, \bar{x}_l$ or x'_l, \bar{x}'_l ($l = 1, 2, 3$) and the variables \hat{q} and \hat{b} are defined as follows

$$\hat{q}_l = \ln[\xi_l Q / (\sqrt{2}\Lambda_{\text{QCD}})] , \quad (148)$$

$$\hat{b}_l = \ln[1/\tilde{b}_l \Lambda_{\text{QCD}}] . \quad (149)$$

The coefficients $A^{(i)}$ and β_i are

$$A^{(1)} = \frac{4}{3}, \quad A^{(2)} = \frac{67}{9} - \frac{1}{3}\pi^2 - \frac{10}{27}n_f + \frac{8}{3}\beta_1 \ln\left(\frac{1}{2}e^\gamma\right) , \\ \beta_1 = \frac{33 - 2n_f}{12} = \frac{1}{4}\beta_0, \quad \beta_2 = \frac{153 - 19n_f}{24} , \quad (150)$$

where n_f is the number of quark flavors and $\gamma = 0.5772\dots$ is the Euler-Mascheroni constant.

The Sudakov function, $s(\xi_l, \tilde{b}_l, Q)$, in Eq. (147) takes into account leading and next-to-leading order gluonic radiative corrections of the form shown in Fig. 23 and accounts for renormalization group evolution from the IR-scale $1/\tilde{b}_l$ to the renormalization scale μ_{ren} via the quark anomalous dimension. The quantities \tilde{b}_l ($l = 1, 2, 3$) are IR cutoff parameters, naturally related to, but not uniquely determined by the mutual separations of the three quarks [72]. A physical perspective on the choice of the IR cutoff is provided by the following analogy to ordinary QED. One expects that because of the color neutrality of a hadron, its quark distribution cannot be resolved by gluons with a wavelength much larger than a

¹⁶A corrected form of this expression was derived by Bolz [142]; see also [143].

characteristic quark separation scale. Hence, long-wavelength gluons probe the color singlet proton and radiation is damped. On the other hand, radiative corrections with wavelengths between the IR cutoff and an upper limit (related to the physical momentum Q) yield to suppression. It is understood that still softer gluonic corrections are already taken care of in the hadron wave function, whereas harder gluons are considered as being part of T_H .

In the pion case, there is only one transverse scale, notably, the quark–anti-quark separation b , so that suppression is automatically accomplished. Indeed, when it happens that one Sudakov function $s(\xi, b, Q) = 0$ (meaning that the corresponding exponential is set equal to unity) the other (negative) Sudakov function in the exponent, $s(1 - \xi, b, Q)$, diverges, thus providing sufficient suppression. This IR-protecting behavior due to the Sudakov form factor, makes it possible to choose a renormalization scale which depends on the initial and final longitudinal momenta. It was shown in Ref. [144], within the collinear approximation, that such a subtraction point minimizes the contributions of the next-to-leading order corrections to the pion form factor, ensuring dominance of the leading-order perturbative contribution. In the standard convolution scheme, such a choice leads to singularities in the running coupling constant α_s , unless it is saturated by additional IR regulators; e.g., a dynamical gluon mass. Here the modification of α_s becomes superfluous because the Sudakov effect inhibits soft-gluon emission, thus effectively *screening* the α_s -singularities. Physically, the Sudakov suppression enhances the dominance of quark configurations with a small color dipole moment and this enhancement becomes more pronounced as Q^2 increases. Concerning the nucleon, the situation is more complicated because several transverse scales are involved and therefore a careful IR regularization is required. Now the Sudakov function comprises six terms ($\xi_l = x_l$ or $\xi_l = x'_l$ for $l = 1, 2, 3$), each depending on its own transverse scale and with corresponding QCD-evolution contributions, driven by the anomalous dimensions associated with quark self energy. Recall that the IR cutoff to be used is the factorization scale, below which operator product expansion becomes a poor approximation. It is also understood that genuine non-perturbative momenta below the IR cutoff are implicitly accounted for in the nucleon wave function.

Different choices of the IR cutoff have been used in the literature: Thus, Li [79] chooses $\tilde{b}_l = b_l$ (this choice is termed hereafter the “L” prescription), whereas Hyer [145] in his analysis of the proton-antiproton annihilation into two photons and of the time-like proton form factor as well as Sotiropoulos and Sterman [146] take $\tilde{b}_1 = b_2$, $\tilde{b}_2 = b_1$, $\tilde{b}_3 = b_3$ (this choice is denoted the “H-SS” prescription). Still another possibility, proposed in [78], is to use for reasons that will be explained below as IR cutoff the maximum of the three inter-quark separations, i.e., to set

$$\tilde{b} \equiv \max\{b_1, b_2, b_3\} = \tilde{b}_1 = \tilde{b}_2 = \tilde{b}_3 . \quad (151)$$

This choice, designated by “MAX”, is analogous to that in the meson case, wherein the quark-anti-quark distance naturally provides a secure IR cutoff. The specific features of each particular cutoff choice will be discussed in detail later.

The integrals in Eq. (146) arise from the application of the renormalization group equation. The evolution from one scale value to another is governed by the anomalous dimensions of the involved operators. The integrals combine the effects of the application of the renormalization group equation on the wave functions and on the hard scattering amplitude. The range of validity of Eq. (147) for the Sudakov functions is limited to not too small \tilde{b}_l

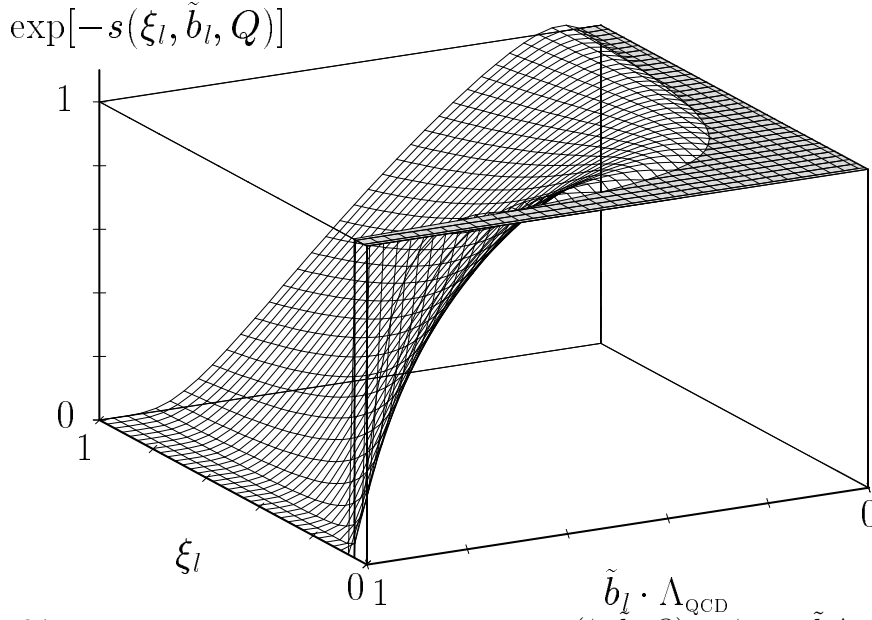


Figure 24. The exponential of the Sudakov function $s(\xi_l, \tilde{b}_l, Q)$ vs ξ_l and $\tilde{b}_l \Lambda_{\text{QCD}}$ for $Q = 30 \Lambda_{\text{QCD}}$. In the hatched area the Sudakov function is set equal to zero according to Li's requirement [79].

values. Whenever $1/\tilde{b}_l$ is large relative to the hard (gluon) scale $\xi_l Q$, the gluonic corrections are to be considered as higher-order corrections to T_H and hence are not included in the Sudakov factor but are absorbed into T_H (hierarchy of scales). For that reason, Li [79] sets any Sudakov function $s(\xi_l, \tilde{b}_l, Q)$ equal to zero whenever $\xi_l \leq \sqrt{2}/(Q\tilde{b}_l)$. Moreover, Li holds the Sudakov factor e^{-S_j} equal to unity whenever it exceeds this value, which is the case in the small \tilde{b}_l -region. Actually, the full expression Eq. (146) shows in this region a small enhancement resulting from the interplay of the next-to-leading logarithmic contributions to the Sudakov exponents and the integrals over the anomalous dimensions.

The IR cutoffs $1/\tilde{b}_l$ in the Sudakov exponents mark the interface between the purely non-perturbative soft momenta, which are implicitly accounted for in the proton wave function, and the contributions from soft gluons, incorporated in a perturbative way in the Sudakov factors. Obviously, the IR cutoff serves at the same time as the gliding factorization scale μ_F to be used in the evolution of the wave function. For that reason, Li [79] as well as Sotiropoulos and Sterman [146] take $\mu_F = \min\{1/\tilde{b}_l\}$. The “MAX” prescription (151), adopted in [78], naturally complies with the choice of the evolution scale proposed in [79,146]. In Fig. 24 we display the exponential of the Sudakov function $\exp[-s(\xi_l, \tilde{b}_l, Q)]$ for $Q = 30 \Lambda_{\text{QCD}}$ by imposing Li's requirement [79]: $s(\xi_l, \tilde{b}_l, Q) = 0$ whenever $\xi_l \leq \sqrt{2}/Q\tilde{b}_l$.

B. MODIFIED NUCLEON FORM FACTOR

The crucial element to incorporate radiative corrections in the calculation of form factors within the modified convolution scheme is to retain the explicit k_\perp -dependence in the convolution of the wave functions with the hard scattering amplitude. This new convolution formula can formally be derived by using the methods described in detail by Botts and Sterman [76]. According to Li [79], the convolution formula for the proton form factor can

be written in the form

$$G_M(Q^2) = \frac{16}{3} \int_0^1 [dx][dx'] \int [d^2\mathbf{k}_\perp][d^2\mathbf{k}'_\perp] \sum_{j=1}^2 T_{H_j}(x, x', \mathbf{k}_\perp, \mathbf{k}'_\perp, Q, \mu) Y_j(x, x', \mathbf{k}_\perp, \mathbf{k}'_\perp, \mu_F) . \quad (152)$$

One recognizes that this formula appears as an intermediate step in the derivation of the standard hard-scattering formula for the proton form factor [21]. Note, however, that the notation adopted in the present exposition is slightly different from that used by Li. Making use of the symmetry properties of the proton wave function under permutation, discussed previously, the contributions from the diagrams involved in the calculation of the proton form factor at Born level can be arranged into two reduced hard-scattering amplitudes of the form

$$T_{H_1} = \frac{2}{3} C_F \frac{(4\pi\alpha_s(\mu))^2}{[(1-x_1)(1-x'_1)Q^2 + (\mathbf{k}_{\perp 1} - \mathbf{k}'_{\perp 1})^2][x_2x'_2Q^2 + (\mathbf{k}_{\perp 2} - \mathbf{k}'_{\perp 2})^2]} , \quad (153)$$

$$T_{H_2} = \frac{2}{3} C_F \frac{(4\pi\alpha_s(\mu))^2}{[x_1x'_1Q^2 + (\mathbf{k}_{\perp 1} - \mathbf{k}'_{\perp 1})^2][x_2x'_2Q^2 + (\mathbf{k}_{\perp 2} - \mathbf{k}'_{\perp 2})^2]} . \quad (154)$$

In the hard scattering amplitudes only the k_\perp -dependence of the gluon propagators is included, whereas that of the quark propagators has been neglected. There is, in principle, no problem to include in the calculation all \vec{k}_\perp -dependence of T_H . In the case of the pion form factor this has been explicitly demonstrated by Li [79]. He found an additional suppression of the final result of about 10%. However, in the proton case, such terms would lead to an 11-dimensional integration which cannot be carried out to sufficient accuracy with present day computers.¹⁷

The functions Y_j in Eq. (152) are short-hand notations for linear combinations of products of the initial- and final-state wave functions Ψ_{ijk} , $\Psi_{i'j'k'}$, weighted by x_i -dependent factors arising from the fermion propagators, namely:

$$\hat{Y}_1 = \frac{1}{\bar{x}_1\bar{x}'_1} \left\{ 4\hat{\Psi}_{123}^{\star'}\hat{\Psi}_{123} + 4\hat{\Psi}_{132}^{\star'}\hat{\Psi}_{132} + \hat{\Psi}_{231}^{\star'}\hat{\Psi}_{231} + \hat{\Psi}_{321}^{\star'}\hat{\Psi}_{321} \right. \\ \left. + 2\hat{\Psi}_{231}^{\star'}\hat{\Psi}_{132} + 2\hat{\Psi}_{132}^{\star'}\hat{\Psi}_{231} + 2\hat{\Psi}_{321}^{\star'}\hat{\Psi}_{123} + 2\hat{\Psi}_{123}^{\star'}\hat{\Psi}_{321} \right\} , \quad (155)$$

$$\hat{Y}_2 = \frac{1}{2\bar{x}_2\bar{x}'_1} \left\{ 3\hat{\Psi}_{132}^{\star'}\hat{\Psi}_{132} - \hat{\Psi}_{231}^{\star'}\hat{\Psi}_{231} - \hat{\Psi}_{231}^{\star'}\hat{\Psi}_{132} - \hat{\Psi}_{132}^{\star'}\hat{\Psi}_{231} \right\} \\ - \frac{1}{\bar{x}_3\bar{x}'_1} \left\{ 4\hat{\Psi}_{321}^{\star'}\hat{\Psi}_{321} + \hat{\Psi}_{123}^{\star'}\hat{\Psi}_{123} + 2\hat{\Psi}_{321}^{\star'}\hat{\Psi}_{123} + 2\hat{\Psi}_{123}^{\star'}\hat{\Psi}_{321} \right\} \quad (156)$$

¹⁷Explorative studies by using, for instance, the k_\perp -dependence of only a certain subset of quark propagators in addition to those of the gluon propagators (leading to a 9-dimensional integration) show that the inclusion of such terms yields an additional suppression of the perturbative result. Since we are mainly interested in estimating rather the maximum perturbative contribution, we dispense with such terms.

for the proton [78] and by

$$\hat{Y}_1^n = \frac{1}{\bar{x}_1 \bar{x}'_1} \left\{ -2\hat{\Psi}_{123}^{\star'} \hat{\Psi}_{123} - 2\hat{\Psi}_{132}^{\star'} \hat{\Psi}_{132} + \hat{\Psi}_{231}^{\star'} \hat{\Psi}_{231} + \hat{\Psi}_{321}^{\star'} \hat{\Psi}_{321} \right. \\ \left. - \hat{\Psi}_{231}^{\star'} \hat{\Psi}_{132} - \hat{\Psi}_{132}^{\star'} \hat{\Psi}_{231} - \hat{\Psi}_{321}^{\star'} \hat{\Psi}_{123} - \hat{\Psi}_{123}^{\star'} \hat{\Psi}_{321} \right\}, \quad (157)$$

$$\hat{Y}_2^n = \frac{1}{\bar{x}_2 \bar{x}'_1} \left\{ \hat{\Psi}_{231}^{\star'} \hat{\Psi}_{231} + \hat{\Psi}_{231}^{\star'} \hat{\Psi}_{132} + \hat{\Psi}_{132}^{\star'} \hat{\Psi}_{231} \right\} \\ + \frac{1}{\bar{x}_3 \bar{x}'_1} \left\{ 2\hat{\Psi}_{321}^{\star'} \hat{\Psi}_{321} - \hat{\Psi}_{123}^{\star'} \hat{\Psi}_{123} + \hat{\Psi}_{321}^{\star'} \hat{\Psi}_{123} + \hat{\Psi}_{123}^{\star'} \hat{\Psi}_{321} \right\} \quad (158)$$

for the neutron [80]. The subscripts on Ψ refer to the order of momentum arguments, for example $\Psi_{123}(x, \mathbf{k}_\perp) = \Psi(x_1, \mathbf{k}_{\perp 1}; x_2, \mathbf{k}_{\perp 2}; x_3, \mathbf{k}_{\perp 3})$. Note that, in general, the wave function depends on the factorization scale μ_F . We make the following convenient ansatz for the wave function:

$$\Psi_{123}(x, \mathbf{k}_\perp) = \frac{1}{8\sqrt{N_c!}} f_N(\mu_F) \Phi_N(x, \mu_F = 1/\tilde{b}_l) \Omega(x, \mathbf{k}_\perp). \quad (159)$$

The k_\perp -dependence of the wave function is contained in the function Ω which is normalized according to

$$\int [d^2 \mathbf{k}_\perp] \Omega_{123}(x, \mathbf{k}_\perp) = 1. \quad (160)$$

Due to Eqs. (91) and (160), f_N is the value of the wave function at the origin of the configuration space. Recall that in contrast to the pion decay constant f_π , which has zero anomalous dimension, f_N exhibits evolution behavior driven by the leading anomalous dimension γ_0 according to

$$f_N(\mu_F) = f_N(\mu_0) \left(\frac{\alpha_s(\mu_F^2)}{\alpha_s(\mu_0^2)} \right)^{2/3\beta_0}. \quad (161)$$

At the starting point of evolution it has the value obtained from QCD sum rules [38,37]: $f_N(\mu_0) = (5.0 \pm 0.3) \times 10^{-3} \text{ GeV}^2$.

In Eq. (159) Ψ represents the soft part of the proton wave function that results by removing the perturbative part and absorbing it into the hard-scattering amplitude T_H . The perturbative tail of the full wave function behaves as $1/k_\perp^4$ for large k_\perp , whereas the soft part vanishes as $1/k_\perp^6$ or faster. The non-perturbative or intrinsic k_\perp -dependence of the soft wave function, being related to confinement, is parameterized in our analysis as a simple Gaussian distribution according to

$$\Omega_{123}(x, \mathbf{k}_\perp) = (16\pi^2)^2 \frac{a^4}{x_1 x_2 x_3} \exp \left[-a^2 \sum_{i=1}^3 \mathbf{k}_{\perp i}^2 / x_i \right]. \quad (162)$$

This parameterization of the intrinsic k_\perp -dependence of the wave function, which is due to Brodsky, Huang, and Lepage [147], seems to be more favorable than the standard form of factorizing x - and k_\perp -dependences. At least for the case of the pion wave function, this has

recently been effected by Zhitnitsky [94] on the basis of QCD sum rules. He found that a factorizing wave function is in conflict with some general theoretical constraints with which any reasonable wave function should comply. Zhitnitsky's QCD sum-rule analysis of the pion wave function seems to indicate that the k_\perp -distribution may also show a double-hump structure (like the distribution over longitudinal momenta in the CZ pion distribution amplitude), which means that small and large values of k_\perp are favored relative to intermediate values. It is likely that the proton wave function may exhibit a similar behavior, though this kind of analysis has yet to be done.

In Eq. (162) the parameter a controls the root mean square transverse momentum (r.m.s.), $\langle k_\perp^2 \rangle^{1/2}$, and the r.m.s. transverse radius of the proton valence Fock state. From the known charge radius of the proton, we expect the r.m.s. transverse momentum to be larger than about 250 MeV. The actual value of $\langle k_\perp^2 \rangle^{1/2}$ may be much larger than 250 MeV, even as large as 600 MeV. Indeed, Sotiropoulos and Sterman [146] show that application of the modified convolution scheme to proton-proton elastic scattering leads to an approximate t^{-8} -behavior of the differential cross section at moderate $|t|$. The behavior $d\sigma/dt \sim t^{-10}$, predicted by dimensional counting, appears only at very large $|t|$. At precisely which value of $|t|$ the transition from the t^{-8} to the t^{-10} behavior occurs, depends on the transverse size of the valence Fock state of the proton. Since the ISR [148] and the FNAL [149] data are rather compatible with a t^{-8} -behavior of the differential cross section, Sotiropoulos and Sterman conclude that the transverse size of the proton is small, perhaps ≤ 0.3 fm. Correspondingly, the r.m.s. transverse momentum is then larger than 600 MeV. It is worth noting that such a large value is supported by the findings of the EMC group [150] in a study of the transverse momentum distribution in semi-inclusive deep inelastic μp scattering. A phenomenologically successful approach to the standard convolution scheme, in which baryons are viewed as bound states of a quark and an effective diquark particle, also uses a value of this size for $\langle k_\perp^2 \rangle^{1/2}$ [151,152,153]. There is a second constraint on the wave function, namely the probability for finding three valence quarks in the proton:

$$P_{3q} = \frac{|f_N|^2}{3} (\pi a)^4 \int_0^1 [dx] \frac{2(\Phi_{123}(x))^2 + \Phi_{132}(x)\Phi_{231}(x)}{x_1 x_2 x_3} \leq 1. \quad (163)$$

Similarly to Sotiropoulos and Sterman [146], we write the valence quark component of the proton state with positive helicity in the form

$$|P, +\rangle = \frac{1}{\sqrt{N_c!}} \int_0^1 [dx] \int [d^2 \mathbf{k}_\perp] \left\{ \Psi_{123} \mathcal{M}_{+-+}^{a_1 a_2 a_3} + \Psi_{213} \mathcal{M}_{-++}^{a_1 a_2 a_3} - (\Psi_{132} + \Psi_{231}) \mathcal{M}_{++-}^{a_1 a_2 a_3} \right\} \epsilon_{a_1 a_2 a_3}, \quad (164)$$

where we assume the proton to be moving rapidly in the 3-direction. Hence, the ratio of transverse to longitudinal momenta of the quarks is small. The 3-quark state with helicities $\lambda_1, \lambda_2, \lambda_3$ and colors a_1, a_2, a_3 is given by

$$\mathcal{M}_{\lambda_1 \lambda_2 \lambda_3}^{a_1 a_2 a_3} = \frac{1}{\sqrt{x_1 x_2 x_3}} |u_{a_1}; x_1, \mathbf{k}_{\perp 1}, \lambda_1\rangle |u_{a_2}; x_2, \mathbf{k}_{\perp 2}, \lambda_2\rangle |d_{a_3}; x_3, \mathbf{k}_{\perp 3}, \lambda_3\rangle. \quad (165)$$

Since the orbital angular momentum is assumed to be zero, the proton helicity is the sum of the quark helicities. The quark states are then normalized as follows

$$\langle q_{a'_i}; x'_i, \mathbf{k}'_{\perp i}, \lambda'_i | q_{a_i}; x_i, \mathbf{k}_{\perp i}, \lambda_i \rangle = 2x_i (2\pi)^3 \delta_{a'_i a_i} \delta_{\lambda'_i \lambda_i} \delta(x'_i - x_i) \delta(\mathbf{k}'_{\perp i} - \mathbf{k}_{\perp i}) . \quad (166)$$

In the numerical analysis of [78,80], to be presented below, we make use of two different values of the r.m.s. transverse momentum: (1) One option is to use that value which is obtained by requiring $P_{3q} = 1$ for a given wave function. [This corresponds to the minimum value of the r.m.s. transverse momentum.] (2) As another option for the r.m.s. transverse momentum, we consider the rather large value of 600 MeV. In the latter case, the probability for the valence quark Fock state is much smaller than unity and depends on the structure of the particular wave function.

In order to include the Sudakov corrections, it is advantageous to re-express Eq. (152) in terms of the variables $\mathbf{b}_{\perp i}$, which are canonically conjugate to $\mathbf{k}_{\perp i}$ and span the transverse configuration space. Then

$$G_M(Q^2) = \frac{16}{3} \int_0^1 [dx] [dx'] \int \frac{d^2 \mathbf{b}_{\perp 1}}{(4\pi)^2} \frac{d^2 \mathbf{b}_{\perp 2}}{(4\pi)^2} \sum_j \hat{T}_j(x, x', \mathbf{b}_{\perp}, Q, \mu) \hat{Y}_j(x, x', \mathbf{b}_{\perp}, \mu_F) e^{-S_j} , \quad (167)$$

where the Fourier transform of a function $f(\mathbf{k}_{\perp}) = f(\mathbf{k}_{\perp 1}, \mathbf{k}_{\perp 2})$ is defined by

$$\hat{f}(\mathbf{b}_{\perp}) = \frac{1}{(2\pi)^4} \int d^2 \mathbf{k}_{\perp 1} d^2 \mathbf{k}_{\perp 2} \exp\{-i\mathbf{b}_{\perp 1} \cdot \mathbf{k}_{\perp 1} - i\mathbf{b}_{\perp 2} \cdot \mathbf{k}_{\perp 2}\} f(\mathbf{k}_{\perp}) . \quad (168)$$

Since the hard scattering amplitudes depend only on the differences of initial- and final-state transverse momenta, there are only two independent Fourier-conjugate vectors $\mathbf{b}_{\perp 1}$ ($= \mathbf{b}_{\perp 1}'$) and $\mathbf{b}_{\perp 2}$ ($= \mathbf{b}_{\perp 2}'$). They are, respectively, the transverse separation vectors between quarks 1 and 3 and between quarks 2 and 3. Accordingly, the transverse separation of quark 1 and quark 2 is given by

$$\mathbf{b}_{\perp 3} = \mathbf{b}_{\perp 2} - \mathbf{b}_{\perp 1} . \quad (169)$$

[Note that Sotiropoulos and Sterman [146] define the transverse separations in a cyclic way which results in the interchange $\mathbf{b}_{\perp 1} \longleftrightarrow -\mathbf{b}_{\perp 2}$, as compared to the definition used here.]

The fact that there are only two independent transverse separation vectors is a consequence of the approximation made in the treatment of the hard scattering amplitudes (given by Eqs. (153) and (154)) which disregards the k_{\perp} -dependence of the quark propagators. This approximation is justified by the enormous technical simplification it entails, given that the thereby introduced errors are very small. Then by virtue of rotational invariance of the system with respect to the longitudinal axis, the form factor (167) can be expressed in terms of a seven-dimensional integral instead of an eleven-dimensional one. Physically, the relations $\mathbf{b}_{\perp 1} = \mathbf{b}_{\perp 1}'$, $\mathbf{b}_{\perp 2} = \mathbf{b}_{\perp 2}'$ mean that the physical probe (i.e., the photon) mediates only such transitions from the initial- to the final-proton state, which have the same transverse configurations of the quarks.

The Fourier-transformed hard scattering amplitudes appearing in Eq. (167) read

$$\hat{T}_1 = \frac{8}{3} C_F \alpha_s(t_{11}) \alpha_s(t_{12}) K_0 \left(\sqrt{(1-x_1)(1-x'_1)} Q b_1 \right) K_0 \left(\sqrt{x_2 x'_2} Q b_2 \right) , \quad (170)$$

$$\hat{T}_2 = \frac{8}{3} C_F \alpha_s(t_{21}) \alpha_s(t_{22}) K_0 \left(\sqrt{x_1 x'_1} Q b_1 \right) K_0 \left(\sqrt{x_2 x'_2} Q b_2 \right) , \quad (171)$$

where K_0 is the modified Bessel function of order 0, and b_l denotes the length of the corresponding vector. We have chosen the renormalization scale in such a way that each hard gluon carries its own individual momentum scale t_{ji} which in turn appears as the argument of the corresponding α_s . The t_{ji} are defined as the maximum scale of either the longitudinal momentum or the inverse transverse separation, associated with each of the gluons:

$$\begin{aligned} t_{11} &= \max \left[\sqrt{(1-x_1)(1-x'_1)}Q, 1/b_1 \right] , \\ t_{21} &= \max \left[\sqrt{x_1x'_1}Q, 1/b_1 \right] , \\ t_{12} &= t_{22} = \max \left[\sqrt{x_2x'_2}Q, 1/b_2 \right] , \end{aligned} \quad (172)$$

One may think of other choices. However, they are not expected to lead to significantly different predictions for the form factor [79].

The quantities \hat{Y}_j contain the same combinations of initial- and final-state wave functions as those in Eq. (155) and Eq. (156), the only difference being that now the products $\Psi_{i'j'k'}^* \Psi_{ijk}$ are replaced by corresponding products of Fourier-transformed wave functions: $\hat{\Psi}_{i'j'k'}^*(x', \mathbf{b}_\perp, \mu_F) \hat{\Psi}_{ijk}(x, \mathbf{b}_\perp, \mu_F)$. Using Eq. (159) and Eq. (162), the Fourier transform of the wave function reads

$$\hat{\Psi}_{123}(x, \mathbf{b}_\perp, \mu_F) = \frac{1}{8\sqrt{N_c!}} f_N(\mu_F) \Phi_{123}(x, \mu_F) \hat{\Omega}_{123}(x, \mathbf{b}_\perp) , \quad (173)$$

where the Fourier-transform of the k_\perp -dependent part is given by

$$\hat{\Omega}_{123}(x, \mathbf{b}_\perp) = (4\pi)^2 \exp \left\{ -\frac{1}{4a^2} [x_1x_3b_1^2 + x_2x_3b_2^2 + x_1x_2b_3^2] \right\} . \quad (174)$$

The exponentials e^{-S_j} in Eq. (167) are the Sudakov factors, discussed previously, which encapsulate the effects of gluonic radiative corrections. This makes it apparent that Eq. (167) is not simply the Fourier transform of Eq. (152) but an expression comprising additional physical input. Thus, with hindsight, Eq. (167) may be termed the “modified convolution formula” in which hard-gluon re-scattering can still be isolated (factored out).

1. Screening of α_s singularities

Using as argument in α_s a renormalization scale, which is independent of the longitudinal momentum fractions, may induce large contributions from higher orders in the endpoint region. Indeed, for the pion form factor this has been explicitly shown, at least at next-to-leading order [144]. Surely such large higher-order contributions would render the leading-order calculation useless. For this reason, one may be tempted to use as a more appropriate choice the renormalization scale $\sqrt{x_2x'_2}Q$, for such a scale would eliminate the large logarithms arising from the higher-order contributions. Unfortunately, this is achieved at the expense that α_s becomes singular in the endpoint regions and the convolution form of the form factors diverges. To render the form factors finite, additional external parameters, like an effective gluon mass [121] or a cutoff prescription have to be introduced, as

we discussed before. One of the crucial advantages of the modified convolution scheme, is that there is no need for external regulators because the Sudakov factor may suppress the singularities of the “bare” (one-loop) α_s inherently. Indeed, in the pion case, it was shown [77] that the transverse quark-anti-quark separation is tantamount to an IR regulator which suffices to suppress all singularities arising from the soft region.

Concerning the proton form factor, we shall effect in the following that the screening of the α_s -singularities by the Sudakov factor depends sensitively on the choice of the IR regularization prescription in transverse configuration space.

Ultimately, the suppression of the α_s -singularities relies on the fact that whenever one of the α_s couplings tends to infinity (owing to the limit $t_{ji} \rightarrow \Lambda_{\text{QCD}}$), the Sudakov factor e^{-S_j} rapidly decreases to zero. As it can be observed from Fig. 24, this is not the case in the region determined by $\xi_l \leq \sqrt{2}\Lambda_{\text{QCD}}/Q$ and simultaneously $\tilde{b}_l\Lambda_{\text{QCD}} \rightarrow 1$, where $\exp[-s(\xi_l, \tilde{b}_l, Q)]$ is fixed to unity. In the pion case this does not matter, since the other $\exp[-s(1-\xi, \tilde{b}, Q)] \rightarrow 0$ faster than any power of $\ln[1/(\tilde{b}\Lambda_{\text{QCD}})]$ and, consequently, the Sudakov factor drops to zero ensuring IR protection. The treatment of the proton form factor is technically more subtle. In that case, e^{-S_j} does not necessarily vanish fast enough to enforce the suppression of the α_s -singularities. This can be illustrated by the following string-like configurations: $x_1 < \sqrt{2}\Lambda_{\text{QCD}}/Q$ and $b_1\Lambda_{\text{QCD}} \rightarrow 1$ and $b_2\Lambda_{\text{QCD}} \simeq b_3\Lambda_{\text{QCD}} \simeq 1/2$. Using the “L” prescription, it is obvious that $s(x_1, \tilde{b}_1, Q) = 0$ and the other two Sudakov functions are finite. Therefore, there is no suppression of the α_s -singularities owing to the limit $\tilde{b}_l\Lambda_{\text{QCD}} \rightarrow 1$. Sufficient suppression of the α_s -singularities is provided only if all three \tilde{b}_l are coerced to be equal. Allowing for the three \tilde{b}_l to be different, the Sudakov factor provides suppression only through the contributions of the anomalous dimensions which are only logarithmic, and hence cannot provide sufficient suppression. Similar observations hold for the “H-SS” prescription. Since the “L” and “H-SS” prescriptions allow for different \tilde{b}_l values in the Sudakov functions, the integrand in (167) has singularities behaving as

$$\sim \ln^{-\kappa} \left(\frac{1}{\tilde{b}_l\Lambda_{\text{QCD}}} \right) \quad (175)$$

for $\tilde{b}_l\Lambda_{\text{QCD}} \simeq 1$ and x_l hold fixed. The maximum degree of divergence is given by

$$\kappa = \frac{1}{\beta_0} \left(\frac{4}{3} + 2\tilde{\gamma}_{\text{max}} - 2 \right) + 1, \quad (176)$$

where the first term $4/3$ comes from the evolution of f_N , Eq. (161), and the constant $\tilde{\gamma}_{\text{max}}$ is related to the anomalous dimension driving the evolution behavior of the proton distribution amplitude (see Eq. (48) and Table 11). Here $\tilde{\gamma}_{\text{max}}$ is the maximum value of the $\{\tilde{\gamma}_n\}$ within a given polynomial order of the eigenfunctions expansion of the distribution amplitude. We reiterate that the $\tilde{\gamma}_n$ are positive fractional numbers increasing with n . Thus, the singular behavior of the integrand becomes worse as the expansion in terms of eigenfunctions extends to higher and higher orders. The term -2 in Eq. (176) stems from the integrations over the anomalous dimensions in the Sudakov factor e^{-S_j} (see Eq. (146)). Finally, the term 1 originates from that $\alpha_s(t_{jk})$ which becomes singular in Eq. (167) (cf. Eq. (172)). Which one of the α_s couplings becomes actually singular depends on the prescription imposed on the IR cutoff parameters \tilde{b}_l . The integral in Eq. (167) does not exist if $\tilde{\gamma}_{\text{max}} \geq \frac{1}{3}$. As Table 11

Table 11. Expansion coefficients for selected nucleon distribution amplitudes, taken from [38] and [51,52], and used in the modified convolution scheme. The notation of [35] is adopted. The $\{\tilde{\gamma}_n\}$ are related to those given in Table 4 as follows: $\tilde{\gamma}_n^{\text{Table I}} = \frac{1}{\beta_0}(\frac{2}{3} + \tilde{\gamma}_n)$, where $\frac{2}{3} = \gamma_0$ in this table. The associated r.m.s transverse momentum and the oscillator parameter for each model wave function, normalized via $P_{3q} = 1$, are shown.

n	$\tilde{\gamma}_n$	$B_n(\text{COZ}^{\text{up}})$	$B_n(\text{COZ})$	$B_n(\text{COZ}^{\text{opt}})$	$B_n(\text{Het})$	$B_n(\text{low})$
1	20/9	3.2185	3.6750	3.5268	3.4437	4.1547
2	24/9	1.4562	1.4840	1.4000	1.5710	1.4000
3	32/9	2.8300	2.8980	2.8736	4.5937	3.3756
4	40/9	-17.3400	-6.6150	-4.5227	29.3125	26.1305
5	42/9	0.4700	1.0260	0.8002	-0.1250	-0.5855
$\langle k_{\perp}^2 \rangle^{1/2}$ [MeV]		271	271	267	317	299
a [GeV $^{-1}$]		0.9893	0.9939	1.0069	0.8537	0.9217

reveals, this happens already for proton distribution amplitudes which include (Appell) polynomials of order 1, i.e., for all distribution amplitudes except for the asymptotic one. Thus application of the “L” and “H-SS” prescriptions to choose the IR cutoff parameters \tilde{b}_l in the proton form factor entails the modified convolution scheme to be invalid. In view of these results, Li’s numerical analysis of the proton form factor [79] is seriously flawed. Nevertheless, his general approach is a decisive step towards a deeper understanding of the electromagnetic baryon form factors.

A simple recipe to bypass the singular behavior of the integrand is to ignore completely the evolution of the distribution amplitude or to “freeze” it at any (arbitrary) value larger than Λ_{QCD} . Hyer [145] suggests, for example, to take for the factorization scale $\mu_F = \max\{1/b_l\}$. In this case, $\tilde{\gamma}_{\text{max}}$ appears in Eq. (176) only if all three \tilde{b}_l tend to $1/\Lambda_{\text{QCD}}$ at once. But then at least one of the $\exp[-s(\xi_l, \tilde{b}_l, Q)]$ drops to 0 faster than any power of $\ln(1/\tilde{b}_l\Lambda_{\text{QCD}})$. Apparently, Hyer’s choice of the factorization scale avoids singularities of the form of Eq. (175), but seems physically implausible. Since he gives numerical results for the proton form factor in the time-like region only, his results cannot be compared directly with those presented here.

Another option, and actually the one favored here, is to use a common IR cutoff not only for the evolution of the wave function but also in the Sudakov exponent [78,80,25]. Indeed, for a common cutoff \tilde{b} , the Sudakov factors always compensate the α_s -singularities, i.e., if, for a given l , it happens that one Sudakov function is in the dangerous region of phase space, $\xi_l < \sqrt{2}\Lambda_{\text{QCD}}/Q$, $\tilde{b}\Lambda_{\text{QCD}} \rightarrow 1$, at least one of the other two Sudakov functions lies in the region $\xi_{l'} > \sqrt{2}\Lambda_{\text{QCD}}/Q$, $\tilde{b}\Lambda_{\text{QCD}} \rightarrow 1$ ($l' \neq l$) and therefore provides sufficient suppression, as outlined above. In particular, we favor $\tilde{b} = \max\{b_l\}$ as the optimum choice (“MAX” prescription), since it does not only lead to a regular integral but also to a non-singular *integrand* of the form factor as well. The Sudakov factor e^{-S_1} subject to the “L” and “MAX” prescriptions is plotted for a specific quark configuration in Fig. 25. This figure makes it apparent that the Sudakov factor in connection with the “MAX” prescription is unencumbered by singularities in the soft regions. As a consequence of the regularizing power of the “MAX” prescription, the perturbative contribution to the proton form factor

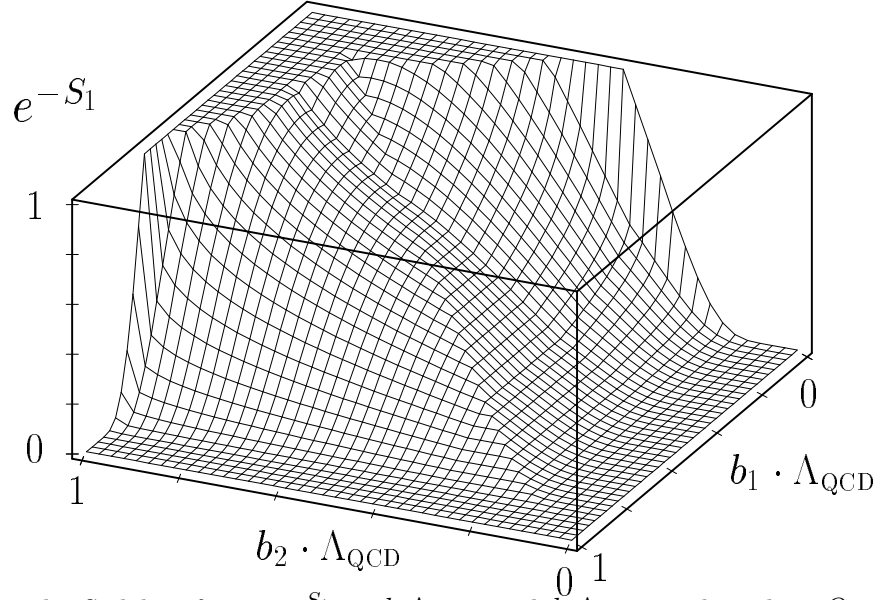
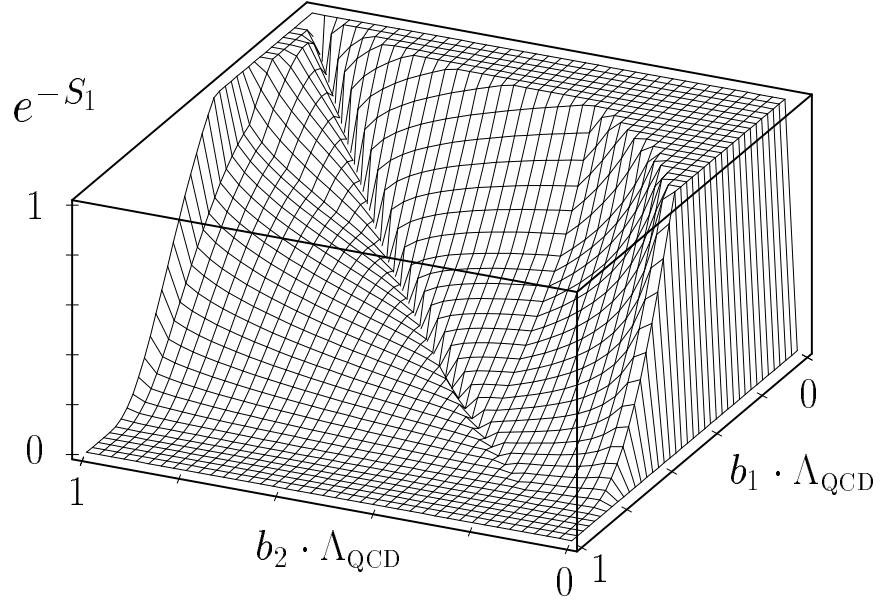


Figure 25. The Sudakov factor e^{-S_1} vs $b_1 \Lambda_{\text{QCD}}$ and $b_2 \Lambda_{\text{QCD}}$ evaluated at $Q = 30 \Lambda_{\text{QCD}}$, and $x_1 = x'_1 = 0.9$, $x_2 = x_3 = x'_2 = x'_3 = 0.05$ assuming a linear quark configuration (i.e., $\mathbf{b}_{\perp 1}$ and $\mathbf{b}_{\perp 2}$ are parallel to each other). The upper and lower figures correspond to the "L" and "MAX" prescriptions, respectively.

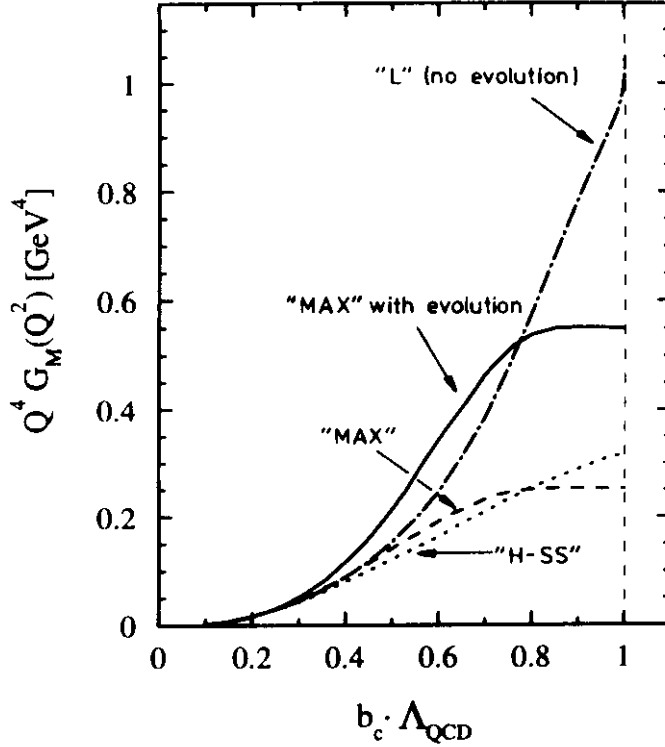


Figure 26. The proton magnetic form factor as a function of $b_c \Lambda_{\text{QCD}}$. The curves shown are obtained at $Q = 30 \Lambda_{\text{QCD}}$ for the COZ distribution amplitude. The solid line corresponds to the “MAX” prescription including evolution. The dotted (dashed, dashed-dotted) line represents results using the “H-SS” (“MAX”, “L”) prescription, by ignoring the intrinsic k_\perp -dependence, and also evolution.

Eq. (167) saturates, i.e., the results become insensitive to the inclusion of the contributions of the soft regions. A saturation as strong as possible should be regarded as a prerequisite for the self-consistency of the perturbative contribution.

To demonstrate the amount of saturation, we calculate the proton form factor through Eq. (167), employing a cutoff procedure to the b_l -integrations at a maximum value b_c . In Fig. 26 the dependence of G_M^p on b_c for the three choices, labeled “L”, “H-SS”, and “MAX” is shown, using, for reasons of an easier comparison with previous works, the COZ distribution amplitude and ignoring evolution.¹⁸

As one sees from this figure, the “MAX” prescription empowers saturation, i.e., the soft region $b_c \Lambda_{\text{QCD}} > 0.7$ does not contribute to the form factor substantially. In fact, already 50 % of the result are obtained from the regions with $b_c \Lambda_{\text{QCD}} < 0.48$, while α_s increases to a value of 0.95 at $b_c \Lambda_{\text{QCD}} \approx 0.48$. This indicates that a sizeable fraction of the contributions to the form factor is indeed accumulated in the perturbative region.

¹⁸Evolution has been dispensed with to avoid a concomitant singularity in $Q^4 G_M^p$ as $b_c \Lambda_{\text{QCD}} \rightarrow 1$ when imposing the “L” and “H-SS” prescriptions.

Unfortunately, this saturation is achieved at the expense of a rather strong damping of the perturbative contribution to the proton (and neutron) form factors. Using the other two prescriptions (“L” and “H-SS”) and ignoring evolution, larger results for G_M^p , and G_M^n can be obtained, but there is no indication for saturation: The additional contributions to the form factor gained this way are accumulated exclusively in the soft regions, i.e., for values of $b_c\Lambda_{\text{QCD}}$ near 1. Hence, this would be a rather deceptive improvement since the criticism of Isgur and Llewellyn-Smith [15] and of Radyushkin [16,17] would again apply.

These findings are in evident contradiction to Li’s results (figure 5 in [79]) for which an acceptable saturation was claimed. On the other hand, the saturation behavior of the proton form factor calculated by Hyer [145] in the time-like region is confirmed. A saturating behavior of the form factor should be regarded as a stringent test for the self-consistent applicability of pQCD. Therefore, calculations, which accumulate large contributions from soft regions (large b_c), can hardly be considered as theoretically legitimate, even if they seem to be phenomenologically successful.

The role of the evolution effect subject to the “MAX” prescription is also effected in Fig. 26. It is evident from this figure that the effect of evolution is large, though finite, owing to the strong suppression provided by the Sudakov factor (recall that the factorization scale is $\mu_F = 1/\tilde{b}$). The significant feature of the evolution effect is that it tends to neutralize the influence of the IR cutoff. Thus one may trade larger values of the proton (neutron) form factor for a slightly worse saturation.

One may criticize the use of the one-loop formula for α_s in the soft region. The “true” α_s coupling may likely differ from that in the soft region. However, the saturation behavior due to the “MAX” prescription (see Fig. 26) reveals that there is practically no contribution to the form factor from soft regions (say for $\tilde{b}\Lambda_{\text{QCD}} \geq 0.8$). The Sudakov factor together with the intrinsic transverse-momentum dependence of the wave function suppresses this region completely. Therefore, it is irrelevant what description of α_s one is using in that region, and hence more involved α_s parameterizations can be avoided.

We now comment on the connection between the modified convolution scheme, employed here, and approaches (e.g., [120]) which make use of an effective gluon mass [121] to regularize the running coupling constant and gluon propagators at small values of Q^2 . The purpose of the following discussion is to show the utility of the k_\perp (or transverse configuration space) representation in compensating the divergent contributions of the soft region of phase space. According to Eq. (152) or equivalently Eq. (167), all values of \mathbf{b}_\perp have been integrated out, in particular those corresponding to large distances, i.e., such of order $1/\Lambda_{\text{QCD}}$, which are not governed by perturbative QCD. As discussed above, once $Q^2 \sim \Lambda_{\text{QCD}}^2$, the external probe (the virtual photon) no longer “sees” the substructure of the nucleon, it rather sees the “diffuse” nucleon as a whole. This means that the strength of the dynamical coupling constant ceases to increase and “freezes” at some scale $Q^2 \leq M^2 = 4m_g^2$ (recall Eq. (117)), below which the long-range forces become saturated [35]. The scale M^2 can be fixed by the requirement that it should lead to the experimentally observed form factors. Then the leading-order coupling constant is replaced by the modified expression [121,122] given by Eq. (117), where the arguments of α_s are $Q_\xi^2 = Q^2\xi_l\xi'_l$ or $Q^2\xi_l\bar{\xi}'_l$ with $\bar{\xi}_l = (1 - \xi_l)$. In this case, the IR-protected α_s remains small enough that perturbation theory still applies. Furthermore, when the longitudinal momentum fractions $\xi_l, \bar{\xi}_l$ tend to zero, the gluon virtuality remains finite and equal to M^2 , and well above the Landau ghost pole. On the other hand,

Table 12. Simulation of Sudakov suppression and intrinsic transverse momentum by an IR-cutoff parameter M in the running coupling constant α_s at the one-loop order. The values of $Q^4 G_M^p$ are calculated with the COZ distribution amplitude and the r.m.s. transverse momentum $\langle k_\perp^2 \rangle^{1/2} = 271$ MeV.

Q^2 [GeV ²]	$Q^4 G_M^p$ [GeV ⁴]	M [MeV]	$\alpha_s(g^2)$
4.0	0.3593	330.9	1.147
6.0	0.3823	343.8	1.079
8.0	0.3962	353.4	1.035
10.0	0.4042	361.6	1.001
12.0	0.4094	368.5	0.974
14.0	0.4134	374.6	0.953
16.0	0.4164	380.0	0.934
18.0	0.4186	384.9	0.919
20.0	0.4195	389.6	0.904
22.0	0.4197	394.1	0.891
24.0	0.4193	398.4	0.879
26.0	0.4185	402.5	0.868
28.0	0.4176	406.4	0.857
30.0	0.4165	410.2	0.848

when Q^2 becomes large enough, the form factor becomes insensitive to the large distances or small momenta, characterized by M . Thus, Eq. (117) simulates the effect of the Sudakov factor in suppressing contributions from large values of $|\mathbf{b}_\perp|$. However, in contrast to the Sudakov damping factor, which has universal character, the IR-cutoff parameter M has to be adjusted to the external momentum. This becomes evident from Table 12, where the results for the Sudakov-suppressed magnetic proton form factor are simulated in the range of momentum transfers 4 to 30 GeV², using again as reference model the COZ distribution amplitude. Evolution is taken into account via the factor $\left(\frac{\alpha_s(Q_\xi^2 + M^2)}{\alpha_s(\mu_0^2 + M^2)} \right)^{\gamma_n/\beta_0}$, where $\mu_0 = 1$ GeV. Indeed, while the form factor begins to scale at $Q^2 \approx 14$ GeV², the values of the *ad hoc* parameter M still increase with Q^2 , in order to provide sufficient IR-protection. Such a Q^2 behavior of M can hardly be associated with the renormalization group controlled evolution of a dynamical gluon mass with a definite anomalous dimension [121].

This exercise demonstrates that IR regularization by such techniques is conceptually inferior to the inclusion of the explicit dependence of k_\perp within the modified convolution scheme. Perhaps the most significant feature of the latter approach is that it remains valid in any regime of momentum transfer without recourse to *ad hoc* assumptions.

2. Numerical form-factor analysis

In this section we present numerical results for the proton and the neutron form factors obtained in [78,80,25]. In these calculations the “MAX” prescription is employed, with

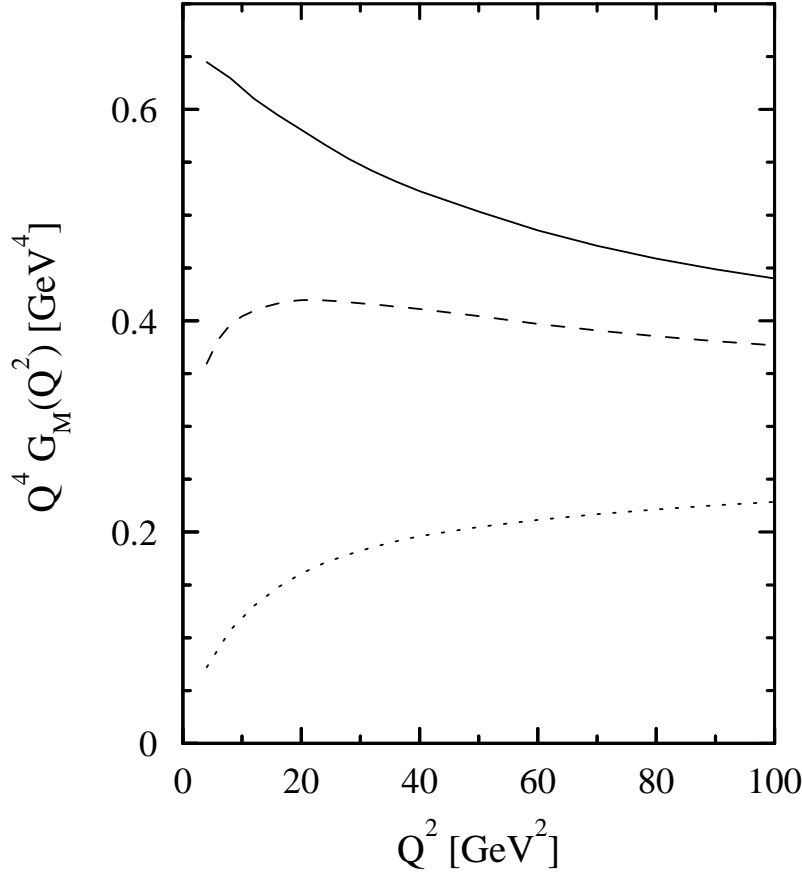


Figure 27. The influence of the intrinsic transverse momentum on the proton magnetic form factor within the modified convolution scheme. The curves shown are obtained for the COZ distribution amplitude by imposing the “MAX” prescription, and including evolution. The solid line represents the result without k_{\perp} -dependence, whereas the dashed and dotted lines are obtained with $\langle k_{\perp}^2 \rangle^{1/2} = 271$ MeV and 600 MeV, respectively.

evolution included, using $\Lambda_{\text{QCD}} = 180$ MeV and $\mu_0 = 1$ GeV. Before proceeding with the presentation of the results, let us first investigate the effect of including the intrinsic transverse momentum in form-factor calculations. The k_{\perp} -dependence of the nucleon wave function effectively introduces a confinement scale in the formalism, the importance of which may be appreciated by looking at Fig. 27.

This figure shows results, obtained for the COZ distribution amplitude without and with k_{\perp} -dependence, using two different values of $\langle k_{\perp}^2 \rangle^{1/2}$. To describe the intrinsic k_{\perp} -dependence, one can use Eq. (162) or, after Fourier-transforming to the transverse configuration space, Eq. (174). Notice that in Li’s approach the Gaussian in Eq. (174) has been replaced by unity. The oscillator parameter a is determined in such a way that either the normalization of the wave function P_{3q} is unity (resulting into $\langle k_{\perp}^2 \rangle^{1/2} = 271$ MeV for the COZ distribution amplitude), or by inputting the value of the r.m.s. transverse momentum. In the second case, a value of 600 MeV is used, which implies $P_{3q} = 0.042$. As can be seen from this and the analogous figure for the neutron (Fig. 28), the predictions for the form

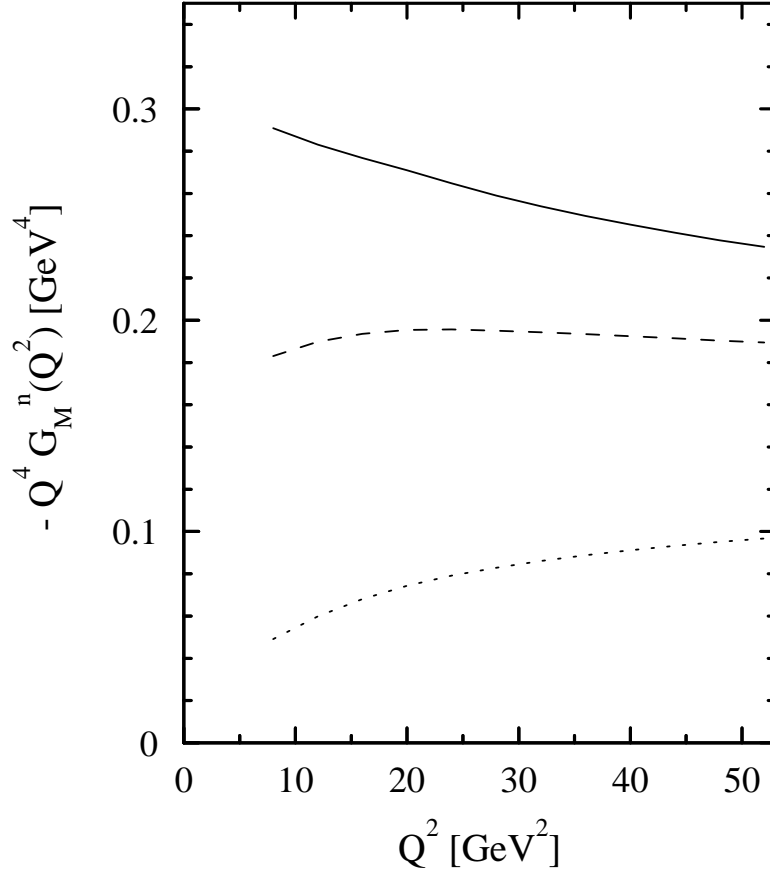


Figure 28. The influence of the intrinsic transverse momentum on the neutron magnetic form factor within the modified convolution scheme. The curves shown are obtained for the COZ distribution amplitude by imposing the “MAX” prescription, and including evolution. The solid line represents the result without k_\perp -dependence, whereas the dashed and dotted lines are obtained with $\langle k_\perp^2 \rangle^{1/2} = 271$ MeV and 600 MeV, respectively.

factor are quite different for the three considered cases.

In fact, the intrinsic k_\perp -dependence of the nucleon wave function leads to further suppression of the perturbative contribution, which becomes substantial if the r.m.s. transverse momentum is large. On the other hand, this suppression is accompanied by an increasing amount of saturation because the Gaussian distribution, Eq. (174), also provides suppression; predominantly of contributions from the soft regions, *viz.*, the large b -regions. In contrast to the Sudakov factor, however, this suppression is Q -independent (there is no evolution). The interplay of the two effects, Sudakov suppression and intrinsic transverse momentum, leads to a different Q -behavior of the form factor, depending on the value of the r.m.s transverse momentum, as can be seen from Figs. 27, 28. The Q -dependence beyond 10 GeV 2 is rather weak, being approximately compatible with dimensional counting (modulo renormalization group generated logarithmic corrections). For very large values of Q^2 , say, beyond 1000 GeV 2 , the three curves have already approached each other within 10% accuracy. This happens when the Sudakov factor dominates the Gaussian k_\perp -distribution

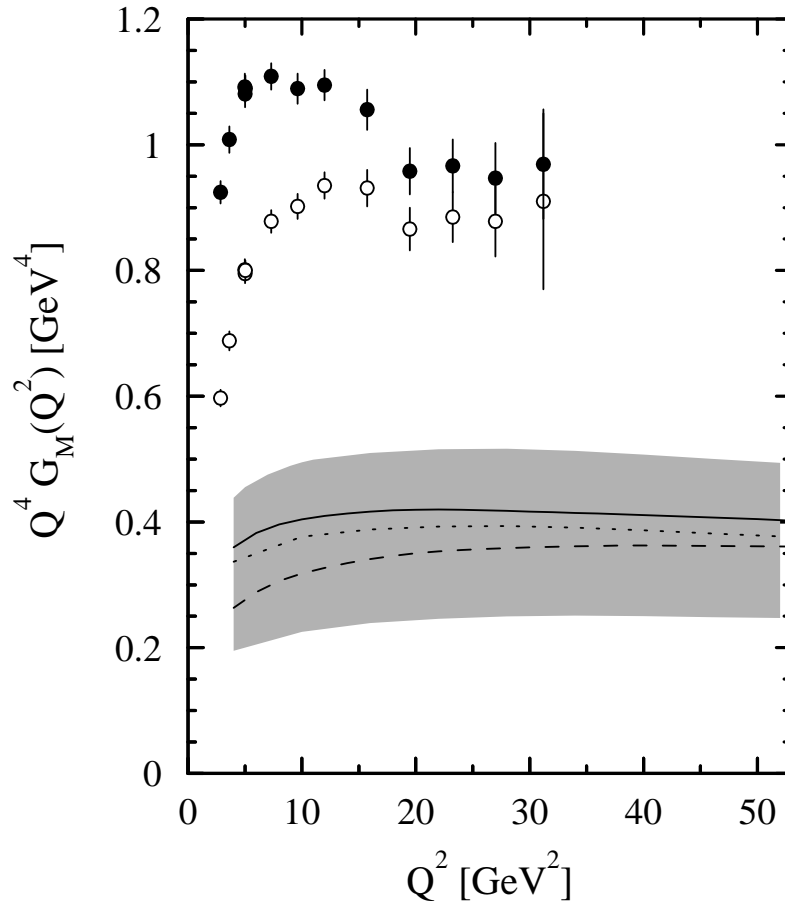


Figure 29. The proton magnetic form factor vs Q^2 . Data are taken from [154,34]. The G_M^p data are represented by black dots, whereas those for F_1^p are indicated by open circles. The theoretical results are obtained using the “MAX” prescription including evolution and normalizing the wave functions to unity. The shadowed strip indicates the range of predictions derived from the set of distribution amplitudes determined in [51,52] in the context of QCD sum rules (see text). The solid (dashed, dotted) line corresponds to the COZ (heterotic, optimized COZ) distribution amplitude.

and selects those configurations with small inter-quark separations. In this region, which one may consider as the pure perturbative region, the results for the form factor are independent of the confinement scale introduced by the r.m.s. transverse momentum.

The penalty of the additional suppression of the perturbative contribution caused by Eq. (174) is mitigated by the advantage of promoting the perturbative contribution to become self-consistent by the *in situ* IR protection due to the Sudakov form factor. This is clearly indicated in the enhanced amount of saturation with increasing r.m.s. transverse momentum. Adapting the criterion of self-consistency, originally suggested by Li and Sterman [77] for the pion case, namely that 50% of the results should accumulate at moderate values of the coupling constant, say, $\alpha_s^2 \leq 0.5$, we find for the nucleon form factors self-consistency for $Q^2 \approx 7 \text{ GeV}^2$ (still referring to the COZ distribution amplitude).

The final results are shown in Fig. 29 (proton) and in Fig. 30 (neutron) for different nucleon distribution amplitudes.

Though we have not considered the pion form factor in the modified convolution scheme, we find it instructive to include it in Fig. 31 which shows the (corrected) calculation by

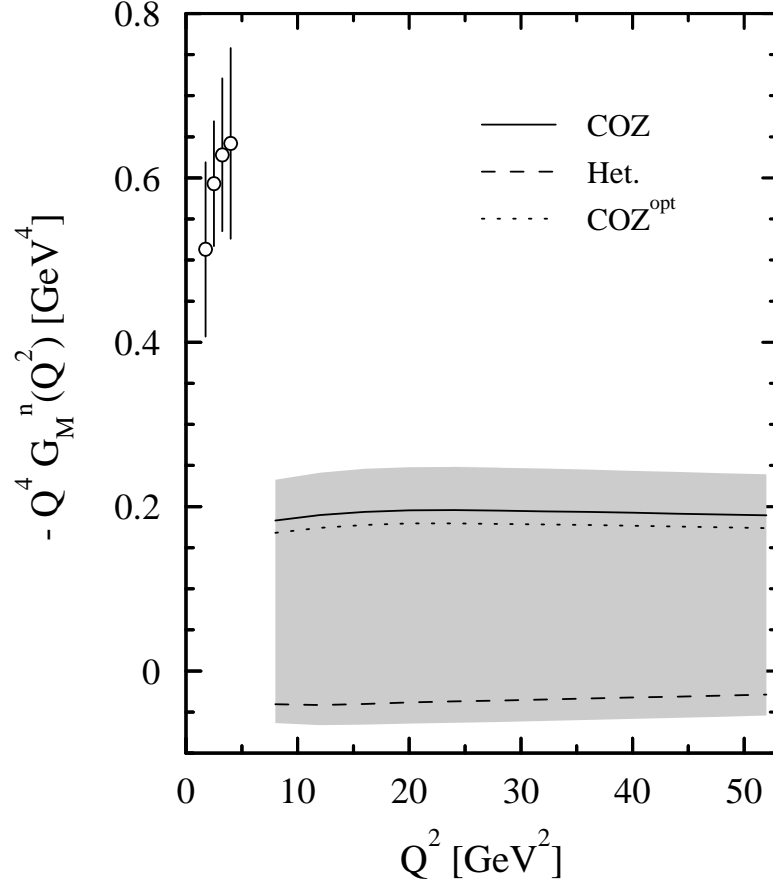


Figure 30. The neutron magnetic form factor vs Q^2 . The theoretical results are obtained using the “MAX” prescription including evolution and normalizing the wave functions to unity. The shadowed strip indicates the range of predictions derived from the set of distribution amplitudes determined in [51] in the context of QCD sum rules (see text). The solid (dashed, dotted) line corresponds to the COZ (heterotic, optimized COZ) distribution amplitude. The data are taken from [154].

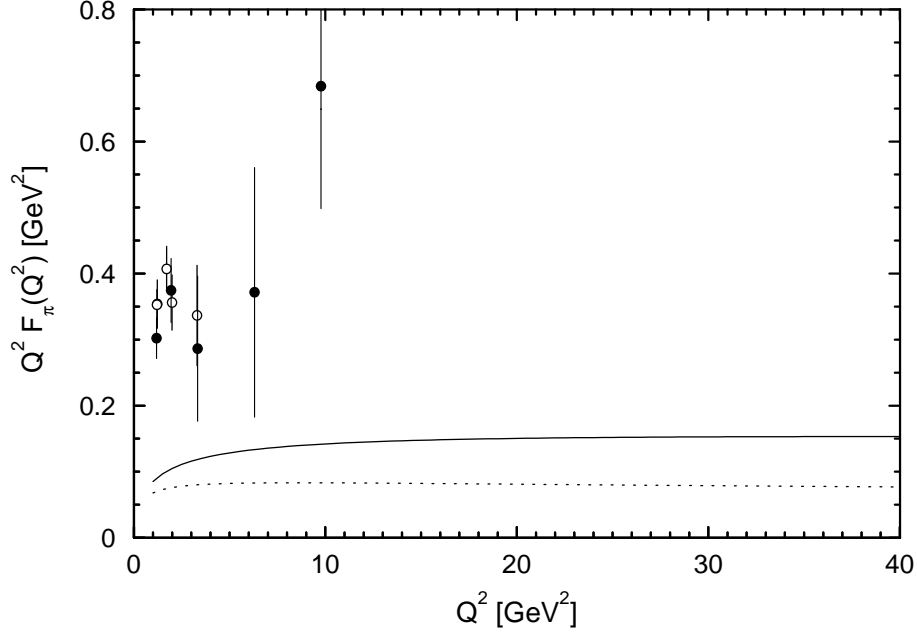


Figure 31. The pion form factor in the space-like region including Sudakov effects and those due to the intrinsic k_{\perp} -dependence of the pion wave function [81], evaluated for $\Lambda_{\text{QCD}} = 200$ MeV. The solid line shows the result for the Chernyak-Zhitnitsky amplitude $\Phi_{CZ} = 30x_1x_2(x_1 - x_2)^2$, and the dotted line that for the asymptotic solution to the evolution equation, $\Phi_{\text{as}} = 6x_1x_2$. The data are taken from [32].

Jakob and Kroll [81].

A set of 45 nucleon distribution amplitudes [51,52] have been investigated, distribution amplitudes which respect the QCD sum-rule constraints [38,37] with comparable χ^2 values. The results for the various distribution amplitudes – or more precisely wave functions, since their intrinsic transverse-momentum dependence is taken into account – obtained under the “MAX” prescription with evolution included, form the shaded area shown in Figs. 29, 30. Note that all wave functions are normalized to unity and that the corresponding r.m.s. transverse momenta vary between 267 MeV and 317 MeV (see Table 11).

The theoretical form-factor predictions span a “band” congruent to the “orbit” of solutions found previously in [51,52] and discussed already in detail in this report. The upper bound of the “band” corresponds to the distribution amplitude COZ^{up} , which yields the maximum value of the form-factor ratio $|G_{\text{M}}^{\text{n}}|/G_{\text{M}}^{\text{p}} = 0.4881$ in the standard convolution scheme. The lower limit of the “band” is obtained using the distribution amplitude “low” (sample 8 in [52]) (cf. Table 4) with $|G_{\text{M}}^{\text{n}}|/G_{\text{M}}^{\text{p}} = 0.175$. Explicitly shown are the results for the COZ distribution amplitude, its optimized version COZ^{opt} , and the heterotic distribution amplitude [42]. We note that the differences among these curves practically disappear already at about $Q^2 = 80 \text{ GeV}^2$, despite the fact that these amplitudes have distinct geometrical characteristics. This behavior effects once more that momentum evolution at larger Q^2 values is enough to wash out shape peculiarities due to the truncation of the eigenfunctions series.

Because the true valence Fock state probability is likely much smaller, or invariably the

r.m.s. transverse momentum larger than a value of order 300 MeV, the “band” describes rather *maximal* expectations for the (leading-order) perturbative contributions to the form factor; at least for proton wave functions of the type we considered. Comparison with the experimental data reveals that the theoretical predictions amount, at best, to approximately 50% of the measured values. This is the benchmark against which we have to discern novelties and aberrations.

Concerning the proton form factor, we note that, since we are calculating only the helicity-conserving part of the current matrix element, it is not obvious whether we should compare the theoretical predictions with the data for the Sachs form factor G_M^p or with those for the Dirac form factor F_1^p . Therefore, we exhibit in Fig. 29 both sets of data [154] for comparison. However, since the two sets of data differ by only 10%, our conclusions concerning the smallness of the theoretical results remain unaffected.

The results for the neutron magnetic form factor are shown in Fig. 30. Unfortunately, there is no form-factor data available in the region where the perturbative contribution is self-consistent. Yet the trend of the low Q^2 data [154] seems to indicate that the size of the perturbative contribution is rather small. Measurements of the neutron magnetic form factor beyond 5 GeV² are extremely important in order to check the validity of the theoretical predictions.

One place to test these results beyond 5 GeV² is in the data [123] for the differential cross sections for elastic electron-proton and electron-neutron scattering, σ_p and σ_n , respectively. For small scattering angles, where the terms $\propto \tan^2(\theta/2)$ can be neglected, and for large Q^2 , the ratio σ_n/σ_p becomes approximately proportional to the square of the ratio of the neutron to the proton magnetic form factor, provided the electric form factors are negligible. For the electric form factor of the proton this assumption has recently been verified experimentally [123]. Its neutron counterpart is experimentally still unknown beyond 5 GeV², but many phenomenological models currently in use predict a small G_E^n . We note that the low Q^2 data on G_E^n [154] are compatible with zero.

Combining the calculations for the proton with those for the neutron, we can extract theoretical predictions for σ_n/σ_p , using the same set of nucleon model distribution amplitudes as before. The results are shown in Fig. 32 (shaded area) in comparison with available data [123]. From this figure we see that the measured values of σ_n/σ_p enter the estimated range already at $Q^2 \approx 8$ GeV². [The corresponding values of the ratio $-G_M^n/G_M^p$, allowed by this analysis, range between -0.2 and 0.5.] It is important to emphasize that the ratio of the magnetic form factors is the first observable for which the modified convolution scheme yields predictions which, albeit in a slightly model-dependent way, indicate overlap with the existing data [123]. This tentative agreement occurs at data points corresponding to the largest momentum transfers measured, where, incidentally, the presented theoretical calculations become self-consistent.

The various model (nucleon) wave functions considered lead to self-consistency of the perturbative contribution, meaning that 50% of the results are accumulated in regions where $\alpha_s^2 \leq 0.5$, i.e., in the range of Q^2 between 6 and 10 GeV².

Closing this chapter we note that using other values of the r.m.s. transverse momentum but the same set of distribution amplitudes, similar “bands” are obtained with about the same relative widths. Even for zero r.m.s. transverse momentum (see Fig. 27), the “band” does not overlap with the data.

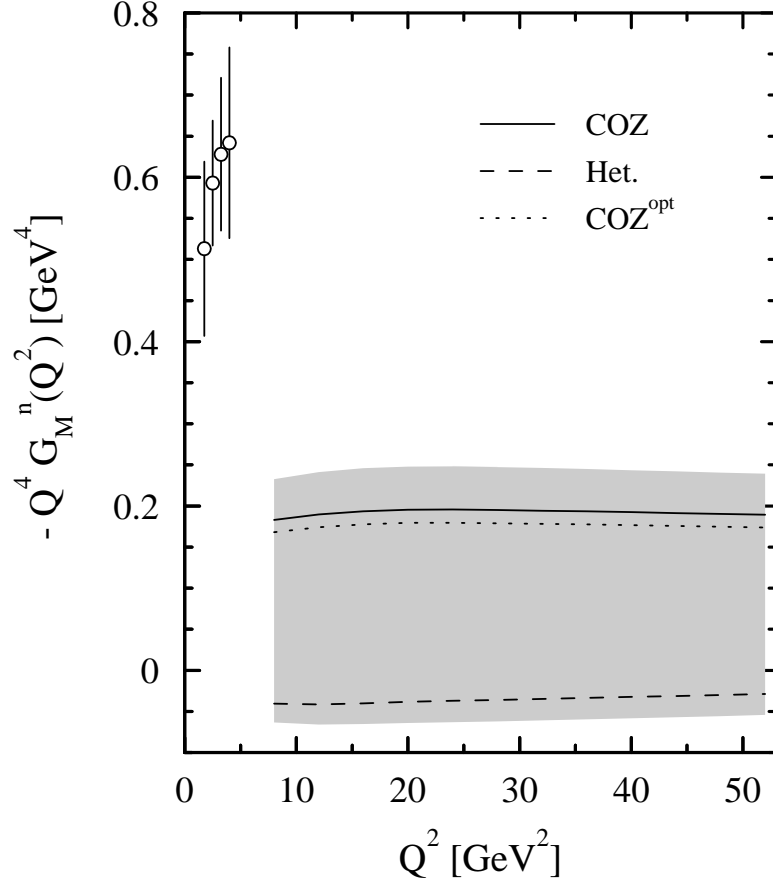


Figure 32. The ratio σ_n/σ_p of the differential elastic electron-neutron to electron-proton cross section vs Q^2 at scattering angles of 10° . The shaded area and the model distribution amplitudes for the nucleon correspond to those shown in Figs. 29 and 30. The data are taken from [123].

Our present knowledge of the proton wave function resides only on QCD sum-rule calculations and is thus rather limited – contrary to the pion case. Therefore, we present two sets of results, such with a minimal r.m.s. transverse momentum (corresponding to $P_{3q} = 1$), and such with 600 MeV (corresponding to $P_{3q} \simeq 0.04$) in order to demonstrate the role of this parameter. The probability of the “true” valence Fock state wave function, say, at $Q^2 = 10 \text{ GeV}^2$, is certainly not 1 but smaller, probably close to the value of the other set. However, according to Botts and Sterman [76] (see also [25]), one may view the Sudakov form factor as part of the wave function, describing the perturbative part of the transverse momentum distribution. Accepting this idea and interpreting the case $P_{3q} = 1$ as the soft wave function in the region $Q^2 \simeq 1 \text{ GeV}^2$, the product of wave function and Sudakov form factor at about $Q^2 = 10 \text{ GeV}^2$ leads to $P_{3q} = 0.21$ and $\langle k_\perp^2 \rangle^{1/2} \simeq 500 \text{ MeV}$. Thus, in order to avoid double counting, it is perhaps reasonable to start with the intrinsic k_\perp -dependence of about $\langle k_\perp^2 \rangle^{1/2} \simeq 300 \text{ MeV}$ and $P_{3q} = 1$.

We finally note that the value of the proton wave function at the origin, f_N , is also burdened by large errors, which in turn induce further uncertainties in the form factor predictions. In present lattice theory calculations [39], the value $f_N^{\text{lat}} = (0.29 \pm 0.6) \times 10^{-3} \text{ GeV}^2$ was found. Literal use of such a value would lead to form factor results even smaller than the predictions shown in Figs. 29, 30.

3. Higher-order nucleon distribution amplitudes

To effect that the depletion of the perturbative contribution is not the consequence of truncating the nucleon distribution amplitude at the level of second-order eigenfunctions, we show in Fig. 33 predictions for the proton and the neutron magnetic form factors calculated with nucleon distribution amplitudes, determined by Schäfer [40], which incorporate Appell polynomials of order three.¹⁹ The solid lines show the results for the amplitude Sch II (in Schäfer’s notation) which deliberately incorporates third-order terms. It is clearly obvious that both form factors G_M^p and G_M^n overshoot the data and have, in addition, a wrong Q^2 evolution. Besides, their saturation behavior deteriorates, for they still increase at Q^2 as large as 50 GeV^2 and insensitivity to the soft region $b_1 \Lambda_{QCD} \rightarrow 1$ sets in at $Q^2 \approx 17 \text{ GeV}^2$, which is a much larger scale compared to that found for the second-order amplitudes: $Q^2 \leq 10 \text{ GeV}^2$. As we have discussed in detail in previous publications [35,103,42,41,51], and also in previous sections of this report, the moment sum rules are not stringent enough to exclude this sort of amplitudes. Additional criteria have to be imposed in order to filter out physically meaningful solutions, i.e., those which ensure dominance of the lowest leading-order contributions.

Along similar lines of thought, Schäfer [40] has determined a collection of amplitudes which, although including third-order Appell polynomials, effectively resemble those of polynomial order two. The dotted lines in Fig. 33 exemplify the form-factor predictions obtained with such amplitudes. To be specific, the underlying amplitude (denoted Sch IVb) was deter-

¹⁹The expansion coefficients B_n for each of these amplitudes can be readily obtained from the corresponding moments via Eqs. (92), (93).

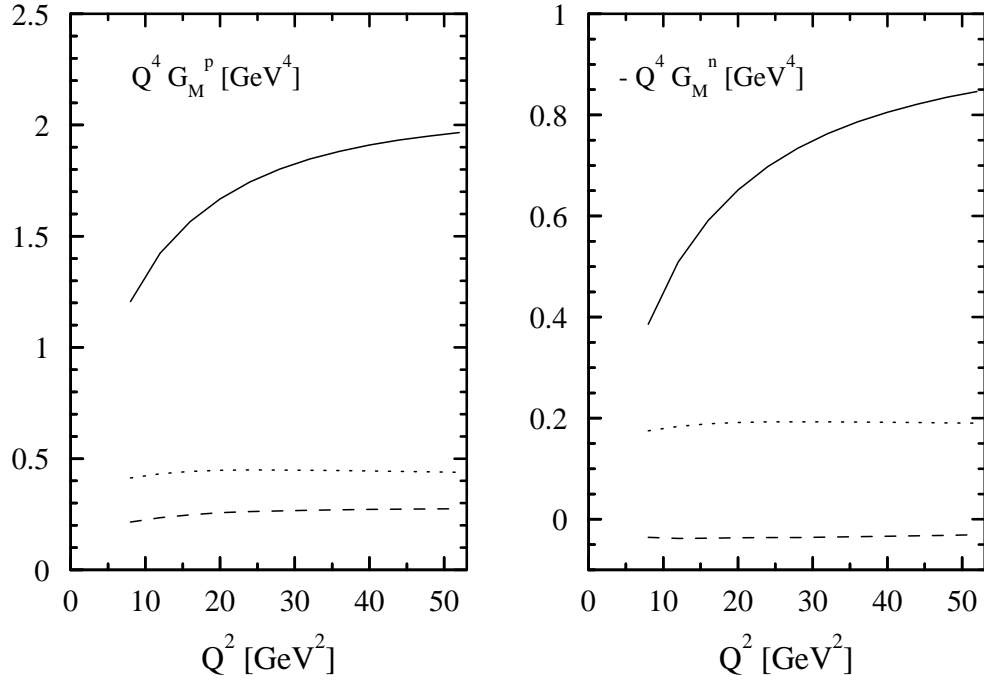


Figure 33. Plots for the proton and neutron magnetic form factor within the modified convolution scheme calculated with nucleon distribution amplitudes, determined by Schäfer [40], which include third-order eigenfunctions (Appell polynomials). As in the previous figures, the “MAX” prescription and the value $\Lambda_{\text{QCD}} = 180$ MeV were used.

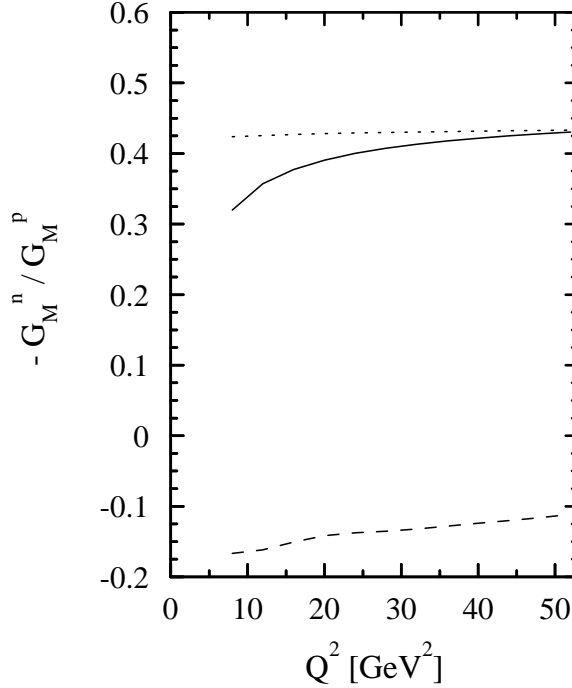


Figure 34. Ratio of the nucleon magnetic form factors computed with the Schäfer amplitudes vs the momentum transfer Q^2 .

mined under the proviso of a “smoothness” criterion with the purpose of excluding spurious oscillations (“wiggles”) caused by the third-order (Appell) polynomials. This criterion is quite restrictive and, as one sees, the obtained results have the same overall quality as those computed with amplitudes truncated after taking into account bilinear combinations of longitudinal momentum fractions. This indicates that the truncation at the second polynomial order is justifiable, since the shape of the corresponding amplitudes is a characteristic property of the *entire* series and that the errors (and amount of cutoff dependence involved) are of sub-leading importance if properly incorporated. For completeness, Fig. 34 shows also form factors, computed with an amplitude (termed Sch III and represented by dashed lines) which exhibits unphysical oscillations. The form-factor ratio $-G_M^n/G_M^p$, as a function of the momentum transfer Q^2 , for the three amplitudes Sch II, Sch III, and Sch IVb is shown in Fig. 34.

4. Global pattern of nucleon distribution amplitudes

It is remarkable that the collective pattern of solutions to the QCD sum rules [38,37], found within the standard convolution scheme [51,52], pertains to the inclusion of transverse-momentum contributions comprising the Sudakov factor and those due to the intrinsic transverse momentum [81] (see Fig. 35).

Indeed, the solutions (nucleon distribution amplitudes) arrange themselves again across an “orbit” in the $(B_4, -G_M^n/G_M^p)$ plane which is, however, somewhat shifted as compared to the original one (Fig. 11). Now the “orbit” is slightly Q^2 -dependent, though its coherent structure is not destroyed but changed in a global way. The solid and

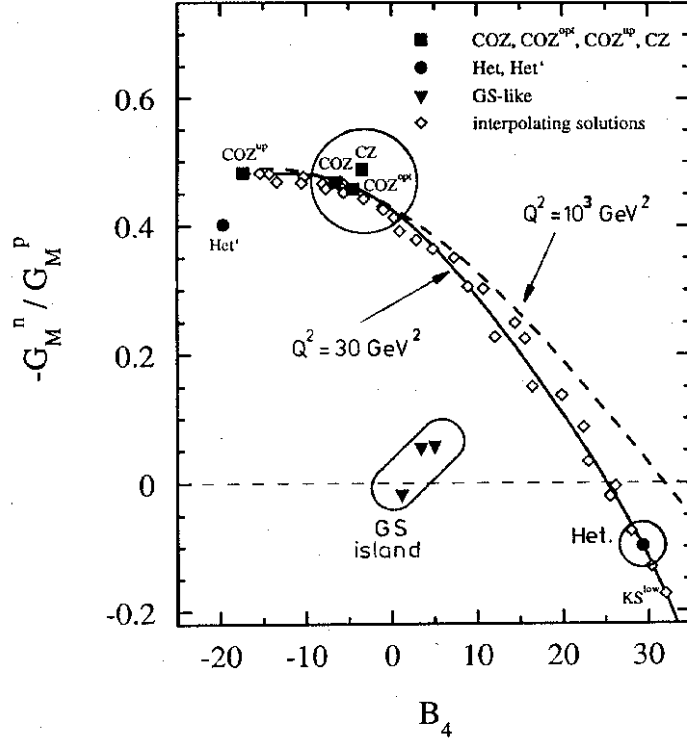


Figure 35. The relation between the ratio $R \equiv |G_M^n|/G_M^p$ of the magnetic nucleon form factors and the expansion coefficient B_4 of the Appell polynomial decomposition of the nucleon distribution amplitude, including the effect of the Sudakov form factor and intrinsic transverse-momentum dependence. The results are obtained at $Q^2 = 30 \text{ GeV}^2$, employing the “MAX” prescription. The superimposed solid line is an empirical polynomial fit similar to the original one given in [51] within the standard convolution scheme. The dashed line serves to illustrate the dependence on the momentum scale ($Q^2 = 10^3 \text{ GeV}^2$).

dashed lines correlate to the calculations within the modified convolution scheme presented above at two different scales, *viz.*, at $Q^2 = 30 \text{ GeV}^2$ and $Q^2 = 10^3 \text{ GeV}^2$, respectively. The orbit at $Q^2 = 30 \text{ GeV}^2$ (solid line) can be characterized by the empirical relation $-G_M^n/G_M^p = 0.426 - 9.91 \times 10^{-3}B_4 - 4.27 \times 10^{-4}B_4^2 + 4.59 \times 10^{-6}B_4^3$, which complies with that found within the standard convolution scheme. The dashed line in Fig. 35 represents a similar fit for $Q^2 = 10^3 \text{ GeV}^2$. We observe that as Q^2 increases the modified orbit approaches again the original one. This observation is double-edged: it means not only that the orbit structure is stable and can be used in both convolution schemes in order to exclude unphysical solutions, for example, Sch III, it also supports the view that in the axial gauge, e^{-S} operates like a finite wave-function renormalization factor [25], as outlined above. This conception may be used reversely to model hadron distribution amplitudes with an improved, i.e., “softened” endpoint behavior relative to those determined by QCD sum rules alone.

VII. CONCLUSIONS AND OUTLOOK

We have reviewed a large body of exclusive processes which relates to testing the validity of perturbative QCD, in particular factorization theorems, and the universality of non-perturbative hadron distribution amplitudes modeled on the basis of QCD sum rules.

Within the standard convolution scheme, our “heterotic” distribution amplitude for the nucleon [42] – which amalgamates the pivotal features of COZ-type [38] with GS-type [33,53,35] distribution amplitudes – successfully correlates a wide variety of unrelated observables to the data without tuning free parameters from case to case and without using additional phenomenological constraints [103]. This agreement is non-trivial; no other theoretical model matches the available experimental data nearly as well.

By analyzing the QCD sum-rule constraints on the moments of nucleon distribution amplitudes [38,37] with the aid of a “hierarchical” χ^2 criterion [42] – that takes into account the higher accuracy [31,35] of lower-order sum rules – we were able to systematically explore the characteristic features of distribution amplitudes complying with the sum-rule constraints [51]. Our extensive analysis does reveal definite evidence for a global pattern of such distribution amplitudes across an orbit in the plane spanned by the ratio $R \equiv |G_M^n|/G_M^p$ of the magnetic form factors of the nucleon and the expansion coefficient B_4 , the latter projecting on to an antisymmetric eigenfunction of order two of the nucleon evolution equation. This orbit is finite, ranging from distribution amplitudes with a ratio value R around 0.1 (heterotic region) up to COZ-type solutions with $R \lesssim 0.49$, where the orbit terminates (fixed point). Proposed nucleon distribution amplitudes which fall outside the orbit turn out to be unphysical, irrespectively of their functional representation in terms of eigenfunctions. Hence, we are inclined to believe that the orbit captures a genuine feature of the true nucleon distribution amplitude, i.e., of the whole eigenfunctions series, resulting in turn into an insensitivity to particular schemes of truncation. We were able to formulate the concept of “heteroticity” in mathematical terms by introducing a “hybridity” angle to quantify the mingling of COZ- and GS-type distribution amplitudes, thus completing the classification scheme of nucleon distribution amplitudes.

Factorizing the exclusive-scattering amplitude for the nucleon form factors according to the modified convolution scheme – which includes gluon radiative corrections in the form of Sudakov-like damping exponentials – the orbit retains its structure and changes only slightly

as a whole. For momentum-transfer values on the order of 10^3 GeV^2 it rotates back to the one obtained within the standard convolution scheme [25,80]. On the phenomenological side, limiting the value of the form-factor ratio by experiment, one could use the orbit to extract the theoretically appropriate nucleon distribution amplitude.

Similar ideas of “heteroticity” could be applied to QCD sum-rule analyses [44,45] which constrain the moments of the Δ^+ distribution amplitude. A theoretical model was derived [43], termed again “heterotic”, that provides the best agreement with existing data [46,47] on the (electromagnetic) transition form factor G_M^* .

Overall, the current status of the QCD sum rules program to exclusive high-momentum processes produced a rich body of theoretical ideas and experimental tests that could be utilized to scrutinize new developments, like the use of nonlocal condensates.

But there are problems, both technical and conceptual. The inversion of few moments cannot fix hadron distribution amplitudes uniquely [53,35,17]. On the other hand, the calculation of higher-order moment constraints is burdened by intrinsic theoretical uncertainties [31,17]; e.g., power corrections grow with the moment order thus overwhelming the perturbative contribution. Clearly, from the theoretical point of view, a QCD sum-rule method to calculate hadron distribution amplitudes as a *whole* would be desirable, but is still to be developed. First steps in this direction [17,93] are promising but have to be further pursued to include baryons.

On the perturbative side, we were able to calculate a total of 55 next-to-leading eigenfunctions of the nucleon evolution equation, tabulating results up to polynomial order $M = 4$ (Tables 4, 5). We investigated the corresponding anomalous dimensions of leading-twist three and estimated their large-order behavior in successive steps from $M = 9$, $M = 20$, $M = 38$, up to $M = 150$. This behavior can be best reproduced by a logarithmic fit, thus confirming previous expectations based on exponentiation of one-loop results.

Repeating the form-factor calculations for the nucleon within the modified convolution scheme [77,79], which incorporates the effect of (soft) gluon radiative corrections by means of Sudakov-type form factors [76], we showed how the screening of α_s singularities in the endpoint region can be enforced by employing an infrared regularization prescription, based on the assumption that quarks at large transverse separations act coherently and thus cannot radiate soft gluons (“MAX” prescription). This prescription renders the calculations finite and reinstates the validity of the perturbative treatment providing sufficient infrared protection, since, even with evolution, the integrand in Eq. (167) remains finite [78,80,25]. A significant feature of this treatment is that the nucleon form factors saturate, i.e., become insensitive to the contributions from large transverse separations. The other choices of infrared-cutoff prescriptions (“L”, “H-SS”) [79,145,146] do not lead to saturation.

However, a heavy price is paid. A reliable saturation and infrared protection of the form factors are achieved at the expense of a strong reduction of the perturbative contribution. The damping of the nucleon form factors becomes enhanced if the intrinsic transverse momentum dependence of the nucleon wave function (see Fig. 26 and Fig. 27) is taken into account. This has been done by assuming a non-factorizing x and k_\perp -dependence of the wave function of the Brodsky-Lepage-Huang type [147], and fixing the value of $\langle k_\perp^2 \rangle^{1/2}$ either via the valence quark probability P_{3q} or by inputting the value 600 MeV by hand [146]. A remarkable finding is that the form factors calculated this way show only a mild dependence on the particular model distribution amplitude used.

The perturbative contribution to the form factor becomes self-consistent in all cases for momentum transfers larger than 6 to 10 GeV², albeit the actual value of the onset of self-consistency depends on the particular wave function and the r.m.s. transverse momentum chosen. Self-consistency is defined such that 50% of the result are accumulated in regions where α_s^2 is smaller than 0.5.

Comparing these theoretical results with the data, it turns out that they fall short by at least 50%. This is true not only for the COZ distribution amplitude (which we have exemplarily used as reference model) but actually for the whole spectrum of amplitudes determined in [51,52] that satisfy existing sum-rule requirements. Depending on the actual value of the r.m.s. transverse momentum, the reduction of the perturbative contribution may be even stronger than 50%.

This damping may perhaps be counteracted by taking into account pairing effects in the hadron, effects which go beyond the simple impulse approximation. The latter assumes that the interaction of the external photon takes place with just one parton at a time. One may argue that non-perturbative vacuum fluctuations, e.g., due to instantons [100], give way to parton correlations and provide additional finite renormalizing factors [25] greater than 1 to bridge the gap to the experimental data at laboratory momentum transfer. Or perhaps higher-order corrections of perturbation theory giving rise to a rather large K-factor of the order 2, as found for other large-momentum transfer (inclusive) processes [155], may improve the theoretical predictions. Furthermore, the failing of the leading-order form-factor contribution to reproduce the existing data, may be a signal that soft contributions (non-logarithmic contributions) not accounted for so far in the formalism should be included. Such contributions include, e.g., improved and/or more complicated wave functions comprising higher-twists, orbital angular momentum, higher Fock components, quark-quark correlations (diquarks), higher-dimensional quark/gluon condensates, quark masses, etc. Also remainders of genuine soft contributions, like vector-meson-dominance terms or the non-factorizing overlap of the soft parts of the wave functions (Feynman contributions), may still be large at accessible momentum transfers. The rather large value of the Pauli form factor F_2 around 10 GeV², as found experimentally (second reference in [123]), indicates that sizeable higher-twist contributions still exist in that region of momentum transfer. One may suspect similar or even larger higher-twist contributions to the helicity non-flip current matrix element controlling F_1 and G_M .

Once all this is accomplished, we shall probably be able to make contact with the data in a more meaningful way.

A real theoretical breakthrough is, however, not a project that simply reconciles form-factor calculations with experimental data. The basic challenge is finding a way to describe an exclusive process in regimes where the impulse approximation becomes invalid. This happens when for some reason the interaction time becomes comparable with that of hadron formation. Then, speaking in terms of pictures, the dynamics is not a “snapshot” (the essence of the impulse approximation) but rather a “blurred” (i.e., “smeared”) field configuration which extends to a large range of scales linking the initial with the final hadron state (scale intrusions). The consequence is that factorization of the amplitude breaks down and a short-distance part amenable to perturbation theory can no more be isolated. This is the case in the kinematic endpoint region when partons can become very “wee”. The appearance of soft propagators in the hard part of the amplitude signals infrared sensitivity and means

that scale locality is lost. These problems cannot be resolved insisting to use valence quarks. These are not asymptotic fields and hence cannot be part of the true asymptotic dynamics (Hamiltonian of the system). One should use instead quark lines which are quark-gluon composites and can inherently accommodate soft modes within an effective approach. The goal is to transcend perturbation theory by providing all-order expressions in the coupling constant for dynamical quantities, like Green and universal vertex functions. Work in this direction is in progress [82,156].

ACKNOWLEDGMENTS

I would like to thank Michael Bergmann, Jan Bolz, Rainer Jakob, and Peter Kroll for valuable contributions at several stages of this work. It is a pleasure to thank Alexander Bakulev, Alexander Dorokhov, Sergey Mikhailov, and Prof. Dmitrij V. Shirkov for useful discussions. I am especially grateful to the members of The Bogoliubov Laboratory of Theoretical Physics, JINR, Dubna for their warm hospitality during several research stays, where and when parts of this manuscript were prepared, and the Landau-Heisenberg-Foundation for travel grants. Finally, I wish to express my gratitude to my wife Annemarie Stefanis for her patience and encouragement during the course of this work, and to thank Peter Druck for technical assistance with the figures.

APPENDIX A: EIGENFUNCTIONS OF THE NUCLEON EVOLUTION EQUATION

The explicit form of the matrix $U_{ij,kl}$ which relates the nucleon evolution kernel to the polynomial basis $|kl\rangle$ is

$$\begin{aligned}
\frac{\hat{V}|kl\rangle}{2w(x_i)} &= \frac{1}{2} \int_0^1 [dy] \frac{V(x_i, y_i)}{w(x_i)} |y_1^k y_3^l\rangle \\
&= x_1^k x_3^l \left(\frac{1}{(k+1)(k+2)} - 3 \sum_{j=2}^{k+1} \frac{1}{j} + \frac{1}{(l+1)(l+2)} - 3 \sum_{j=2}^{l+1} \frac{1}{j} \right) + \\
&\quad \left[\sum_{i=1}^k \frac{k-i+2}{i(k+2)} x_1^{k-i} \sum_{j=0}^i \binom{i}{j} (-1)^j x_3^{l+j} + \right. \\
&\quad \left. \sum_{i=1}^l \frac{l-i+2}{i(l+2)} x_3^{l-i} \sum_{j=0}^i \binom{i}{j} (-1)^j x_1^{k+j} \right] - \\
&\quad \left[\sum_{i=1}^l x_1^{k+i} x_3^{l-i} \sum_{j=0}^i \binom{l}{j} \binom{l-j}{l-i} (-1)^j \sum_{m=2}^{k+j+1} \frac{1}{m} + \right. \\
&\quad \left. \sum_{i=1}^k x_3^{l+i} x_1^{k-i} \sum_{j=0}^i \binom{k}{j} \binom{k-j}{k-i} (-1)^j \sum_{m=2}^{l+j+1} \frac{1}{m} \right] \\
&= \frac{1}{2} \sum_{i,j}^{i+j \leq M} |ij\rangle U_{ij,kl}
\end{aligned} \tag{A1}$$

with $w(x_i) = x_1 x_2 x_3 = x_1(1-x_1-x_3)x_3$. The operation of \hat{V} on a polynomial $|kl\rangle$ of degree $M = k+l$ projects on another polynomial of degree $i+j \leq M$. This projection is expressed through the matrix U . In the present work U is represented in terms of Appell polynomials which are defined on the triangle $T = T(x_1, x_3)$ with $x_1 > 0$, $x_3 > 0$, $x_1 + x_3 < 1$ as follows

$$\begin{aligned}
\mathcal{F}_{mn}(\chi_0, \chi_1, \chi_3; x_1, x_3) &= w^{-1}(\chi_0, \chi_1, \chi_3; x_1, x_3) \frac{\Gamma(\chi_1 + m) \Gamma(\chi_3 + n)}{\Gamma(\chi_1) \Gamma(\chi_3)} \\
&\quad \frac{\partial^{m+n}}{\partial x_1^m \partial x_3^n} \left[x_1^{m+\chi_1-1} x_3^{n+\chi_3-1} (1-x_1-x_3)^{m+n+\chi_0-\chi_1-\chi_3} \right].
\end{aligned} \tag{A2}$$

Here Γ denotes the Γ -function with

$$\frac{\Gamma(\chi_i + j)}{\Gamma(\chi_i)} = \chi_i (\chi_i - 1) \cdots (\chi_i + j - 1) \tag{A3}$$

and the weight function is defined by

$$w(\chi_0, \chi_1, \chi_3; x_1, x_3) = x_1^{\chi_1-1} x_3^{\chi_3-1} (1-x_1-x_3)^{\chi_0-\chi_1-\chi_3}. \tag{A4}$$

The polynomials \mathcal{F}_{mn} are of order $M = m+n$ and analytical, provided the χ_i are real, i.e.,

$$\Re(\chi_1) > 0, \quad \Re(\chi_3) > 0, \quad \Re(\chi_0) > \Re(\chi_1 + \chi_3) - 1. \tag{A5}$$

The scalar product of an arbitrary function $f(x_1, x_3)$ on the triangle T with \mathcal{F}_{mn} gives

$$\langle f | \mathcal{F}_{mn} \rangle := \frac{\Gamma(\chi_1+m)\Gamma(\chi_3+n)}{\Gamma(\chi_1)\Gamma(\chi_3)} \int_G dx_1 dx_3 f(x_1, x_3) \frac{\partial^{m+n}}{\partial x_1^m \partial x_3^n} \left[x_1^{m+\chi_1-1} x_3^{n+\chi_3-1} (1-x_1-x_3)^{m+n+\chi_0-\chi_1-\chi_3} \right], \quad (\text{A6})$$

where a “bracket” notation, resembling that in Chapter III C 3, is used. If the function $f(x_1, x_3)$ is another Appell polynomial, then the following two relations hold:

- (1) $m + n \neq m' + n'$

$$\langle \mathcal{F}_{m'n'} | \mathcal{F}_{mn} \rangle = 0 \quad (\text{A7})$$

meaning that Appell polynomials of different degree are mutually orthogonal.

- (2) $m + n = m' + n'$

$$\begin{aligned} \langle \mathcal{F}_{mn} | \mathcal{F}_{m'n'} \rangle &= (-1)^{m+n} \frac{\Gamma(\chi_1+m)\Gamma(\chi_3+n)}{\Gamma(\chi_1)\Gamma(\chi_3)} \frac{\partial^{m+n} \mathcal{F}_{m'n'}}{\partial x_1^m \partial x_3^n} \\ &= \frac{\Gamma(\chi_1)\Gamma(\chi_3)\Gamma(\chi_0+m+n-\chi_1-\chi_3+1)}{\Gamma(\chi_0+2m+2n+1)} (-1)^{m+n} \frac{\partial^{m+n} \mathcal{F}_{m'n'}}{\partial x_1^m \partial x_3^n} \end{aligned} \quad (\text{A8})$$

meaning that Appell polynomials of the same degree are not *a priori* orthogonal to each other.

In the nucleon case, $M = m + n = 0, 1, 2, 3, \dots$ equals the total number of derivatives in the interpolating three-quark operators between the nucleon and the vacuum. In order to ensure that the asymptotic behavior of the nucleon distribution amplitude predicted by perturbative QCD is described by the amplitude $\Phi_{\text{as}}(x_i) = 120x_1x_2x_3$, the weight function of the Appell polynomials has to be $w(x_i) = x_1x_2x_3$ with $x_2 = 1 - x_1 - x_3$ because of momentum conservation. Hence, $\chi_1 = \chi_3 = 2$ and $\chi_0 = 0$, so that the relevant Appell polynomials are

$$\begin{aligned} \mathcal{F}_{mn}^{(M)}(5, 2, 2; x_1, x_3) &= w(x_i)^{-1} \frac{1}{(m+1)!(n+1)!} \frac{\partial^{(M)}}{\partial x_1^m \partial x_3^n} \left[x_1^{m+1} x_3^{n+1} (1-x_1-x_3)^{m+n+1} \right] \\ &= \sum_{k,l}^{k+l \leq m+n} a_{kl}^{(mn)} |kl\rangle. \end{aligned} \quad (\text{A9})$$

The symmetrized Appell polynomials used in the text are defined by the differential equation

$$\begin{aligned} \tilde{\mathcal{F}}_{mn}(x_1, x_3) &= x_1x_3(1-x_1-x_3) \frac{\Gamma(2+m)\Gamma(2+n)}{2(\Gamma(2))^2} \\ &\quad \frac{\partial^{m+n}}{\partial x_1^m \partial x_3^n \pm \partial x_1^n \partial x_3^m} \left[x_1^{m+1} x_3^{n+1} (1-x_1-x_3)^{m+n+1} \right], \end{aligned} \quad (\text{A10})$$

where the plus sign refers to the case $m \geq n$ and the minus sign to the case $m < n$.

APPENDIX B: ELASTIC FORM FACTORS OF THE NUCLEON

The functions $I^p(B_n)$ and $I^n(B_n)$, entering, respectively, the calculation of the proton and neutron Dirac form factors are:

$$\begin{aligned}
 I^p = & 1400 B_0 B_1 + \frac{2000 B_1^2}{9} + 1800 B_0 B_2 + \frac{2800 B_1 B_2}{3} + 1200 B_2^2 + \\
 & 6600 B_0 B_3 + \frac{22000 B_1 B_3}{9} + 4800 B_2 B_3 + \frac{18800 B_3^2}{3} - \frac{1000 B_0 B_4}{3} - \\
 & \frac{2600 B_1 B_4}{27} - \frac{2200 B_2 B_4}{9} - \frac{4600 B_3 B_4}{9} + \frac{2600 B_4^2}{243} - 1400 B_0 B_5 - \\
 & \frac{3500 B_1 B_5}{9} - \frac{1100 B_2 B_5}{9} - \frac{5900 B_3 B_5}{9} + \frac{4100 B_4 B_5}{27} + \frac{7700 B_5^2}{27} - \\
 & \frac{135 B_0 B_6}{9} - \frac{855 \sqrt{w_1} B_0 B_6}{3} - \frac{715 B_1 B_6}{3} - \frac{265 \sqrt{w_1} B_1 B_6}{27} - \\
 & \frac{1025 B_2 B_6}{8} - \frac{625 \sqrt{w_1} B_2 B_6}{8} - \frac{3775 B_3 B_6}{24} - \frac{4175 \sqrt{w_1} B_3 B_6}{8} + \\
 & \frac{35 B_4 B_6}{8} + \frac{65 \sqrt{w_1} B_4 B_6}{8} - \frac{1025 B_5 B_6}{24} + \frac{325 \sqrt{w_1} B_5 B_6}{24} + \\
 & \frac{3}{94901 B_6^2} + \frac{9}{2629 \sqrt{w_1} B_6^2} - \frac{48}{135 B_0 B_7} + \frac{16}{855 \sqrt{w_1} B_0 B_7} - \\
 & \frac{768}{715 B_1 B_7} + \frac{768}{265 \sqrt{w_1} B_1 B_7} - \frac{8}{1025 B_2 B_7} + \frac{8}{625 \sqrt{w_1} B_2 B_7} - \\
 & \frac{24}{3775 B_3 B_7} + \frac{8}{4175 \sqrt{w_1} B_3 B_7} + \frac{8}{35 B_4 B_7} - \frac{8}{65 \sqrt{w_1} B_4 B_7} - \\
 & \frac{24}{1025 B_5 B_7} - \frac{24}{325 \sqrt{w_1} B_5 B_7} - 227 B_6 B_7 + \frac{94901 B_7^2}{9} - \\
 & \frac{48}{2629 \sqrt{w_1} B_7^2} + \frac{16}{8309 B_0 B_8} + \frac{109 \sqrt{w_2} B_0 B_8}{768} + \frac{67525 B_1 B_8}{1188} + \\
 & \frac{768}{925 \sqrt{w_2} B_1 B_8} + \frac{44}{17197 B_2 B_8} + \frac{44}{197 \sqrt{w_2} B_2 B_8} + \frac{1188}{120643 B_3 B_8} + \\
 & \frac{1188}{1643 \sqrt{w_2} B_3 B_8} - \frac{132}{10939 B_4 B_8} - \frac{132}{139 \sqrt{w_2} B_4 B_8} - \frac{396}{94717 B_5 B_8} - \\
 & \frac{396}{1717 \sqrt{w_2} B_5 B_8} - \frac{891}{331907 B_6 B_8} - \frac{891}{265651 \sqrt{w_1} B_6 B_8} - \frac{2376}{2507 \sqrt{w_2} B_6 B_8} - \\
 & \frac{63360}{3451 \sqrt{w_1 w_2} B_6 B_8} - \frac{63360}{331907 B_7 B_8} + \\
 & \frac{63360}{265651 \sqrt{w_1} B_7 B_8} - \frac{63360}{2507 \sqrt{w_2} B_7 B_8} + \frac{63360}{3451 \sqrt{w_1 w_2} B_7 B_8} + \\
 & \frac{63360}{2390087 B_8^2} + \frac{63360}{33287 \sqrt{w_2} B_8^2} + \frac{8309 B_0 B_9}{109 \sqrt{w_2} B_0 B_9} + \\
 & \frac{348480}{67525 B_1 B_9} - \frac{348480}{925 \sqrt{w_2} B_1 B_9} + \frac{44}{17197 B_2 B_9} - \frac{44}{197 \sqrt{w_2} B_2 B_9} + \\
 & \frac{1188}{120643 B_3 B_9} - \frac{1188}{1643 \sqrt{w_2} B_3 B_9} - \frac{132}{10939 B_4 B_9} + \frac{132}{139 \sqrt{w_2} B_4 B_9} - \\
 & \frac{396}{94717 B_5 B_9} + \frac{396}{1717 \sqrt{w_2} B_5 B_9} - \frac{891}{331907 B_6 B_9} + \frac{891}{2507 \sqrt{w_2} B_6 B_9} - \\
 & \frac{2376}{265651 \sqrt{w_1} B_6 B_9} + \frac{2376}{3451 \sqrt{w_1 w_2} B_6 B_9} - \frac{63360}{331907 B_7 B_9} + \frac{63360}{63360} +
 \end{aligned}$$

$$\frac{265651 \sqrt{w_1} B_7 B_9}{63360} + \frac{2507 \sqrt{w_2} B_7 B_9}{63360} - \frac{3451 \sqrt{w_1 w_2} B_7 B_9}{63360} + \frac{791 B_8 B_9}{1188} + \frac{2390087 B_9^2}{348480} - \frac{33287 \sqrt{w_2} B_9^2}{348480}, \quad (\text{B1})$$

$$\begin{aligned} I_n = & 1800 B_0^2 - 1400 B_0 B_1 + \frac{2200 B_1^2}{9} - 1800 B_0 B_2 - \frac{2800 B_1 B_2}{3} - \\ & 200 B_2^2 - 1000 B_0 B_3 - \frac{22000 B_1 B_3}{9} - 2000 B_2 B_3 - \frac{17000 B_3^2}{9} + \\ & \frac{1000 B_0 B_4}{3} - \frac{2600 B_1 B_4}{27} + \frac{2200 B_2 B_4}{9} + \frac{4600 B_3 B_4}{9} + \frac{2600 B_4^2}{9} + \\ & \frac{2000 B_0 B_5}{3} + \frac{3500 B_1 B_5}{27} + \frac{500 B_2 B_5}{9} + \frac{6500 B_3 B_5}{9} - \frac{243 B_4 B_5}{4100} - \\ & \frac{7250 B_5^2}{3} + \frac{725 B_0 B_6}{9} + \frac{325 \sqrt{w_1} B_0 B_6}{9} + \frac{715 B_1 B_6}{9} + \frac{265 \sqrt{w_1} B_1 B_6}{81} + \\ & \frac{81 B_2 B_6}{115} + \frac{195 \sqrt{w_1} B_2 B_6}{8} + \frac{5815 B_3 B_6}{8} + \frac{4295 \sqrt{w_1} B_3 B_6}{8} - \\ & \frac{35 B_4 B_6}{8} - \frac{65 \sqrt{w_1} B_4 B_6}{9} + \frac{1705 B_5 B_6}{72} - \frac{935 \sqrt{w_1} B_5 B_6}{72} - \\ & \frac{91813 B_6^2}{3} - \frac{2357 \sqrt{w_1} B_6^2}{9} + \frac{144 B_0 B_7}{725} - \frac{144 \sqrt{w_1} B_0 B_7}{325} + \\ & \frac{2304 B_1 B_7}{715} - \frac{2304 \sqrt{w_1} B_1 B_7}{265} + \frac{8 B_2 B_7}{115} - \frac{8 \sqrt{w_1} B_2 B_7}{195} + \\ & \frac{5815 B_3 B_7}{4295} - \frac{8 \sqrt{w_1} B_3 B_7}{4295} - \frac{35 B_4 B_7}{3} + \frac{65 \sqrt{w_1} B_4 B_7}{9} + \\ & \frac{1705 B_5 B_7}{72} + \frac{935 \sqrt{w_1} B_5 B_7}{72} + 77 B_6 B_7 - \frac{91813 B_7^2}{9} + \\ & \frac{144 \sqrt{w_1} B_7^2}{2357} - \frac{144 B_0 B_8}{8309} - \frac{109 \sqrt{w_2} B_0 B_8}{197} + \frac{2304 B_1 B_8}{69973} + \\ & \frac{2304 \sqrt{w_2} B_1 B_8}{973} - \frac{44 B_2 B_8}{17197} - \frac{44 \sqrt{w_2} B_2 B_8}{197} - \frac{1188 B_3 B_8}{120643} - \\ & \frac{1643 \sqrt{w_2} B_3 B_8}{132} - \frac{10939 B_4 B_8}{139} - \frac{132 \sqrt{w_2} B_4 B_8}{139} + \frac{396 B_5 B_8}{94717} + \\ & \frac{396 \sqrt{w_2} B_5 B_8}{1717} + \frac{891 B_6 B_8}{331907} + \frac{265651 \sqrt{w_1} B_6 B_8}{63360} + \\ & \frac{2376 \sqrt{w_1 w_2} B_6 B_8}{3451} + \frac{63360 B_7 B_8}{331907} - \frac{63360 \sqrt{w_1} B_7 B_8}{265651} + \\ & \frac{63360 \sqrt{w_2} B_7 B_8}{2507} - \frac{63360 \sqrt{w_1 w_2} B_7 B_8}{3451} + \frac{4062433 B_8^2}{580800} + \\ & \frac{63360 \sqrt{w_2} B_8^2}{169699} - \frac{63360 B_0 B_9}{8309} + \frac{109 \sqrt{w_2} B_0 B_9}{17197} + \frac{2507 \sqrt{w_2} B_6 B_8}{197} + \\ & \frac{1742400 B_1 B_9}{69973} - \frac{44 \sqrt{w_2} B_1 B_9}{973} - \frac{44 B_2 B_9}{17197} + \frac{63360 \sqrt{w_2} B_2 B_9}{197} - \\ & \frac{1188 B_3 B_9}{120643} + \frac{1188 \sqrt{w_2} B_3 B_9}{1643} - \frac{132 B_4 B_9}{10939} + \frac{132 \sqrt{w_2} B_4 B_9}{139} + \\ & \frac{396 B_5 B_9}{94717} - \frac{396 \sqrt{w_2} B_5 B_9}{1717} + \frac{891 B_6 B_9}{331907} - \frac{891 \sqrt{w_2} B_6 B_9}{2507} + \\ & \frac{2376 \sqrt{w_1} B_6 B_9}{265651} - \frac{2376 \sqrt{w_1 w_2} B_6 B_9}{3451} + \frac{63360 B_7 B_9}{331907} - \frac{63360 \sqrt{w_1} B_7 B_9}{63360} - \end{aligned}$$

$$\frac{2507 \sqrt{w_2} B_7 B_9}{63360} - \frac{265651 \sqrt{w_1} B_7 B_9}{63360} + \frac{4062433 B_9^2}{580800} + \frac{3451 \sqrt{w_1 w_2} B_7 B_9}{63360} + \frac{695 B_8 B_9}{1188} - \frac{169699 \sqrt{w_2} B_9^2}{1742400}, \quad (\text{B2})$$

where $w_1 = 97$ and $w_2 = 4801$.

Particularly useful expressions are obtained by recasting these formulae in terms of strict moments $\Phi_N^{(n_1 \bar{0} n_3)} \equiv (n_1 0 n_3)$ via Eq. (90). The results up to order $M = 2$ (in correspondence to the nucleon distribution amplitudes on the orbit) are

$$I_p = 196 \left[4899 - 9851 (001) + 47231 (001)^2 + 24954 (002) - 163098 (001)(002) + 138696 (002)^2 - 29425 (100) + 95825 (001)(100) - 175500 (002)(100) + 67625 (100)^2 + 20790 (101) + 30720 (001)(101) - 30780 (002)(101) - 22350 (100)(101) + 37800 (101)^2 + 29310 (200) - 132120 (001)(200) + 231780 (002)(200) - 161550 (100)(200) + 101400 (200)^2 \right], \quad (\text{B3})$$

$$I_n = 490 \left[-485 - 982 (001) + 3799 (001)^2 - 5028 (002) + 30300 (001)(002) - 26544 (002)^2 + 4792 (100) - 16184 (001)(100) + 34176 (002)(100) - 12680 (100)^2 - 1728 (101) - 6744 (001)(101) + 5976 (002)(101) + 1200 (100)(101) - 3420 (101)^2 - 5400 (200) + 26880 (001)(200) - 44520 (002)(200) + 30720 (100)(200) + 2520 (101)(200) - 19020 (200)^2 \right]. \quad (\text{B4})$$

Similar expressions can be obtained also for the other nucleon form factors displayed below.

The axial form factor of the nucleon in terms of nucleon eigenfunctions, including next-to-leading ($M = 3$) contributions, is

$$Q^4 g_A(Q^2) = \left(\frac{16\pi\bar{\alpha}_S}{3} \right)^2 |f_N|^2 \left[\frac{75 B_0^2}{4} + \frac{175 B_0 B_1}{6} + \frac{25 B_1^2}{108} + \frac{25 B_0 B_2}{2} + \frac{175 B_1 B_2}{9} + \frac{75 B_2^2}{4} + \frac{625 B_0 B_3}{6} + \frac{1375 B_1 B_3}{27} + \frac{125 B_2 B_3}{2} + \frac{9625 B_3^2}{108} - \frac{125 B_0 B_4}{18} - \frac{275 B_2 B_4}{54} - \frac{575 B_3 B_4}{54} - \frac{625 B_0 B_5}{36} - \frac{875 B_1 B_5}{108} - \frac{625 B_2 B_5}{108} - \frac{2875 B_3 B_5}{108} + \frac{1025 B_4 B_5}{972} + \frac{15625 B_5^2}{3888} + \frac{125 B_0 B_6}{192} - \frac{275 \sqrt{97} B_0 B_6}{192} - \frac{715 B_1 B_6}{1152} - \frac{265 \sqrt{97} B_1 B_6}{384} - \frac{1195 B_2 B_6}{635 \sqrt{97}} - \frac{635 \sqrt{97} B_2 B_6}{3265} - \frac{3265 B_3 B_6}{4145 \sqrt{97}} - \frac{4145 \sqrt{97} B_3 B_6}{1728} + \frac{35 B_4 B_6}{144} + \frac{65 \sqrt{97} B_4 B_6}{432} - \frac{95 B_5 B_6}{384} + \frac{985 \sqrt{97} B_5 B_6}{3456} + \frac{31891 B_6^2}{18432} + \frac{899 \sqrt{97} B_6^2}{18432} + \frac{125 B_0 B_7}{192} + \frac{275 \sqrt{97} B_0 B_7}{192} - \right]$$

$$\begin{aligned}
& \frac{715 B_1 B_7}{1152} + \frac{265 \sqrt{97} B_1 B_7}{384} - \frac{1195 B_2 B_7}{576} + \frac{635 \sqrt{97} B_2 B_7}{576} - \\
& \frac{3265 B_3 B_7}{1728} + \frac{4145 \sqrt{97} B_3 B_7}{1728} + \frac{35 B_4 B_7}{144} - \frac{65 \sqrt{97} B_4 B_7}{432} - \\
& \frac{95 B_5 B_7}{384} - \frac{985 \sqrt{97} B_5 B_7}{3456} - \frac{113 B_6 B_7}{36} + \frac{31891 B_7^2}{18432} - \\
& \frac{899 \sqrt{97} B_7^2}{18432} + \frac{8309 B_0 B_8}{2112} + \frac{109 \sqrt{4801} B_0 B_8}{2112} + \frac{17 B_1 B_8}{792} + \\
& \frac{\sqrt{4801} B_1 B_8}{17197} + \frac{17197 B_2 B_8}{197 \sqrt{4801}} + \frac{197 \sqrt{4801} B_2 B_8}{6336} + \\
& \frac{120643 B_3 B_8}{1643 \sqrt{4801}} + \frac{6336 B_3 B_8}{94717 B_5 B_8} - \\
& \frac{19008}{1717 \sqrt{4801} B_5 B_8} - \frac{19008}{331907 B_6 B_8} - \frac{114048}{265651 \sqrt{97} B_6 B_8} - \\
& \frac{114048}{2507 \sqrt{4801} B_6 B_8} - \frac{3041280}{3451 \sqrt{w_1 w_2} B_6 B_8} - \frac{3041280}{331907 B_7 B_8} + \\
& \frac{3041280}{265651 \sqrt{97} B_7 B_8} - \frac{3041280}{2507 \sqrt{4801} B_7 B_8} + \frac{3041280}{3451 \sqrt{w_1 w_2} B_7 B_8} + \\
& \frac{3041280}{3701 B_8^2} + \frac{17 \sqrt{4801} B_8^2}{8309 B_0 B_9} - \frac{109 \sqrt{4801} B_0 B_9}{2613600} + \\
& \frac{17 B_1 B_9}{\sqrt{4801} B_1 B_9} + \frac{871200}{17197 B_2 B_9} - \frac{2112}{197 \sqrt{4801} B_2 B_9} + \\
& \frac{792}{120643 B_3 B_9} - \frac{2376}{1643 \sqrt{4801} B_3 B_9} - \frac{6336}{94717 B_5 B_9} + \\
& \frac{19008}{1717 \sqrt{4801} B_5 B_9} - \frac{19008}{331907 B_6 B_9} - \frac{114048}{265651 \sqrt{97} B_6 B_9} + \\
& \frac{114048}{2507 \sqrt{4801} B_6 B_9} + \frac{3041280}{3451 \sqrt{w_1 w_2} B_6 B_9} - \frac{3041280}{331907 B_7 B_9} + \\
& \frac{3041280}{265651 \sqrt{97} B_7 B_9} + \frac{3041280}{2507 \sqrt{4801} B_7 B_9} - \frac{3041280}{3451 \sqrt{w_1 w_2} B_7 B_9} - \\
& \left. \frac{3041280}{1188} + \frac{3701 B_9^2}{2613600} - \frac{17 \sqrt{4801} B_9^2}{871200} \right] . \tag{B5}
\end{aligned}$$

This expression verifies the leading-order results obtained by Carlson and Poor [126].

References

- [1] E. V. Shuryak, Nucl. Phys. B 203 (1982) 93, 116, 140; V. N. Baier and Yu. F. Pinelis, Report Nr. IYF-81-115, Report Nr. IYF-81-141; D. Gromes, Phys. Lett. 115B (1982) 482.
- [2] A. G. Grozin, Int. J. Mod. Phys. A 10 (1995) 3497.
- [3] M. Campostrini, A. Di Giacomo, and G. Mussardo, Z. Phys. C 25 (1984) 173; A. Di Giacomo and H. Panagopoulos, Phys. Lett. B 285 (1992) 133.
- [4] M. A. Shifman, A. I. Vainshtein, and V. I. Zakharov, Nucl. Phys. B 147 (1979) 385, 448, 519.
- [5] K. G. Wilson, Phys. Rev. D 10 (1974) 2445.
- [6] D. Daniel et al., Phys. Rev. D 46 (1992) 3130; M. C. Chu, M. Lissia, and J. W. Negele, Nucl. Phys. B 360 (1991) 31; R. Gupta, D. Daniel, and J. Grandy, Phys. Rev. D 48 (1993) 3330.
- [7] C. V. Christov et al., Prog. Part. Nucl. Phys. 37 (1996) 91.
- [8] D. I. Diakonov and V. Yu. Petrov, Nucl. Phys. B 272 (1986) 457.
- [9] D. Amati, R. Petronzio, and G. Veneziano, Nucl. Phys. B 140 (1978) 54; S. Libby and G. Sterman, Phys. Rev. D 18 (1978) 3252; A. H. Mueller, Phys. Rev. D 18 (1978) 3705; R. Ellis et al., Nucl. Phys. B 152 (1979) 285.
- [10] J. C. Collins, D. E. Soper, and Sterman, Phys. Lett. 134B (1984) 263.
- [11] J. C. Collins, D. E. Soper, and Sterman, in: Perturbative Quantum Chromodynamics, ed. A. H. Mueller (World Scientific, 1989), p. 1.
- [12] F. Bloch and A. Nordsieck, Phys. Rev. 52 (1937) 54.
- [13] R. Doria, J. Frenkel, and J. C. Taylor, Nucl. Phys. B 168 (1980) 93; J. Frenkel, J. G. M. Gatheral, and J. C. Taylor, Nucl. Phys. B 233 (1984) 307; F. T. Brandt, J. Frenkel, and J. C. Taylor, Nucl. Phys. B 312 (1989) 589.
- [14] C. Di'Lieto et al., Nucl. Phys. B 183 (1981) 223.
- [15] N. Isgur and C. H. Llewellyn-Smith, Phys. Rev. Lett. 52 (1984) 1080; Phys. Lett. B 217 (1989) 535; Nucl. Phys. B 317 (1989) 526.
- [16] A. V. Radyushkin, Acta Phys. Pol. 15 (1984) 403.
- [17] A. V. Radyushkin, in: Particles and Nuclei, Proc. Twelfth International Conference, Cambridge, Massachusetts, 1990, eds. J. L. Matthews et al., Nucl. Phys. A 527 (Proc. Suppl.) (1991) 153c; Proc. European Workshop on Hadronic Physics with Electrons Beyond 10 GeV, Dourdan, France, 1990, eds. B. Frois and J.-F. Matthiot; *ibid.* A 532 (Proc. Suppl.) (1991) 141c.
- [18] P. Kroll, in: SPIN95 Conference, Protvino, Russia, 1995, Wuppertal Report Nr. WU-B 95-31 (October 1995).
- [19] G. P. Lepage and S. J. Brodsky, Phys. Lett. 87B (1979) 359.
- [20] G. P. Lepage and S. J. Brodsky, Phys. Rev. Lett. 43 (1979) 545.
- [21] G. P. Lepage and S. J. Brodsky, Phys. Rev. D 22 (1980) 2157.
- [22] A. V. Efremov and A. V. Radyushkin, in: XIX International Conference on High Energy Physics, Tokyo, Japan, 1978, Dubna Report Nr. E2-11535 (June 1978).
- [23] A. V. Efremov and A. V. Radyushkin, Dubna Report Nr. E2-11983 (December 1978) published in Teor. Mat. Fiz. 42 (1980) 97; 42 (1980) 147; 44 (1981) 573, 664, 774; Phys. Lett. 94B (1980) 245.

- [24] D. J. Gross and F. A. Wilczek, Phys. Rev. Lett. 30 (1973) 1343; H. D. Politzer, Phys. Rev. Lett. 30 (1973) 1346.
- [25] N. G. Stefanis, Mod. Phys. Lett. A 10 (1995) 1419.
- [26] K. G. Wilson, Phys. Rev. 179 (1969) 1499.
- [27] B. L. Ioffe and A. V. Smilga, Phys. Lett. 114B (1982) 353; Nucl. Phys. B 216 (1983) 373.
- [28] V. A. Nesterenko and A. V. Radyushkin, Phys. Lett. 115B (1982) 410; Phys. Lett. 128B (1983) 439.
- [29] V. L. Chernyak and A. R. Zhitnitsky, Nucl. Phys. B 201 (1982) 492; Nucl. Phys. B 214 (1983) 547(E).
- [30] V. L. Chernyak and I. R. Zhitnitsky, Nucl. Phys. B 246 (1984) 52.
- [31] V. L. Chernyak and A. R. Zhitnitsky, Phys. Rept. 112 (1984) 173.
- [32] C. J. Bebek et al., Phys. Rev. D 13 (1976) 25; D 17 (1978) 1693.
- [33] M. Gari and N. G. Stefanis, Phys. Lett. B 175 (1986) 462.
- [34] R. G. Arnold et al., Phys. Rev. Lett. 57 (1986) 174.
- [35] N. G. Stefanis, Phys. Rev. D 40 (1989) 2305; D 44 (1991) 1616(E).
- [36] V. L. Chernyak, A. A. Ogloblin, and I. R. Zhitnitsky, Z. Phys. C 42 (1989) 583.
- [37] I. D. King and C. T. Sachrajda, Nucl. Phys. B 279 (1987) 785.
- [38] V. L. Chernyak, A. A. Ogloblin, and I. R. Zhitnitsky, Z. Phys. C 42 (1989) 569.
- [39] D. G. Richards, C. T. Sachrajda, and C. J. Scott, Nucl. Phys. B 286 (1987) 683; G. Martinelli and C. T. Sachrajda, Phys. Lett. B 217 (1989) 319.
- [40] A. Schäfer, Phys. Lett. B 217 (1989) 545.
- [41] N. G. Stefanis, in: 4th Hellenic School on Elementary Particle Physics, Corfu, Greece, September 2-20, 1992, eds. E. N. Gazis, G. Koutsoumbas, N. D. Tracas, and G. Zoupanos, Physics Department, National Technical University, Athens, Greece, Vol. II, p. 528.
- [42] N. G. Stefanis and M. Bergmann, Phys. Rev. D 47 (1993) R3685.
- [43] N. G. Stefanis and M. Bergmann, Phys. Lett. B 304 (1993) 24.
- [44] G. R. Farrar et al., Nucl. Phys. B 311 (1988/89) 585.
- [45] C. E. Carlson and J. L. Poor, Phys. Rev. D 38 (1988) 2758.
- [46] L. Stuart et al., in: Proc. Workshop on Exclusive Reactions at High Momentum Transfer, Elba, Italy, 24-26 June, 1993, eds. C. E. Carlson, P. Stoler, and M. Taiuti (World Scientific, Singapore, 1994), p. 44.
- [47] L. Stuart et al., Phys. Rev. D 58 (1998) 032003.
- [48] P. Stoler, Phys. Rev. Lett. 66 (1991) 1003; Phys. Rev. D 44 (1991) 73.
- [49] N. G. Stefanis and M. Bergmann, in: Proc. Workshop on Exclusive Reactions at High Momentum Transfer, Elba, Italy, 24-26 June, 1993, eds. C. E. Carlson, P. Stoler, and M. Taiuti (World Scientific, Singapore, 1994) p. 137; M. Bergmann and N. G. Stefanis, in: ibid p. 146.
- [50] N. G. Stefanis and M. Bergmann, in: Proc. International Conference on Hadron Structure '93, Banská Štiavnica, Slovakia, 5-10 September, 1993 edited by S. Dubnička and A. Z. Dubničková, Bratislava, Slovakia, 1994, p. 111.
- [51] M. Bergmann and N. G. Stefanis, Phys. Rev. D 48 (1993) R2990.
- [52] M. Bergmann and N. G. Stefanis, Phys. Lett. B 325 (1994) 183.
- [53] M. Gari and N. G. Stefanis, Phys. Rev. D 35 (1987) 1074.
- [54] S. V. Mikhailov and A. V. Radyushkin, Yad. Fiz. 52 (1990) 1095 [Sov. J. Nucl. Phys. 52 (1990) 697].

- [55] J. Bolz and P. Kroll, Z. Phys. A 356 (1996) 327.
- [56] S. V. Mikhailov and A. V. Radyushkin, JETP Lett. 43 (1986) 712; Yad. Fiz. 49 (1989) 794 [Sov. J. Nucl. Phys. 49 (1989) 494]; Phys. Rev. D 45 (1992) 1754.
- [57] A. P. Bakulev and A. V. Radyushkin, Phys. Lett. B 271 (1991) 223.
- [58] S. V. Mikhailov, Phys. At. Nucl. 56 (1993) 650.
- [59] V. M. Belyaev and B. L. Ioffe, Zh. Eksp. Teor. Fiz. 83 (1982) 876 [Sov. Phys. JETP 56 (1982) 493].
- [60] E. V. Shuryak, Nucl. Phys. B 328 (1989) 85.
- [61] A. E. Dorokhov, S. V. Esaibegyan, and S. V. Mikhailov, Phys. Rev. D 56 (1997) 4062.
- [62] J. M. Cornwall and G. Tiktopoulos, Phys. Rev. D 13 (1976) 3370; D 15 (1977) 2937.
- [63] V. Sudakov, Sov. Phys. JETP 3 (1956) 65.
- [64] R. Jackiw, Ann. Phys. (N.Y.) 48 (1968) 292.
- [65] P. M. Fishbane and J. D. Sullivan, Phys. Rev. D 4 (1971) 458.
- [66] T. Appelquist and J. R. Primack, Phys. Rev. D 1 (1970) 1144; D 5 (1972) 1555(E); Phys. Rev. D 4 (1971) 2454.
- [67] A. H. Mueller, Phys. Rev. D 20 (1979) 2037.
- [68] J. C. Collins, Phys. Rev. D 22 (1980) 1478.
- [69] V. V. Belokurov and N. I. Ussyukina, Phys. Lett. 94B (1980) 251.
- [70] H. D. Dahmen and F. Steiner, Z. Phys. C 11 (1981) 247.
- [71] A. Sen, Phys. Rev. D 24 (1981) 3281.
- [72] J. C. Collins and D. E. Soper, Nucl. Phys. B 193 (1981) 381; B 194 (1982) 445.
- [73] J. C. Collins, D. E. Soper, and G. Sterman, Nucl. Phys. B 261 (1985) 104.
- [74] G. Sterman, in: Theoretical Advanced Study Institute, QCD and Beyond, Boulder, Colorado, June 1995, [hep-ph/9606312, 12 June 1996].
- [75] G. Grammer and D. R. Yennie, Phys. Rev. D 8 (1973) 4332.
- [76] J. Botts and G. Sterman, Nucl. Phys. B 325 (1989) 62.
- [77] H.-N. Li and G. Sterman, Nucl. Phys. B 381 (1992) 129.
- [78] J. Bolz, R. Jakob, P. Kroll, M. Bergmann, and N. G. Stefanis, Z. Phys. C 66 (1995) 267.
- [79] H.-N. Li, Phys. Rev. D 48 (1993) 4243.
- [80] J. Bolz, R. Jakob, P. Kroll, M. Bergmann, and N. G. Stefanis, Phys. Lett. B 342 (1995) 345.
- [81] R. Jakob and P. Kroll, Phys. Lett. B 315 (1993) 463; B 319 (1993) 545(E).
- [82] N. G. Stefanis (unpublished).
- [83] S. J. Brodsky and G. P. Lepage, in: Perturbative Quantum Chromodynamics, ed. A. H. Mueller (World Scientific, 1989), p. 93.
- [84] Yu. L. Dokshitzer, Zh. Eksp. Teor. Fiz. 73 (1977) 1216 [Sov. Phys. JETP 46 (1977) 641].
- [85] V. N. Gribov and L. Lipatov, Yad. Fiz. 15 (1972) 781 [Sov. J. Nucl. Phys. 15 (1972) 438]; Yad. Fiz. 15 (1972) 1218 [Sov. J. Nucl. Phys. 15 (1972) 675].
- [86] G. Altarelli and G. Parisi, Nucl. Phys. B 126 (1977) 298.
- [87] D. E. Soper, Nucl. Phys. B 163 (1980) 93.
- [88] A. V. Efremov and A. V. Radyushkin, Riv. Nuovo Cimento 3 (1980) 1.
- [89] S. J. Brodsky et al., Phys. Rev. D 33 (1985) 1881.
- [90] S. J. Brodsky, Y. Frishman, and G. P. Lepage, Phys. Lett. 167B (1986) 347.
- [91] A. Erdelyi et al., Higher Transcendental Functions (McGraw-Hill, New York, 1953), Vol. II.

- [92] G. R. Farrar and D. R. Jackson, Phys. Rev. Lett. 43 (1979) 246; D. R. Jackson, Ph. D. Thesis, Cal. Tech. (1977) (unpublished); V. L. Chernyak and A. R. Zhitnitsky, Pis'ma Zh. Eksp. Teor. Fiz. 25 (1977) 544 [JETP Lett. 25 (1977) 510]; G. Parisi, Phys. Lett. 84B (1979) 225.
- [93] A. P. Bakulev and S. V. Mikhailov, Z. Phys. C 68 (1995) 451; Mod. Phys. Lett. A 11 (1996) 1611.
- [94] A. R. Zhitnitsky, Phys. Lett. B 329 (1994) 493.
- [95] Z. Dziembowski and L. Mankiewicz, Phys. Rev. Lett. 58 (1987) 2175.
- [96] V. M. Braun and I. E. Filyanov, Z. Phys. C 44 (1989) 157; T. Huang and Q.-X. Shen, Z. Phys. C 50 (1991) 139; T. Huang, B.-Q. Ma, and Q.-X. Shen, Phys. Rev. D 49 (1994) 1490; A. Szczepaniak, C.-R. Ji, and S. R. Cotanch, Phys. Rev. D 49 (1994) 3466; D. Müller, Phys. Rev. D 51 (1995) 3855; A. V. Belitsky, Phys. Lett. B 386 (1996) 359.
- [97] V. M. Braun and I. Halperin, Phys. Lett. B 328 (1994) 457.
- [98] V. Anisovich, D. Melikhov, and V. Nikonov, Phys. Rev. D 52 (1995) 5295; D 55 (1997) 2918.
- [99] R. Jakob, P. Kroll, and M. Raulfs, J. Phys. G 22 (1996) 45; P. Kroll, and M. Raulfs, Phys. Lett. B 387 (1996) 848.
- [100] A. E. Dorokhov, Nuovo Cim. 109A (1996) 391.
- [101] N. G. Stefanis and M. Bergmann, in: Proc. Workshop on Quantum Field Theoretical Aspects of High Energy Physics, Kyffhäuser, Germany, September 20-24, 1993, eds. B. Geyer and E.-M. Ilgenfritz, p. 112.
- [102] N. G. Stefanis, in: International Conference on Quark Confinement and the Hadron Spectrum, Villa Olmo, Como, Italy, 20-24 June, 1994, eds. N. Brambilla and G. M. Prosperi (World Scientific, Singapore, April 1995) p. 258; M. Bergmann and N. G. Stefanis, in: ibid, p. 269; N. G. Stefanis, in: Workshop on Hadron Structure and QCD in Hard Processes, 3 July-13 August, 1994, European Theory Center, Trento, Italy; XII International Seminar on High Energy Physics Problems, Relativistic Nuclear Physics & Quantum Chromodynamics, September 12-17, 1994, Dubna, Russia.
- [103] N. G. Stefanis, Acta Phys. Pol. B 25 (1994) 1777.
- [104] M. Bergmann, Dissertation, Bochum University, January 1994, in German (unpublished).
- [105] M. Peskin, Phys. Lett. 88B (1979) 128.
- [106] M. Kremer, Nucl. Phys. B 168 (1979) 272.
- [107] K. Tesima, Phys. Lett. 110B (1981) 319; Nucl. Phys. B 202 (1982) 523.
- [108] Th. Ohrndorf, Nucl. Phys. B 198 (1982) 26.
- [109] A. Duncan and A. H. Mueller, Phys. Lett. 90B (1980) 159; A. H. Mueller, Phys. Rept. 73 (1981) 237.
- [110] G. P. Korchemsky, Mod. Phys. Lett. A 4 (1989) 1257.
- [111] A. Ali, V. M. Braun, and G. Hiller, Phys. Lett. B 266 (1991) 117.
- [112] P. Kroll, in: International Conference on Physics with GeV-Particle Beams, Jülich, Germany, 22-25 August, 1994, Wuppertal Report Nr. WU-B 94-17 (August 1994).
- [113] N. G. Stefanis, Nuovo Cimento 83A (1984) 205.
- [114] N. S. Craigie and H. Dorn, Nucl. Phys. B 185 (1980) 204.
- [115] A. B. Henriques, B. H. Kellett, and R. G. Moorhouse, Ann. Phys. (N.Y.) 93 (1975) 125.
- [116] V. A. Avdeenko, S. E. Korenblit, and V. L. Chernyak, Yad. Fiz. 33 (1981) 481 [Sov. J. Nucl. Phys. 33 (1981) 252].

- [117] P. M. Stevenson, Phys. Lett. B 100 (1981) 61; Phys. Rev. D 23 (1981) 2916; Nucl. Phys. B 231 (1984) 65.
- [118] I. Tamm, J. Phys. (UdSSR) 9 (1945) 449; S. M. Dancoff, Phys. Rev. 78 (1950) 382; F. J. Dyson, Phys. Rev. 90 (1953) 994; W. Zimmermann, Nuovo Cim. Suppl. 11 (1954) 43.
- [119] J. Hansper, R. Eckardt, and M. F. Gari, Z. Phys. A 341 (1992) 339; R. Eckardt, J. Hansper, and M. F. Gari, Z. Phys. A 343 (1992) 443.
- [120] C.-R. Ji, A. F. Sill, and R. M. Lombard-Nelsen, Phys. Rev. D 36 (1987) 165.
- [121] J. M. Cornwall, Phys. Rev. D 26 (1982) 1453.
- [122] G. Parisi and R. Petronzio, Phys. Lett. 94B (1980) 51.
- [123] S. Platchkov et al., Nucl. Phys. A 510 (1990) 740; P. E. Bosted et al., Phys. Rev. Lett. 68 (1992) 3841; S. Rock et al., Phys. Rev. D 46 (1992) 24, and references cited therein.
- [124] M. F. Gari and N. G. Stefanis, Phys. Lett. B 187 (1987) 401.
- [125] J. G. Körner and M. Kuroda, Phys. Rev. D 16 (1977) 2165; R. G. Arnold, C. E. Carlson, and F. Gross, Phys. Rev. C 21 (1980) 1426; M. Gari and W. Krümpelmann, Z. Phys. A 322 (1985) 689; Phys. Lett. B 173 (1986) 10.
- [126] C. E. Carlson and J. L. Poor, Phys. Rev. D 34 (1986) 1478.
- [127] C. E. Carlson and J. L. Poor, Phys. Rev. D 36 (1987) 2169.
- [128] N. J. Baker et al., Phys. Rev. D 23 (1981) 2499; K. L. Miller et al., Phys. Rev. D 26 (1982) 537; T. Kitagaki et al., Phys. Rev. D 28 (1983) 436.
- [129] C. E. Carlson, Phys. Rev. D 34 (1986) 2704.
- [130] W. Bartel et al., Phys. Lett. 28B (1968) 148; S. Galster et al., Phys. Rev. D 5 (1972) 519; J. C. Alder et al., Nucl. Phys. B 46 (1972) 573; S. Stein et al., Phys. Rev. D 12 (1975) 1884; R. Siddle et al., Nucl. Phys. B 35 (1975) 93.
- [131] V. M. Belyaev and A. V. Radyushkin, Phys. Lett. B 359 (1995) 194; Phys. Rev. D 53 (1995) 6509.
- [132] C. E. Carlson, M. Gari, and N. G. Stefanis, Phys. Rev. Lett. 58 (1987) 1308.
- [133] S. J. Brodsky and G. P. Lepage, Phys. Rev. D 24 (1981) 2848.
- [134] A. Andrikopoulou, Z. Phys. C 22 (1984) 63.
- [135] P. H. Damgaard, K. Tsokos, and E. L. Berger, Nucl. Phys. B 259 (1985) 285.
- [136] R. Barbieri, R. Gatto, and R. Kögerler, Phys. Lett. 60B (1976) 183; R. Barbieri, R. Gatto, and E. Remiddi, Phys. Lett. 61B (1976) 465; R. Barbieri et al, Phys. Lett. 95B (1980) 93; 106B (1981) 497.
- [137] T. A. Armstrong et al., Nucl. Phys. B 373 (1992) 35.
- [138] J. Bolz, private communication.
- [139] Particle Data Group, K. Hikasa et al., Phys. Rev. D 45 (1992) 1.
- [140] R. P. Feynman, *Photon-Hadron Interactions* (Benjamin, Reading, MA, 1972).
- [141] N. G. Stefanis, in: Hadron Structure '96. High Energy Interactions: Theory and Experiment, Stará Lesná, High Tatra, Slovak Republic, February 12-17, 1996, eds. by Ľubomír Martinovič and Pavol Stríženec, p. 29, [hep-ph/9607230, 4 July 1996].
- [142] J. Bolz, Dissertation, Wuppertal University Internal Report Nr. WUB-DIS 95-10, August 1995, in German (unpublished).
- [143] M. Dahm, R. Jakob, and P. Kroll, Z. Phys. C 68 (1995) 595.
- [144] F. M. Dittes and A. V. Radyushkin, Yad. Fiz. 34 (1981) 293 [Sov. J. Nucl. Phys. 34 (1981) 2931]; Phys. Lett. 134B (1984) 359; R. D. Field et al., Nucl. Phys. B 186 (1981) 429; M. H. Sarmadi, Phys. Lett. 143B (1984) 471; E. Braaten and S.-M. Tze, Phys. Rev.

- D 35 (1987) 2255.
- [145] T. Hyer, Phys. Rev. D 47 (1993) 3875.
 - [146] M. G. Sotiropoulos, G. Sterman, Nucl. Phys. B 425 (1994) 489.
 - [147] S. J. Brodsky, G. P. Lepage, and T. Huang, Banff Summer Institute, Particles and Fields 2, eds. A. Z. Capri, A. N. Kamal (1983), p. 143.
 - [148] E. Nagy et al., Nucl. Phys. B 150 (1979) 221.
 - [149] J. L. Hartmann et al., Phys. Rev. Lett. 39 (1977) 975; W. Faissler et al., Phys. Rev. D 23 (1981) 33.
 - [150] J. J. Aubert et al., Phys. Lett. 95B (1980) 306; A. Schlagböhmer, Ph. D thesis, Freiburg (1981).
 - [151] P. Kroll, in: Proc. Adriatic Research Conference on Spin and Polarization Dynamics in Nuclear and Particle Physics, Trieste, Italy, 1988; P. Kroll, M. Schürmann, W. Schweiger, Z. Phys. A 338 (1991) 339; *ibid.* A 342 (1992) 429; P. Kroll, M. Schürmann, W. Schweiger, Int. J. Mod. Phys. A 6 (1991) 4107.
 - [152] P. Kroll et al., Phys. Lett. B 316 (1993) 546.
 - [153] R. Jakob et al., Z. Phys. A 347 (1993) 109.
 - [154] S. Rock et al., Phys. Rev. Lett. 49 (1982) 1139; A. Lung et al., Phys. Rev. Lett. 70 (1993) 718; A. F. Sill et al., Phys. Rev. D 48 (1993) 29.
 - [155] N. G. Antoniou et al., Phys. Lett. B 128 (1983) 257.
 - [156] N. G. Stefanis, in: 10th International Conference on Problems of Quantum Field Theory, Alushta, Crimea, Ukraine, 13-18 May, 1996, eds. D. V. Shirkov, D. I. Kazakov, and A. A. Vladimirov (Publishing Department, JINR, Dubna, 1996) p. 199 [hep-th/9607063, 8 July 1996]; A. I. Karanikas, C. N. Ktorides, and N. G. Stefanis, Phys. Rev. D 52 (1995) 5898; A. Kernemann and N. G. Stefanis, Phys. Rev. D 40 (1989) 2103; R. Jakob and N. G. Stefanis, Ann. Phys. (N.Y.) 210 (1991) 112.